3-D FINITE ELEMENT ANALYSIS

OF

VISCOELASTIC FLOW

By

FARHAD SHARIF, M.A.Sc.

A Thesis

Submitted to the School of Graduate Studies

in Partial Fulfillment of the Requirements

for the Degree

Doctor of Philosophy

McMaster University

3-D FINITE ELEMENT ANALYSIS OF VISCOELASTIC FLOW

DOCTOR OF PHILOSOPHY
(Chemical Engineering)

McMASTER UNIVERSITY
Hamilton, Ontario

Title: 3-D Finite Element Analysis of Viscoelastic Flow

Author: Farhad Sharif
M.A.Sc. in Chemical Engineering, University of Toronto
Toronto, Canada
B.Sc. in Petrochemical Engineering, Amir-Kabir university of Technology, Tehran, Iran

Supervisors: Drs:A.N.Hrymak and J.Vlachopolous
Department of Chemical Engineering, McMaster University

Number of pages: xvii, 200

ABSTRACT

3-D numerical analysis of a viscoelastic flow is a necessity for better understanding of viscoleastic fluids and viscoelastic flow. It is important both from the scientific and technological points of view. Analysis of viscoelastic flow is a difficult task as it is associated with the problems arising from intrinsic complexity of the fluid. Progress in the area of 3-D analysis of viscoelastic flow has been further hindered by the increase in the size of the problem and number of variables. The outlet boundary condition for 3-D flow of a viscoelastic fluid is another problem.

Segregated methods were used to solve the creeping flow formulation of the duct flow to save computer time and memory. A pressure correction method was selected and compared with the fully coupled method.

A 3-D and 2.5-D segregated algorithm were proposed using the modified Phan-Thien Tanner constitutive equation and the EVSS method to decouple the calculation of stresses from the flow kinematics. Results from the 2.5-D algorithm were verified by comparison with the reported results from literature. Results for cases of high Wi were obtained and it was shown that for MPTT fluid, the intensity of the secondary flows becomes independent of Wi at high Wi. The effects of Re on the secondary flows were

also studied and new patterns of secondary flows involving up to eight vortices in each quarter were reported.

Results from the 2.5-D analysis were compared with the results of a 3-D algorithm in the analysis of the viscoelastic flow in straight ducts. Different cases of boundary conditions were studied and observations are reported. It is reported for the first time that a deviation from a fully developed solution occurs near the outlet. The problem of the destruction of the vortex pattern and the consequent increase in the primary flow velocity component were then analysed. It was established that the fully developed flow solution is a valid solution for the 3-D formulation of the problem and the problem arises from a combination of the decoupling of the stresses and imposing outlet boundary conditions. The 3-D algorithm was further evaluated for the cases of flow in complex geometries, using two test cases from the literature. One of the cases involved a converging duct and the other involved a 4:1 abrupt contraction. Results from 3-D and 2-D planar analysis were compared with the reported experimental results.

ACKNOLEDGEMENTS

First and foremost, I 'd like to thank God for his help, during this study in various stages.

Secondly, I wish to thank my wife Bahareh for her patience, and all the efforts and sacrifices she made to provide comfort for the family. I am greatly indebted to her for sharing with me all the troubles in these years. I'd love to thank my son, Mohammad-Mahdi and my daughter Mina for contributing to love and affection in the family. I wish there was a way to split and share my degree with them.

I 'd like to thank Professor Andrew Hrymak for his sharp, bitter and constant criticism throughout this study. I also wish to thank Professor John Vlachopolous for accepting me one of his last few students on his way to retirement. I am very grateful to Dr. Philip Wood for his patience in listening to me and for his precious advice. I am very thankful to Dr. Mark Hattan for his great help in a crucial moment of my Ph.D. that I shall never forget.

I am very grateful to the Ministry of Culture and Higher Education in Islamic Republic of Iran, for their generous financial support. I hope I can be useful for my country, as well.

Apart from the people mentioned above there is an army of people that I am very thankful for their help, kindness and thoughtfulness. This includes but is not limited to;

- My teachers from primary to high school and university
- Friends in the CAPPA-D group; Shawn, Andrew, Vassilis, Mariana, Victor, Alberto, Alex, ...
- Mr. Mark Hollomby and Mr.Fred Kus who helped me with problems with computers
- Department's staff; Barbera, Loura and Sara
- Many more people that I should recall but I do not, and I deeply regret.

TABLE OF CONTENTS

LIST OF FIGURES

LIST OF TABLES

LIST OF SYMBOLS

A: arbitrary tensor

C: Cauchy-Green strain tensor, stiffness matrix component

D: width of the duct

De: Deborah number

G: relaxation modulus

H: height

I: first invariant

II: second invariant

K: stiffness matrix component

L: length

N : interpolation function

N_1: first normal stress difference

N_2: second normal stress difference

P: pressure

Q: flow-rate

Re: Reynold number

S: deformation dependent tensor

T: stress (tensor)

V: velocity (tensor)

Wi: Weissenberg number

a: parameter

f: function

m: memory function

n: power-law index, stage number

p: pressure

t: time

tr: trace

u: velocity in x direction

v: velocity in y direction

w: velocity in z direction

x: flow direction

y: width direction

z: height direction

∇: gradient operator

Ψ: normal stress difference coefficient

α: parameter, relaxation factor

β: ratio of solvent viscosity to solution viscosity

ε: material constant in viscoelastic model, tolerance

ϕ: arbitrary function

γ: strain

$\dot{\gamma}$: shear rate

η: viscosity

μ: viscosity coefficient

ρ: density

ζ: material constant in viscoelastic model

Superscripts

^{c}: corrected values

^{p}: related to pressure

^{T}: Transpose

^{x}: in x direction

*: known values

$^{\sim}$: approximation

Subscript

$_{av}$: average

$_{p}$: related to pressure/polymer

$_{sl}$: related to slip

$_{s}$: related to solvent

$_{w}$: wall

$_{\infty}$: infinite

$_{o}$: Zero (zero shear)

Chapter 1

Introduction

Polymer melts and solutions often behave drastically differently from Newtonian fluids. These behaviors include rod climbing in a mixer, large vortices in velocity fields near a sudden contraction, vortex inhibition in a mixing tank, die swell and many more as collected by Bird et al. (1987).

The cause of these types of behavior is attributed to the viscoelastic nature of the fluids, resulting in a departure from a purely viscous behavior and approaching solid-like, elastic behavior. Viscoelastic behavior has been attributed to the long chain structure of the polymer molecules.

There is an increasing need to analyze the flow of viscoelastic fluids in simple and complex geometries in order to understand and predict polymer behavior. It is often

necessary to model a three-dimensional flow of a viscoelastic fluid to provide an accurate picture of the state of the velocity and stress components. Knowledge of the velocity and stress field in a viscoelastic flow helps to design better products (by reducing frozen stresses for example) or tools (e.g. dies) that can increase the rate of production.

Modeling of three-dimensional flow of a viscoelastic fluid in simple or complex geometries has been a challenge for many years. This is because of a number of problems, including the large number of variables due to the inclusion of viscoelastic stress components as well as the large number of grid points required to produce meaningful results. There is uncertainty about the validity of the constitutive equations and boundary conditions of 3-D viscoelastic flows. The incorporation of viscoelastic constitutive equations usually results in convergence difficulties in numerical analysis of the flow. This study proposes a method to model the three-dimensional flow of a viscoelastic fluid in simple and complex geometries, considering reduction in time and storage requirements and addressing the outlet boundary conditions.

1.1- Thesis outline

This chapter includes a review of constitutive equations which are used to describe the stresses resulting from the deformation of the polymer in the flow field and are in fact the source of the complexity in the analysis of the viscoelastic flow. This

review is followed by a literature summary of different problems and various approaches to numerical analysis of viscoelastic flow. This chapter also includes a review on the secondary flows of the viscoelastic fluids in non-circular straight ducts.

The primary task in modeling 3-D flow is to find an appropriate formulation and algorithm that is most efficient in terms of computational storage and speed for the numerical solution. Addition of another dimension to the flow model can easily increase the number of unknowns by an order of magnitude. Therefore, it is absolutely essential to find an appropriate method that solves the problem more efficiently in terms of memory requirements and speed. Another problem to be addressed is the definition of the inlet and outlet boundary conditions for the 3-D analysis of viscoelastic fluids. In order to address these concerns (efficiency and boundary conditions) a marching method based on a parabolic formulation of the flow was examined. This formulation results in reducing a 3-D problem to a series of planar (2-D) problems in the direction of the flow and the elimination of the need for exit boundary conditions. This formulation is based on a segregated strategy for solving the governing equations of the flow. In segregated methods, flow variables are analyzed separately and equations for each variable are solved one at a time. This results in a dramatic reduction in the size of the problem and memory requirement. However, the marching method fails in analysis of the flow in complex geometries, and for this reason the marching method was abandoned. The

assumptions and algorithm for this formulation along with its results, problems and, drawbacks are discussed in Appendix A.

In Chapter Two, the 3-D algorithm based on creeping flow formulation, EVSS (Elastic Viscous Split Stress) method to decouple the elastic stresses, and equations of the stress for MPTT (Modified Phan-Thien Tanner) constitutive equation are described. A segregated method is applied to the creeping flow of a generalized Newtonian fluid and compared to a non-segregated, fully-coupled formulation.

In Chapter Three, the 2.5-D algorithm to analyze the fully developed flow of a viscoelastic fluid in a duct is fully described. The results from the 2.5-D analysis is verified for mesh independence and compared to the results from the literature. This chapter also includes new results on the effect of the flow parameters on the intensity and pattern of the secondary flows.

In Chapter Four, results of the 3-D analysis of viscoelastic flow in a straight duct is presented. The results from a 3-D analysis is compared with results from 2.5-D analysis. The 3-D analysis produces the same vortex pattern as the 2.5-D analysis for the secondary flows in major part of the domain. However, the vortex pattern collapses near the outlet. This problem occurs for various inlet boundary conditions, duct lengths and

mesh densities. The source of the problem at the outlet is addressed and modifications to the algorithm are suggested.

In Chapter Five, results of the application of the fully segregated 3-D algorithm in modeling the flow in a converging duct and a sudden contraction are presented. Results from the 3-D analysis are compared with a 2-D analysis and experimental results from the literature.

1.2- Constitutive equations

A flow analysis includes the solution of the conservation equations (mass and momentum) and a constitutive equation that describes the fluid response to any imposed stress or deformation. For a Newtonian fluid, the stress resulting from the deformation of the fluid in the flow field is described in a simple form, using one parameter.

$$T = \eta_o \dot{\gamma} \qquad (1.1)$$

Where T is the stress tensor, and η_o is the viscosity of the fluid. $\dot{\gamma}$ is the rate of deformation tensor defined as

$$\dot{\gamma} = \nabla V + \nabla V^T \qquad (1.2)$$

where V is the velocity vector, and superscript ^{T} denotes the transpose of a tensor.

Polymers have a complex response when subjected to a stress. When polymers are placed under load in shear or extension, an immediate deformation occurs. The initial deformation is followed by a continuous deformation, which is called creep. This time-dependent response is a manifestation of viscoelasticity. It can also be demonstrated that if a piece of polymer or polymeric liquid is subjected to a sudden increase in strain, the stress that is required to maintain that strain relaxes (Macosko, 1994). The relaxation modulus is defined as

$$G(t) = \frac{T(t)}{\gamma} \tag{1.3}$$

where γ is strain. At short times, the relaxation modulus approaches a constant value for polymers. This linear dependence of stress relaxation on strain is called linear viscoelasticity (Macosko, 1994). As the deformation increases, the relaxation modulus becomes

$$G(t,\gamma) = \frac{T(t,\gamma)}{\gamma} \tag{1.4}$$

When the relaxation modulus depends on time and strain it is called non-linear viscoelastic behavior.

Viscoelasticity is associated with some nonlinear behavior that a viscoelastic constitutive equation must be able to describe. These nonlinear phenomena include shear-thinning, appearance of normal stress differences, extensional thickening and time-

dependence of rheological material functions. The simplest group of models for describing polymer behavior is the one that only describes the shear-thinning and is called the generalized Newtonian constitutive equation. Generalized Newtonian constitutive equations consider the viscosity to be a function of shear rate rather than having a constant value as for Newtonian fluids. For an arbitrary shearing flow of an incompressible fluid, the viscosity (η) maybe described as

$$\eta = f(|\dot{\gamma}|) \tag{1.5}$$

Where $|\dot{\gamma}|$ is the magnitude of $\dot{\gamma}$ defined as the square root of half of the second invariant of the strain rate tensor

$$|\dot{\gamma}| = \sqrt{\frac{1}{2}\sum_i \sum_j \dot{\gamma}_{ij}\dot{\gamma}_{ji}} \tag{1.6}$$

With $\dot{\gamma}_{ij}$ being the components of the rate of deformation tensor from equation 1.2.

There are several models to describe the shear dependence of polymer melts. The simplest model is the power-law model where the viscosity is defined as

$$\eta = m|\dot{\gamma}|^{n-1} \tag{1.7}$$

where m is the consistency index and n is the power-law exponent. If $n<1$ the fluid is called pseudoplastic or shear thinning, and if $n>1$ the fluid is called dilatant or shear thickening. A typical range of n for polymer melts is between 0.15 and 0.6. The power-

law model does not describe the viscosity curve near $|\dot{\gamma}| = 0$, as η goes to zero, which may cause some problems in numerical solutions.

Another model that describes the shear dependence of the fluids is Carreau-Yasuda model. The Carreau-Yasuda model is defined (Bird et al, 1987) as:

$$\frac{\eta - \eta_\infty}{\eta_0 - \eta_\infty} = \left[1 + (\lambda|\dot{\gamma}|)^a\right]^{n-1/a} \qquad (1.8)$$

where η_o is zero shear rate viscosity, η_∞ is the infinite shear rate viscosity, λ is the time constant, and n is the power-law exponent. The dimensionless parameter, a, describes the transition region between zero shear rate and the power law regions (usually a=2, and in this case the model is called the Carreau model).

For steady state shear flow of the polymers, where elastic properties are not important, the generalized Newtonian constitutive equations can be used for design and engineering purposes. In these cases, the most important rheological characteristic of polymer melts is their shear rate dependent viscosity.

1.2.1-Viscoelastic constitutive equations

The general, linear, viscoelastic constitutive equation is the simplest expression of viscoelasticity that can describe some time-dependent behavior of viscoelastic fluids in

the flow field. General linear viscoelastic constitutive equations can be applied when the fluid does not move very far (or very fast) from its initial configuration. The Maxwell model is the basic model in this class and can be derived based on the concept of a spring (Hooke's law) and dash-pot (Newton's law)

$$T + \lambda_o \frac{\partial T}{\partial t} = -\eta_o \dot{\gamma} \qquad (1.9)$$

where λ_o is a time constant. For the case of steady state flow where there is no change of stress in time, equation (1.9) predicts Newtonian behavior. For a rapidly changing stress, the time derivative dominates the left hand side of the equation resulting in Hookean behavior. λ_o is a time constant which determines the stress rate that is required to show Hookean behavior of the fluid. Equation (1.9) can be written in integral form as:

$$T(t) = \int_{-\infty}^{t} [\frac{\eta_o}{\lambda_o^2} \exp((t'-t)/\lambda_o)]\gamma(t')dt' \qquad (1.10)$$

where γ is the state of the fluid when $t'=t$. The quantity in the square braces is called the memory function, representing the notion of fading memory in viscoelastic fluids. Fading memory of the fluid means that deformations experienced by the fluid element in the recent past have a larger effect on the present state of stress in the fluid than the deformations experienced in the distant past.

The major drawback of the Maxwell constitutive equation is that the stress prediction depends on the frames of reference. To overcome this problem, constitutive equations based on other frames of reference have been developed. One of these frame of

reference is called corotating coordinates. The corotating coordinates base vectors stretch and rotate with material lines. The simplest constitutive equation, based on a corotating frame of reference is the second order fluid described as:

$$T = -pI + \eta_o \dot{\gamma} + \frac{1}{2}\Psi_{1,o}\overset{\nabla}{\dot{\gamma}} + \Psi_{2,o}\dot{\gamma}\cdot\dot{\gamma} \qquad (1.11)$$

where $\Psi_{1,o}$ and $\Psi_{2,o}$ are the first and second normal stress coefficients at zero shear rate. Ψ_1 and Ψ_2 are defined in terms of normal stress differences N_1 and N_2 as follows

$$\Psi_1 = \frac{N_1}{\dot{\gamma}^2} = \frac{T_{xx} - T_{yy}}{\dot{\gamma}^2} \qquad (1.12)$$

$$\Psi_2 = \frac{N_2}{\dot{\gamma}^2} = \frac{T_{yy} - T_{zz}}{\dot{\gamma}^2} \qquad (1.13)$$

where T_{xx}, T_{yy} and T_{zz} are the normal stresses in the direction of the flow, normal to the shearing plane and the neutral direction, respectively.

Figure 1-1: Demonstration of normal stress components

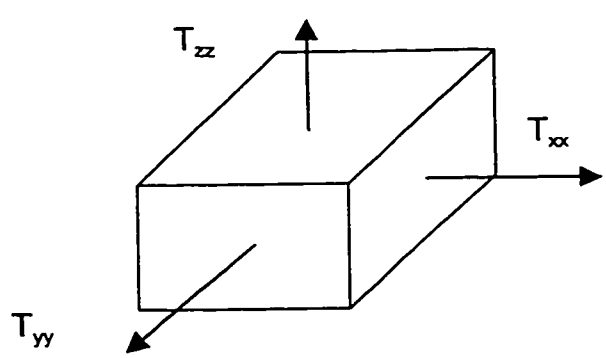

The upper-convected derivative of the rate of strain tensor is defined for an arbitrary tensor A as

$$\overset{\nabla}{A} = \dot{A} - (\nabla V)^T \cdot A - A \cdot \nabla V \qquad (1.14)$$

$$\dot{A} = \frac{\partial}{\partial t} A + V \cdot \nabla A \tag{1.15}$$

It can be shown that for a slowly varying flow (i.e. retarded motion expansion) a viscoelastic fluid can be described by equation (1.11). For example, in a shear flow equation (1.11) holds if the flow is so slow that coefficients in the equation do not depart from their low shear rate values (i.e. no shear-thinning). The second-order fluid constitutive equation can be made applicable to polymer melts by modifying its coefficients (η_o, $\Psi_{1,o}$, $\Psi_{2,o}$ defined for the limiting low shear rate values) to shear dependent coefficients. The resulting constitutive equation is called the Criminale-Erickson-Filbey (CEF) constitutive equation and is applicable to steady shearing flows (Bird, 1987)

$$T = \eta\dot{\gamma} + \frac{1}{2}\Psi_1 \overset{\nabla}{\dot{\gamma}} + \Psi_2 \dot{\gamma} \cdot \dot{\gamma} \tag{1.16}$$

The CEF equation is not able to capture any time-dependent viscoelastic behavior.

Using a corotational frame of reference and an upper-convected time derivative the Maxwell model can be modified to the upper-convected Maxwell (UCM) model that predicts time-dependent behavior of viscoelastic fluids.

$$T + \lambda_o \overset{\nabla}{T} = -\eta_o \dot{\gamma} \tag{1.17}$$

Many sophisticated constitutive equations of Maxwell type have been developed that can capture one or two nonlinear phenomena associated with viscoelasticity. These may be described (Macosko, 1994) in the general form:

$$\overset{\nabla}{T} + f_c(T, \frac{\dot{\gamma}}{2}) + \frac{1}{\lambda}T + f_d(T) = G\dot{\gamma} \qquad (1.18)$$

where f_c modifies the rate of stress build-up and f_d modifies the rate of stress decay. In Table 1-1, a few differential constitutive equations based on equation (1.18) are presented.

Table 1-1: Maxwell type constitutive equations for viscoelastic fluids

Model	f_c	f_d	Parameters
White - Metzner (1977)	$f_c = a(\frac{1}{2}\dot{\gamma} : \dot{\gamma})$	–	a
Larson (1984)	$f_c = \frac{\alpha}{3G}\dot{\gamma} : T(T + GI)$	–	α, G
Geisekus (1982)	–	$f_d = \frac{\alpha}{\lambda G}T \cdot T$	α, λ, G
Phan-Thien Tanner (1977, 1978)	$f_c = \frac{\zeta}{2}(\dot{\gamma} \cdot T + T \cdot \dot{\gamma})$	$f_d = \frac{1}{\lambda}(1 + \frac{\varepsilon}{G}tr(T))(T - I)$	ε, λ, ζ, G

The White-Metzner constitutive equation is a relatively simple model but it fits the data poorly from a step shear test, and does not predict the second normal stress

differences (Ψ_2=0). The Larson model works reasonably well with different types of flow, but it predicts a zero second normal stress difference.

The Geisekus model is excellent in modeling shear flows. However, it is not the best one for extensional flows as it occurs in flow through complex geometries (Macosko, 1994) . The Phan-Thien Tanner (PTT) constitutive equation works reasonably well for different types of the flow, except in the start-up of steady shearing flow. The modified Phan-Thien Tanner (MPTT) model is obtained from the PTT model by the following modification.

$$G = \mu G_o \tag{1.19}$$

$$\mu = \frac{1+\zeta(2-\zeta)\lambda^2\dot{\gamma}^2}{(1+\Gamma^2\dot{\gamma}^2)^{(1-n)/2}} \tag{1.20}$$

where n and Γ are new parameters.

Differential constitutive equations can be stated in a more general form of multi-mode constitutive equations as follows.

$$T = \sum_{i=1}^{m} T_i \tag{1.21}$$

where m is the number of modes and i refers to the contribution of each mode to that stress component. That is to say that polymer response is the sum of the responses from different molecules with different properties. Considering more parameters results in better fit and better prediction of viscoelastic properties.

The selection of an appropriate constitutive equation is the first step in the modeling of viscoelastic flow. It is important to note there is no constitutive equation that is best from all aspects. Appropriate models are selected based on the type of the flow. In this study, the Modified Phan-Thien Tanner constitutive equation has been selected, and will be fully described in Chapter Two. This model predicts a non-zero second normal stress coefficient, which is the main factor in ensuing secondary flows in flow of viscoelastic fluid in straight ducts. It also works reasonably well for the extensional flow, which is important in modeling complex geometries. Its weakness is in the case of start-up flows, which is not of interest in this study.

1.3- Numerical analysis of viscoelastic flows

After selecting a suitable constitutive equation, the second challenge is to solve the set of governing equations, which include the mass and momentum conservation equations. The success of this step depends on many factors, some of which are discussed here.

There are two main approaches in solving the set of governing equations for viscoelastic flow. In a coupled method, the conservation equations and the viscoelastic constitutive equation are solved simultaneously. In a decoupled method, the calculation of the viscoelastic extra stress is done separately based on previously known kinematics

of the flow. Kinematics of the flow is obtained from the solution of an elliptic Newtonian like flow where viscoelastic stresses are treated as a known body-force term. Since calculation of the viscoelastic stresses are done separately, special techniques can be used for calculation of the stresses.

There are also two methods used to calculate the viscoelastic extra stress. One is to use a discretized method to calculate the stress components at grid points. The other is to integrate the constitutive equation along a streamline (Luo and Tanner,1986,1989). Both methods can be used with both types of constitutive equations (i.e. differential and integral). The streamwise integration method faces convergence difficulties in cases such as flow in a sudden contraction where longitudinal vortices appear (Keunings 1989).

The speed of calculation for each of these methods very much depends on the type and size of the problems. In each of these approaches, discretization techniques based on finite element, boundary element, finite difference and finite volume methods have been used; however, it should be noted that most published simulations have been done using finite element techniques (Keunings, 1989).

Based on different assumptions and approaches, different mathematical formulations of the problem may be used. Formulation of the problem also depends on the mathematical nature of the equations and the mathematical behavior of the equations

is influenced by the elastic nature of the flow. The elastic character of the flow is usually quantified by Wi (Weissenberg number) or De (Deborah number). Wi is defined as

$$Wi = \frac{\lambda u^{*}}{L^{*}} \tag{1.22}$$

where λ is the time constant of the fluid and, u^{*} and L^{*} are characteristic velocity and length scales for the flow. Deborah number is defined in terms of λ and characteristic shear rate of the flow (γ^{*}) as;

$$De = \lambda\gamma^{*} \tag{1.23}$$

In the study of viscoelastic flow it has been observed that as Wi increases numerical computations fail to converge. This problem has been attributed to the irregular points in the solution domain. The occurrence of irregular points in the solution may have a mathematical or numerical origin. Mathematically speaking, the behavior of the solution in terms of Wi may be classified within the following five classes (Keunings 1989).

1- Smooth solution with no irregular points as Wi increases. It has been observed that even in this case, Picard type solvers used in decoupled methods failed to converge. This could be attributed to the excessive numerical errors that can easily occur in the solution of the viscoelastic flow. The underlying cause for such errors could be the severe non-linearity that arises from increasing Wi.

2- Smooth solution everywhere but at one point ($Wi = Wi_{crit}$). The solution is well behaved before and after the critical point. For this case, it is very well possible that such a critical point is reached locally and results in failure of the solution.

3- Smooth solution up to the point $Wi = Wi_{crit}$ where upon the solution abruptly terminates. This can happen as a local loss of solution that results in the divergence of the numerical solution.

4- Presence of a turning point, which implies the multiplicity of the solution for some $Wi < Wi_{crit}$.

5- Presence of bifurcation point which implies multiplicity of the solution after $Wi > Wi_{crit}$. Turning points and bifurcation points may result in unstable solutions and for Picard type iterative methods may result in divergence. For the coupled methods, these points may be discovered and avoided locally.

Irregular points appear in the solution of viscoelastic flows due to the presence of boundary layers or singularities in the velocity and stress field. One of the cases involving a singularity is the flow through a sudden contraction. Several methods have been suggested to deal with the problem of a singular point in the case of a sudden

contraction. These methods include the introduction of a slip boundary condition at the corner and/or modifying the sharp corner to a curved corner (Brown et al. 1986). However, even with those considerations the solution seems to have a turning point in terms of Wi.

Another source of problem in the solution of viscoelastic fluid flow is the hyperbolic nature of the set of governing equations that results from the introduction of a viscoelastic constitutive equation. The hyperbolic nature of the equations along with the presence of irregular points could result in oscillatory results in the solution field. The hyperbolic nature of the equations may also result in loss of evolution. Loss of evolution is an instability in which short wave disturbances increase in amplitude. Furthermore, it has been shown (Joseph et al. 1985) that the set of governing equations is of a mixed type, meaning that the system is never strictly elliptic or hyperbolic. This means that the set of equations may change type either in a global or local sense depending on the flow and fluid parameters. Change of type and loss of evolution cannot occur when a constitutive equation contains a Newtonian component (Keunings, 1989).

Another challenge in modeling viscoelastic flows lies in specifying appropriate boundary conditions. Because of the fluid memory, it is difficult to specify the state of the fluid at the entrance plane because this requires information about the state of the flow prior to entrance. It is also difficult to specify boundary conditions at the exit plane

after experiencing deformations in the flow domain, because it is not known how the flow domain affects the fluid behavior. In practice, no flow pre-history (deformation history experienced by fluid before entering) is assumed based on fully developed flow upstream.

A second difficulty arises in applying boundary conditions at the solid boundaries. Unlike the case of Newtonian fluids, the no-slip condition at the wall is not necessarily true in polymers (Hatzikiriakos et al, 1991, 1992). Different slip models have been proposed (Dussan et al. 1974; Hill et al. 1990; Denn, 1992). The linear slip model for one-dimensional movements can be demonstrated as follows:

$$u_{sl} = \beta_{sl} T_w \qquad (1.24)$$

where u_{sl} is the slip velocity at the solid boundary, β_{sl} is the slip constant and T_w is the shear stress at the wall.

Finally it must be pointed out that no mathematical substantiation for the existence or uniqueness of solutions for viscoelastic flows has yet been found (Keunings, 1989). Therefore the set of governing equations including conservation equations and viscoelastic constitutive equation does not necessarily have a unique solution if a solution at all.

1.4- Secondary flows of viscoelastic fluids

It has long been established that flow of viscoelastic fluids in non-circular ducts involves secondary flows (flows with transverse velocity components normal to the main flow), Langlois et al. (1959,1963) and Langlois (1964). Apart from previous scientific interest in studying secondary flows, recently; the research in this area has been greatly motivated by an increasing demand for a better understanding of polymer melt processing in industry. Polymer melts are good examples of highly elastic materials, and they are processed in conditions where their viscoelastic behavior is important.

Secondary flows have an important effect on mixing and heat transfer in the duct flow of polymer melts and solutions. They also influence the residence time distribution. Another issue is the prediction of the state of the stress that is caused by the viscoelastic nature of the fluid in flow through straight ducts. The stress prediction is used in the estimation of frozen stresses in polymer products resulting from the solidification of polymer melt.

Analysis by Langlois and Rivlin (1963) showed that fully developed flow in non-circular ducts of a fourth order fluid shows a transverse flow that is superimposed on the rectilinear flow, thereby resulting in streamlines that are spirals rather than straight lines. Flow in an elliptical duct was predicted to have four symmetric secondary flow

patterns. In each quadrant, the fluid moves toward the centre along the major axis and toward the wall along the minor axis.

Wheeler and Whistler (1966) used the Reiner-Rivlin constitutive equation with a variable viscosity and a constant normal stress coefficient in a finite difference scheme to simulate the flow in a straight square duct. They assumed the flow to be fully developed and therefore velocity components did not depend on the axial position. They solved the momentum equation in the direction of the flow as a nonlinear Poisson equation and used stream functions to combine the momentum and continuity equations. They found a pattern of eight vortices with two counter-rotating vortices in each symmetric quadrant of the duct.

Dodson et al. (1974) applied the same fully developed assumption but used a more complex constitutive equation. Dodson et al. employed a CEF constitutive equation for their study. For a Reiner-Rivlin fluid, the first normal stress coefficient is zero, while the CEF model has a non-zero first normal stress coefficient. Assuming the second normal stress difference is small, they used N_2 (second normal stress difference) as a perturbation parameter. They expanded the flow variables in powers of N_2 and neglected terms of order $(N_2)^2$ to obtain the velocity components:

$$v = N_2 \frac{\partial \psi_1}{\partial z} \tag{1.25}$$

$$w = -N_2 \frac{\partial \psi_1}{\partial y} \tag{1.26}$$

$$u = u_o(y,z) + N_2 u_1(y,z) \tag{1.27}$$

In which ψ_1 is the secondary flow stream function, v and, w are the transverse velocity components. $u_o(y,z)$ represents the general solution in the absence of secondary flows for the main velocity, and u_1 is an extra component due to the presence of secondary flows. They used a finite difference method to solve equations that are obtained from the perturbation analysis. Dodson et al. (1974) found that the sufficient condition for rectilinear flow is to have N_2 as zero or a constant multiple of η. They also found the eight vortices pattern for square cross-sections and for the rectangular cross-sections with aspect ratios of less than 4/3. They report that the secondary flows change direction if the sign of N_2 changes.

Townsend et al. (1976), used a perturbation analysis with an independent perturbation parameter instead of N_2. They considered N_2 to be a function of shear rate (not constant as in the previous work) resulting in more complicated equations than those of Dodson et al's (1974) work. They found that the functional form of the N_1 also affects the characteristics of the secondary flows and the direction of the secondary flow cannot be considered as a sign test for N_2.

Thangham et al. (1987) used a method similar to that of Wheeler et al. (1966), employing the Maxwell constitutive equation. They also obtained the eight vortices pattern. Their study included an investigation of the effects of Re and Wi number on the intensity of the secondary flows.

Gervang and Larson (1991) used a finite volume formulation to simulate the secondary flow of a CEF fluid in straight ducts. They used a four plane grid with the inlet boundary condition to be a known velocity field (either guessed or obtained from solution at the outlet) and gradients for velocities and pressure in the outwards direction were forced to zero. They investigated several aspect ratios for a straight rectangular duct and obtained the eight vortices pattern for low aspect ratios, with the appearance of a third vortex in each quadrant in higher aspect ratios (1/16 for instance). They found qualitative agreement between their predictions of the magnitude of the secondary flows and their experimental measurements. The quantitative disagreement was attributed to inaccurate measurement of N_2.

More recently, Xue et al. (1995), used a finite volume formulation to study the pattern of secondary flows in a straight rectangular duct, using a one mode MPTT constitutive equation for the fluid. Since the MPTT constitutive equation is not explicit in terms of stress, they used a decoupled scheme. The stress components were calculated from the constitutive equation using the known values of the velocities. Pressure and

velocity components were calculated by solving the equations of momentum and mass conservation. The pressure was decoupled with a pressure drop component in the direction of the flow and another component representing pressure non-uniformity in each cross-section plane. They studied the effects of model parameters for Wi up to 0.135 and found that while the intensity of secondary flows is highly dependent on the viscoelastic material parameters, their pattern did not depend on material parameters. They also studied effects of different aspect ratios on the shape and number of secondary flows. They concluded that in the range of 1 to 16 for the aspect ratio of the rectangular duct, secondary flows have the same pattern of two vortices in each quadrant.

Dooley and Hughes (1995) used a set of experiments to show the effect of viscoelasticity on layer non-uniformity in the flow of polymer melts through ducts. Dooley and Dietsche (1996) used a finite element package (Polyflow) to model the secondary flows using the PTT constitutive equation. The numerical results were dependent on the portion of the viscometric data that were used to obtain the model parameters. There was an order of magnitude difference between predictions that used fitted parameters for shear rates in the range 1-10 (1/sec) compared with others obtained over the range of 10–100 (1/sec).

Torres (1995) used a marching code (see Appendix A) to simulate flow of CEF and MPTT fluids in a straight square duct. In contrast to other theoretical and

experimental work, the results did not produce the previously reported patterns of eight vortices, with the same rheological parameters as in previous work. However, with the assumption that N_2 changes sign as the shear rate changes in the flow domain, the eight vortices pattern was obtained. This assumption is supported by observations made for polymer solutions (Magda et al., 1991, 1993). The algorithm was checked for the case of zero secondary flows and also for different meshes. The pattern of the secondary flows obtained from the CEF and MPTT constitutive equations were consistent with each other but not with the previous studies.

In an attempt to predict layer displacement in coextrusion flows of polymers due to secondary flows, Debbaut et al. (1997) used a finite element method to study different duct cross sections based on the fully developed flow assumption. They used a five-mode Geisekus constitutive equation to predict the displacement of the particles from inlet to different length in the duct. They also performed an experimental study on the layer distortion of the polymer and compared it with numerical results. While there was generally good agreement between the results (prediction and observation of the interface), they concluded that as the flow progresses the difference between prediction of the interface and observations grows.

1.5 - Concluding remarks

In this chapter, viscoelastic fluid concepts were introduced and some equations that have been proposed for characterizing such fluids were reviewed. Nonlinear phenomena associated with viscoelasticity were also mentioned, indicating the complexity of the viscoelastic flow. The first issue is therefore finding an appropriate description of the fluid behavior in the flow domain that involves both choosing a suitable constitutive equation and finding the correct parameters for that model. Finding the parameters becomes more difficult as the models become more complex and have more parameters.

One of the viscoelasticity-related phenomena that has been observed and studied, is the presence of secondary flows in flows of viscoelastic fluids through straight non-circular ducts. From an analytical point of view, studies of secondary flows in 3-D straight ducts constitutes a good test problem for evaluating 3-D algorithms, as this flow field does not contain any of the complexities that are involved in flow in other geometries.

In section 1.3, some of the difficulties that arise in the analysis of viscoelastic flows were reviewed. Due to the number of difficulties in analysis of visoelastic flow, most of the studies in this area have been focused on 2-D analysis of the flow. While 2-D

analysis of the flow is helpful in evaluating different methods or different constitutive equations, it is obvious that the assumption of planar flow in complex geometries is unrealistic. Seeking a 3-D algorithm to analyze viscoelastic flow is a natural step toward achieving a better understanding of the viscoelastic flow. Ultimately, reliable quantitative assessment of the flow in real geometries hinges on a 3-D analysis using an accurate constitutive equation.

This study seeks to find an appropriate 3-D algorithm for modeling viscoelastic flow with special attention to saving memory and time in the calculations, and the problem of the outlet boundary condition. In the next chapter, a 3-D algorithm is presented that is based on the creeping flow formulation.

Chapter 2

Fully Segregated Algorithm for 3-D Analysis of Viscoelastic Flow

The purpose of this chapter is to describe the 3-D segregated algorithm that was used for the analysis of viscoleastic flow in this study. The first part of this chapter describes the segregated method used to solve creeping flow of a generalized Newtonian fluid. It also includes the study of convergence of the method and a comparison of its speed with that of the fully coupled method.

In the second part of this chapter, the EVSS (Elastic Viscous Split Stress) method, used to decouple the elastic component of the stresses and equations for stress components from the MPTT (Modified Phan-Thien Tanner) constitutive equation, is described.

2.1- Segregated method for creeping flow

In a fully coupled formulation, all of the algebraic equations resulting from the discretization of the flow equations are assembled, to form a global system of equations. Solving these equations gives the simultaneous values for all nodal unknowns (i.e. u, v, w and p). In a segregated formulation, the global system of discretized equations is never fully assembled, instead one or some of the variables (but not all of them) are calculated one step at a time, on the entire mesh. The other variables are treated as temporarily "known". These methods save memory and could also result in faster calculations for denser meshes. This makes these methods promising for solving 3-D viscoelastic flow problems.

The application of three different segregated methods, as proposed by Haroutunian et al. (1993), to the analysis of creeping flow was investigated. These algorithms are denoted as Pressure Correction (PC), Pressure Projection (PP), and Pressure Update (PU). Only the application of the PC method resulted in convergence. The formulation of the problem and the PC algorithm, as well as some modifications that were made to improve the algorithm in terms of speed and convergence are discussed. The accuracy and performance of the PC algorithm, was compared against the fully coupled method developed by Bravo (1998).

2.1.1- Pressure correction algorithm

The creeping flow formulation is obtained from the Navier-Stokes equations by assuming Re=0, resulting in the following set of linear second order differential equations.

$$\frac{\partial^2 u}{\partial x^2}+\frac{\partial^2 u}{\partial y^2}+\frac{\partial^2 u}{\partial z^2}=-\frac{\partial p}{\partial x} \qquad (2.1)$$

$$\frac{\partial^2 v}{\partial x^2}+\frac{\partial^2 v}{\partial y^2}+\frac{\partial^2 v}{\partial z^2}=-\frac{\partial p}{\partial y} \qquad (2.2)$$

$$\frac{\partial^2 w}{\partial x^2}+\frac{\partial^2 w}{\partial y^2}+\frac{\partial^2 w}{\partial z^2}=-\frac{\partial p}{\partial z} \qquad (2.3)$$

Equations 2.1 to 2.3 have been made dimensionless, by considering the average velocity (u_{av}) and the width of the duct (D) as velocity and length scales. Pressure (p') is made dimensionless using

$$p = p'D/\eta_o\, u_{av} \qquad (2.4)$$

The creeping flow formulation has been successfully applied in modeling low Re (Re→ 0) flows such as polymer melt flows, both, in simple and complex geometries.

The structure of the global equation system that results from the application of the Galerkin finite element method to the equations of momentum and continuity can be stated as follows (Reddy, 1984; Burnett, 1987):

$$\begin{bmatrix} K_{uu} & K_{uv} & K_{uw} & -C_x \\ K_{vu} & K_{vv} & K_{vw} & -C_y \\ K_{wu} & K_{wv} & K_{ww} & -C_z \\ C_x^T & C_y^T & C_z^T & 0 \end{bmatrix} \begin{bmatrix} u \\ v \\ w \\ p \end{bmatrix} = \begin{bmatrix} 0 \\ 0 \\ 0 \\ 0 \end{bmatrix} \tag{2.5}$$

$$K_{uu} = K_u = \int_{\Omega_e} (2\frac{\partial N_i}{\partial x}\frac{\partial N_j}{\partial x} + \frac{\partial N_i}{\partial y}\frac{\partial N_j}{\partial y} + \frac{\partial N_i}{\partial z}\frac{\partial N_j}{\partial z})d\Omega \tag{2.6}$$

$$K_{vv} = K_v = \int_{\Omega_e} (\frac{\partial N_i}{\partial x}\frac{\partial N_j}{\partial x} + 2\frac{\partial N_i}{\partial y}\frac{\partial N_j}{\partial y} + \frac{\partial N_i}{\partial z}\frac{\partial N_j}{\partial z})d\Omega \tag{2.7}$$

$$K_{ww} = K_w = \int_{\Omega_e} (\frac{\partial N_i}{\partial x}\frac{\partial N_j}{\partial x} + \frac{\partial N_i}{\partial y}\frac{\partial N_j}{\partial y} + 2\frac{\partial N_i}{\partial z}\frac{\partial N_j}{\partial z})d\Omega \tag{2.8}$$

$$K_{uv} = \int_{\Omega_e} (\frac{\partial N_i}{\partial y}\frac{\partial N_j}{\partial x})d\Omega \tag{2.9}$$

$$K_{uw} = \int_{\Omega_e} (\frac{\partial N_i}{\partial z}\frac{\partial N_j}{\partial x})d\Omega \tag{2.10}$$

$$K_{vu} = \int_{\Omega_e} (\frac{\partial N_i}{\partial x}\frac{\partial N_j}{\partial y})d\Omega \tag{2.11}$$

$$K_{vw} = \int_{\Omega_e} (\frac{\partial N_i}{\partial z}\frac{\partial N_j}{\partial y})d\Omega \tag{2.12}$$

$$K_{wu} = \int_{\Omega_e} (\frac{\partial N_i}{\partial x}\frac{\partial N_j}{\partial z})d\Omega \tag{2.13}$$

$$K_{wv} = \int_{\Omega_e} (\frac{\partial N_i}{\partial y}\frac{\partial N_j}{\partial z})d\Omega \tag{2.14}$$

$$C_x = \int_{\Omega_e} \frac{\partial N_i^p}{\partial x} N_j d\Omega \tag{2.15}$$

$$C_x^T = \int_{\Omega_e} N_i \frac{\partial N_j^p}{\partial x} d\Omega \tag{2.16}$$

$$C_y = \int_{\Omega_e} \frac{\partial N_i^p}{\partial y} N_j d\Omega \tag{2.17}$$

$$C_y^T = \int_{\Omega_e} N_i \frac{\partial N_j^p}{\partial y} d\Omega \tag{2.18}$$

$$C_z = \int_{\Omega_e} \frac{\partial N_i^p}{\partial z} N_j d\Omega \tag{2.19}$$

$$C_z^T = \int_{\Omega_e} N_i \frac{\partial N_j^p}{\partial z} d\Omega \tag{2.20}$$

where **N** is the interpolation function for velocity and $\mathbf{N^P}$ is the interpolation function for pressure. Using the terms defined above, the algorithmic steps can be described as follows (Haroutunian et al., (1993)):

1- Find the pressure correction from the following simplified consistent pressure equation (SCPE), using known values of u^i, v^i and w^i (either guessed or calculated in the previous iteration). Superscript "i" denotes the number of iterartion.

$$\left[C_x^T(\tilde{K}_u^*)^{-1}C_x + C_y^T(\tilde{K}_v^*)^{-1}C_y + C_z^T(\tilde{K}_w^*)^{-1}C_z\right]\Delta p^{i+1/2} = -C_x^T u^i - C_y^T v^i - C_z^T w^i \tag{2.21}$$

where ~ denotes an approximation to K, and * denotes an expression involving the latest available field data. Any approximations for $\tilde{K}^*$ that results in a diagonal matrix,

including the identity matrix, can be used. It is important to have a diagonal matrix since it is easy to invert. One of the approximations is to sum up all the K values in the row to make a diagonal matrix $\tilde{K}$;

$$(\tilde{K}_u)_{ii} = \sum_e \sum_j |(K_u)_{ij}| \tag{2.22}$$

$$(\tilde{K}_v)_{ii} = \sum_e \sum_j |(K_v)_{ij}| \tag{2.23}$$

$$(\tilde{K}_w)_{ii} = \sum_e \sum_j |(K_w)_{ij}| \tag{2.24}$$

where $\sum_e$ is a sum or assembly of element-level contributions.

2- Using the pressure correction, mass-adjust the velocity field and update pressure.

$$u^{i+1/2} = u^i + (\tilde{K}_u^{-1}) * C_x \Delta p^{i+1/2} \tag{2.25}$$

$$v^{i+1/2} = v^i + (\tilde{K}_v^{-1}) * C_y \Delta p^{i+1/2} \tag{2.26}$$

$$w^{i+1/2} = w^i + (\tilde{K}_w^{-1}) * C_z \Delta p^{i+1/2} \tag{2.27}$$

$$p^{i+1} = p^i + (1-\alpha_p)\Delta p^{i+1/2} \tag{2.28}$$

α_p is the relaxation factor for pressure.

3-Solve x-momentum equation for u,

$$\left[\left(\frac{\alpha_u}{1-\alpha_u}\right)\tilde{K}_u + K_u\right]^* u^{i+1} = -K_{uv}^* v^{i+1/2} - K_{uw}^* w^{i+1/2} + C_x p^{i+1} + \left(\frac{\alpha_u}{1-\alpha_u}\right)\tilde{K}_u^* u^{i+1/2} \tag{2.29}$$

4- Solve y-momentum equation for v,

$$\left[\left(\frac{\alpha_v}{1-\alpha_v}\right)\widetilde{K}_v + K_v\right]^{*} v^{i+1} = -K^{*}_{vu}u^{i+1} - K^{*}_{vw}w^{i+1/2} + C_y p^{i+1} + \left(\frac{\alpha_v}{1-\alpha_v}\right)\widetilde{K}^{*}_{v}v^{i+1/2} \qquad (2.30)$$

5- Solve z-momentum equation for w,

$$\left[\left(\frac{\alpha_w}{1-\alpha_w}\right)\widetilde{K}_w + K_w\right]^{*} w^{i+1} = -K^{*}_{wu}u^{i+1} - K^{*}_{wv}v^{i+1} + C_z p^{i+1} + \left(\frac{\alpha_w}{1-\alpha_w}\right)\widetilde{K}^{*}_{w}w^{i+1/2} \qquad (2.31)$$

α_u , α_v, and α_w are the relaxation factors for velocity components u, v, and w. Terms involving α represent implicit preconditioning of momentum equations.

2.1.2- Performance and accuracy of PC algorithm (Newtonian fluid)

The accuracy of the segregated code was investigated by comparing the results with those from a code that uses a fully coupled method for the solution of creeping flow equations. Three meshes (6x2x4, 6x3x6, and 6x4x8 in x, y, and z direction respectively) were used to model one half of a square duct. The length of the duct was L=3D. The tolerance for maximum variation of pressure between two iterations in the segregated code was 10^{-4}. This resulted in an error less than 0.1% in mass conservation. The results for the streamwise velocity component and pressure values of flow of a Newtonian fluid in a square duct, over the whole domain (at all grid points) were compared. Results of the comparison are shown in Table 2-1.

Table 2-1: Comparison between the results from segregated method and fully coupled method

	Difference in u velocity		Difference in pressure	
	Max	Average	Max	Average
Mesh I 6x2x4	0.13%	0.09%	0.33%	0.1%
Mesh II 6x3x6	0.12%	0.07%	0.15%	0.09%
Mesh III 6x4x8	0.14%	0.07%	0.2%	0.078%

The second issue concerned the comparison between the speeds of the two methods. Using the same meshes that were used above both codes were run on the same machine (IBM RS 6000-370). Table 2-2 shows that the segregated method is more efficient in solving problems with denser meshes.

Table 2-2: Comparison between the speed of fully coupled and segregated method (min:sec)

	Fully coupled	Segregated 3D	Degrees of freedom
Mesh I 6x2x4	1:26	8:06	916
Mesh II 6x3x6	33:00	25:20	2236
Mesh III 6x4x8	175:00	117:00	4140

The pressure relaxation factor (α_p) was found to be the single most important parameter that influences the convergence and its speed. The velocity relaxation factors

did not have any effect on the convergence rate. The range of allowable α_p that resulted in convergence depends on the choice of approximation for $\tilde{K}^*$ in the SCPE and the density of the mesh. When the identity matrix was used for $\tilde{K}^*$, relaxation factors as small as α_p=0.75 could be used for coarse meshes (6x2x4). When the other approximations for $\tilde{K}^*$ (summing up all the K values in the row and defining it as the diagonal term) were used, larger relaxation factors had to be used. For a coarse mesh (6x2x4) the smallest α_p that could be used was 0.92. Finer meshes required larger relaxation factors. The number of iterations and the corresponding α_p has been shown in the following table for three meshes (6x2x4, 6x3x6, 6x4x8).

Table 2-3: Effects of the mesh and relaxation factor on number of iterations

	α_p	Number of iterations
Mesh I 6x2x4	0.942	106
Mesh II 6x3x6	0.97	107
Mesh III 6x4x8	0.985	132

Figure 2-1 shows the schematic view of the duct. Typical results for pressure and velocity of are shown in Figures 2-2 to 2-4. Figure 2-2 shows the u-velocity component at the middle of exit plane. Figure 2-3 shows the progress of the u-velocity component along the duct. In Figure 2-4 progress of the pressure along the duct is shown. All the quantities are reported in dimensionless form.

Figure 2-1: Schematic view of the duct

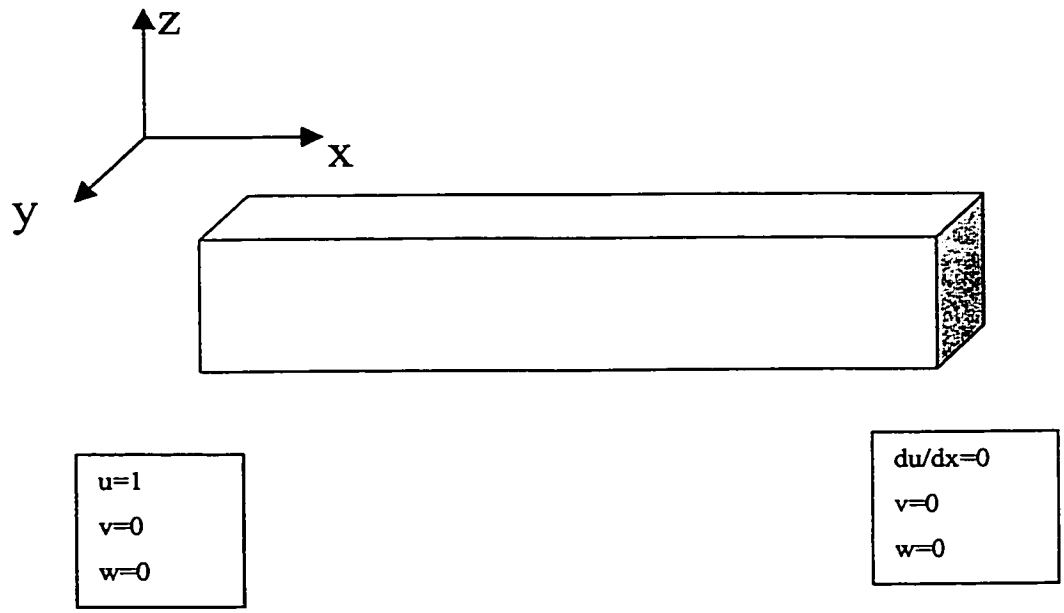

Figure 2-2: u distribution at the exit plane (Newtonian Fluid)

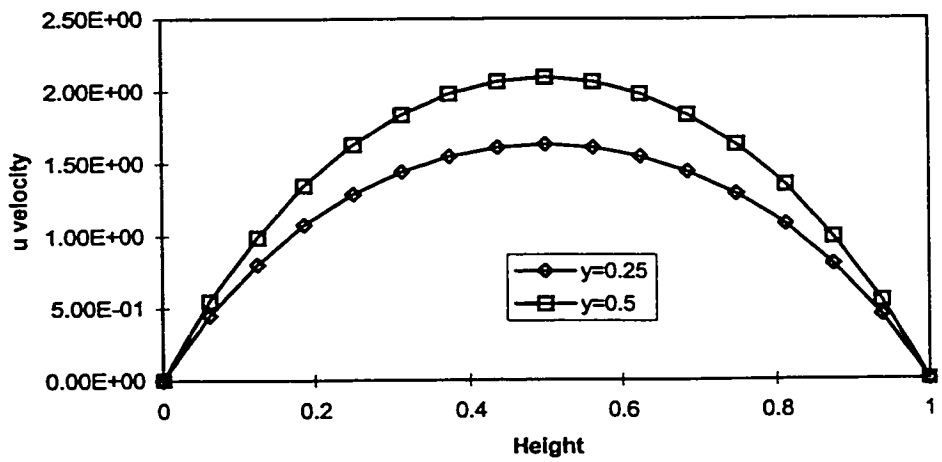

Figure 2-3: u velocity distribution along the duct (Newtonian fluid)

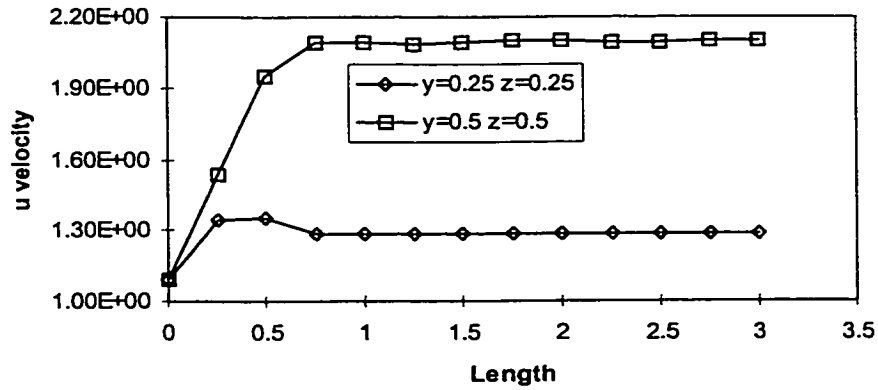

Figure 2-4: Pressure distribution along the duct (Newtonian fluid)

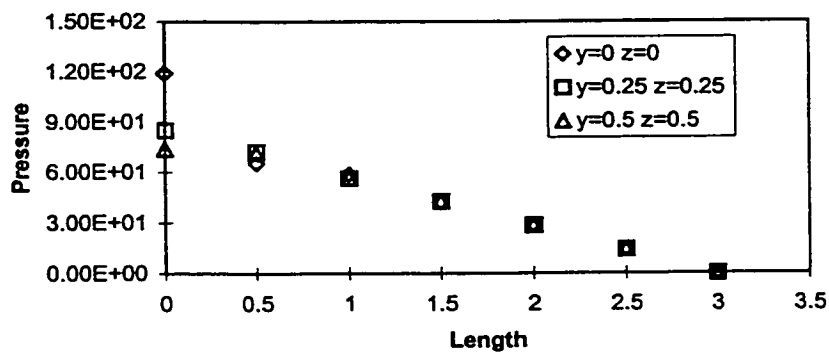

2.1.3- Performance and accuracy of PC algorithm (Carreau Model)

The next stage in evaluating the segregated code was implementing the Carreau model as the constitutive equation representing generalized Newtonian Fluid (GNF). Viscosity is defined by the Carreau model as follows (Bird, 1987):

$$\eta(|\dot{\gamma}|) = \eta_o (1 + (\lambda \cdot |\dot{\gamma}|)^2)^{(n-1)/2} \tag{3.32}$$

where η_0 is the zero shear rate viscosity, λ is a time constant and n is the power-law exponent. Results from fully coupled methods were compared with those of the segregated method using n=0.5 and λ=1.0 (λ becomes dimensionless by dividing by D/u_{av}). The tolerance for maximum variation of pressure between iterations was 10^{-4}. This resulted in less than 0.01% error in continuity. The maximum difference and average difference for the main velocity component and pressure are shown in Table 2-4;

Table 2-4: Comparison between the results from fully coupled and segregated methods for Carreau model (n=0.5, λ=1.0)

	Difference in u velocity		Difference in p	
	Max	Average	Max	Average
Mesh I 6x2x4	9%	0.37%	4%	0.33%
Mesh II 6x3x6	17.5%	0.53%	3.9%	0.28%
Mesh III 6x4x8	23%	0.6%	4.5%	0.27%

The maximum differences for pressure occurred in the first plane and the maximum errors for u-velocity occurred at third plane (x=0.5D) in flow direction (second plane for pressure nodes) and it also increased the average difference. The error was highest near the wall which could have been caused by the unrealistic initial condition of a step profile at the inlet.

The number of iterations and the corresponding relaxation factors for the three meshes are shown Table 2-5.

Table (2-5) : Typical number of iterations for case n=0.5 and λ=1.0

	α_p	Number of iterations
Mesh I 6x2x4	0.95	88
Mesh II 6x3x6	0.98	116
Mesh III 6x4x8	0.98	288

The results of the velocity and pressure distribution are shown in Figures 2-5 to 2-7.

Figure 2-5: u distribution at the exit plane (Carreau model n=0.5, λ=1.0)

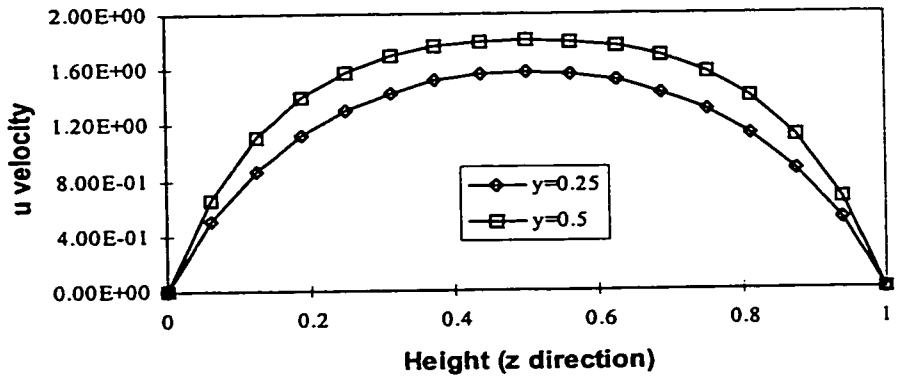

Figure 2-6: u distribution along the duct (Carreau model n=0.5, λ=1.0)

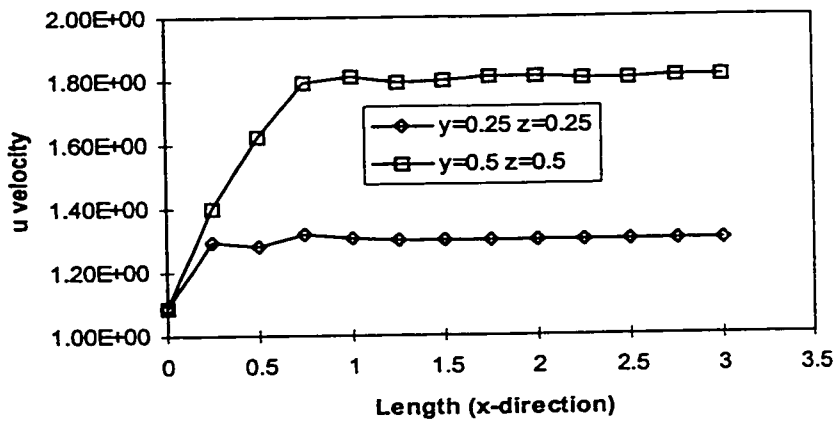

Figure 2-7: Pressure distribution along the duct (Carreau model n=0.5, λ=1.0)

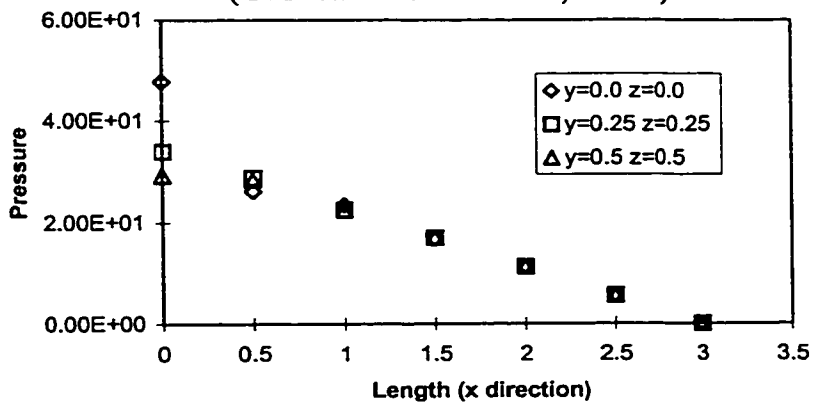

2.1.3- Performance of PC segregated method (Rectangular Duct)

To further verify the performance of the code, half of a rectangular duct with an aspect ratio of 4:1 and L=2D (D is the larger side) was studied. For the Newtonian case, the results of the velocity distribution at the exit plane was compared to the numerical solution of the Poisson equation for a two dimensional problem, and the maximum difference between the numerical predictions of velocity values found to be less than 10^{-3}.

The flow in the rectangular duct was also examined for the non-Newtonian case (Carreau model). It was found that when n becomes smaller than 0.5, convergence becomes difficult. The calculations were expected to be more mesh sensitive because of the non-linearity that is involved in the viscosity. Therefore different meshes were

studied to see if the problem arises from inappropriate element aspect ratios. But this was not the main problem as divergence continued even when using meshes with less than 2:1 aspect ratios.

After extensive, step by step studies on the algorithm it was discovered that the second step (equations 2.25 to 2.27) of the algorithm which provides updates to velocities, was the main cause of the divergence. It was further determined that this step did not have much effect in improving the solution even in the Newtonian case. Removal of velocity update resulted in convergence, while preserving continuity, and, also reduced computational work.

The results for the streamwise velocity component at the exit plane were then compared to the fully developed flow solution and the maximum difference was less than 4×10^{-4}. The mesh for the cross-section of the rectangular duct is shown in Figure 2-8. Results of the velocity and pressure distribution are shown in Figures 2-9 to 2-11.

Figure 2-8 : Mesh for the cross-section of the rectangular duct

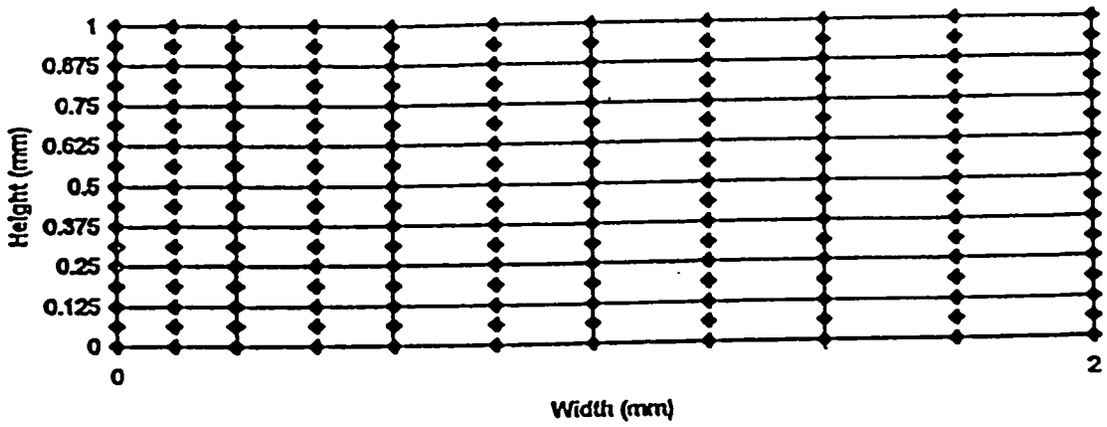

Figure 2-9 : u velocity distribution along the z-axis (height) at the midplane (y=0.5D), (Carreau model n=0.5, λ=1.0)

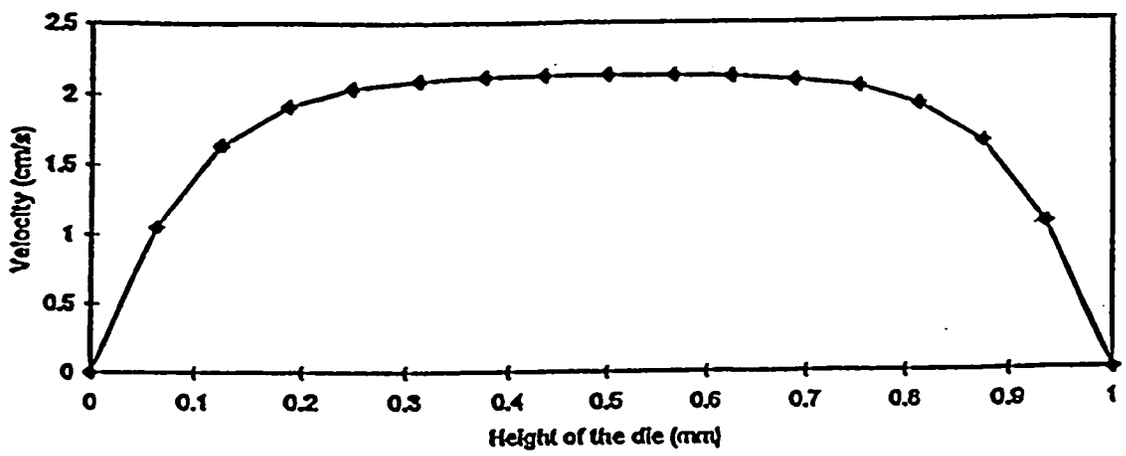

Figure 2-10 : u velocity distribution across y-axis (width), at midplane (z=0.5H), (Carreau model n=0.25, λ=1.0)

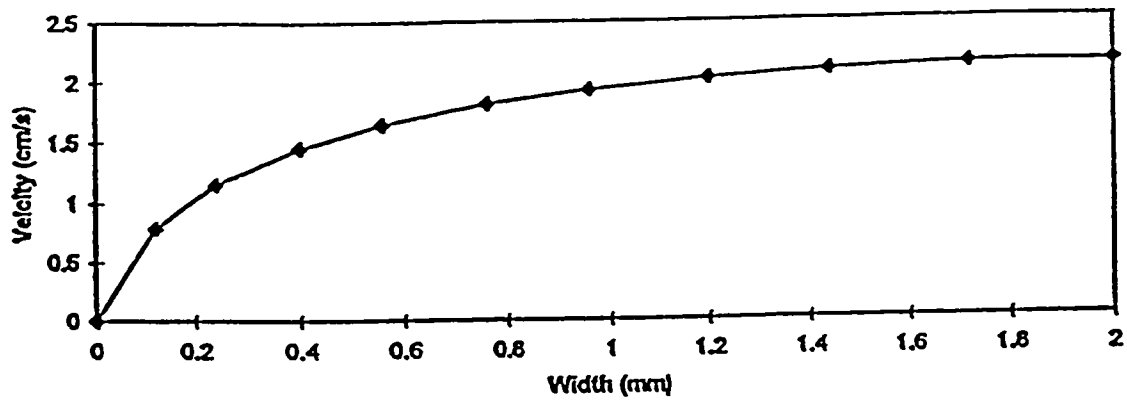

Figure 2-11 : Pressure distribution along the duct (Carreau model n=0.25, λ=1.0)

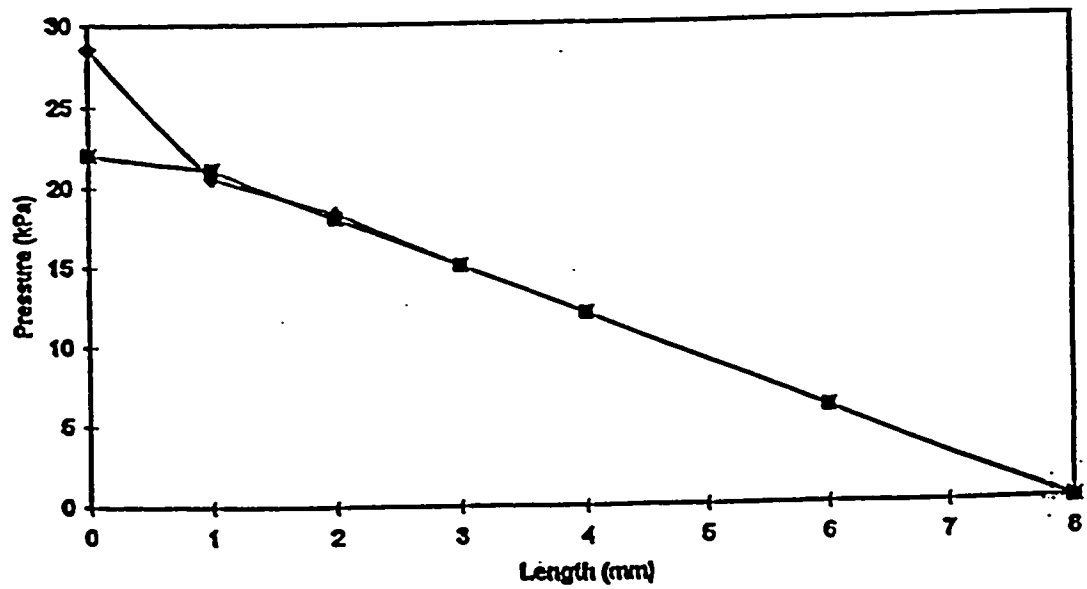

2.2- Modified Algorithm

After explaining the modifications that have been made to the algorithm described in section 2.1.1, the formulation for the final algorithm is described as follows:

1- In the calculation of the first step (equation 2.21) the left hand side (LHS) matrix is the same for each iteration and it is only the right hand side that is changing (at least for the Newtonian case). Therefore the LHS can be calculated and stored at the beginning, and read back at each iteration, instead of being re-calculated. This resulted in improving the speed of each iteration (iterations for the mesh III were completed 20% faster and the savings increased as the number of unknowns and number of iterations increased).

   For the case of non-Newtonian fluids, the LHS of equation 2.21 is not the same in each iteration in general, because $\tilde{K}^{*}$ is a function of viscosity that is changing for each iteration based on the velocity field. To take advantage of the proposed method, the identity matrix was chosen for $\tilde{K}^{*}$ to make it independent of the viscosity that changes in the velocity field.

2- In the analysis of the Carreau fluid in rectangular ducts, it was found that updating the velocities according to continuity and using pressure updates (equations 2.25 to 2.28) had a destabilizing effect as n became smaller than 0.5. Therefore that step was

removed. Removing step 2 (equations 2.25 to 2.27) did not have any effect on preserving continuity or the number of iterations required for convergence and in fact removing it resulted in less computational effort at each step. Equations of continuity and conservation of the momentum are still being satisfied through satisfying equations 2.21 and 2.29 to 2.31.

The modified PC algorithm with reduced equations can be written as follows.

1- Find the pressure correction from the following simplified consistent pressure equation (SCPE), using known values of u^i, v^i and w^i .

$$\left[C_x^T C_x + C_y^T C_y + C_z^T C_z\right]\Delta p^{i+1/2} = -C_x^T u^i - C_y^T v^i - C_z^T w^i \qquad (2.33)$$

The RHS of equation of 2.33 is calculated once and only the LHS is calculated for each iteration. Equation 2.33 ensures that when the continuity is preserved the pressure correction will be zero.

2- Update the pressure according to equation 2.28.

3- Solve x-momentum equation for u,

$$K_u^* u^{i+1} = C_x p^{i+1} \qquad (2.34)$$

4- Solve y-momentum equation for v,

$$K_v^* v^{i+1} = C_y p^{i+1} \qquad (2.35)$$

5- Solve momentum equation for w,

$$K_w{}^{\bullet} w^{i+1} = C_z p^{i+1} \tag{2.36}$$

where

$$K_u = \int_{\Omega_e} \frac{\partial N_i}{\partial x} \frac{\partial N_j}{\partial x} d\Omega \tag{2.37}$$

$$K_v = \int_{\Omega_e} \frac{\partial N_i}{\partial y} \frac{\partial N_j}{\partial y} d\Omega \tag{2.38}$$

$$K_w = \int_{\Omega_e} \frac{\partial N_i}{\partial z} \frac{\partial N_j}{\partial z} d\Omega \tag{2.39}$$

6- Check for convergence. As a test for convergence, the variation in each variable ϕ_i relative to the maximum nodal value of variables was compared against the tolerance

$$\frac{\left|\phi_i^{n+1} - \phi_i^{n}\right|}{\max[\phi]} < \varepsilon' \tag{2.40}$$

Where ϕ_i^{n+1} is the calculated value and ϕ_i^{n} is the previous value at the same node, and ε' is the tolerance.

2.3- Constitutive Equation

A constitutive equation is required to complete the set of the governing equations. The Modified Phan-Thien Tanner (MPTT) constitutive equation (Phan-Thien and Tanner 1977), that has been used in this study can be written in terms of following equations.

The stress components T are divided into two parts, T_s (solvent contribution) and T_p (polymer contribution) as follows.

$$T = T_p + T_s \tag{2.41}$$

$$T_s = (1-\beta)\dot{\gamma} \tag{2.42}$$

where β is the ratio of polymer viscosity at zero shear (η_{po}) to the viscosity of the fluid at zero shear (η_s is the viscosity of the solvent), given by

$$\beta = \frac{\eta_{P_o}}{\eta_{P_o} + \eta_s} \tag{2.43}$$

and $\dot{\gamma}$ is:

$$\dot{\gamma} = \nabla V + \nabla V^T \tag{2.44}$$

$$\begin{aligned} gT_p + Wi[\frac{\partial T_p}{\partial t} + V \cdot \nabla T_p + \frac{\zeta}{2}(\nabla V \cdot T_p + T_p \cdot (\nabla V)^T) \\ -(1-\frac{\zeta}{2})(\nabla V^T \cdot T_p + T_p \cdot \nabla V)] - \mu(1-\beta)\dot{\gamma} = 0 \end{aligned} \tag{2.45}$$

ζ is a constant of the order 0.1 (between 0 and 1) and is directly related to the second normal stress coefficient. Wi is the Weissenberg number, defined as;

$$Wi = \frac{\lambda u_{av}}{D} \tag{2.46}$$

where λ is the relaxation time of the fluid, u_{av} is the average velocity in the primary flow direction and, D is the width of the duct. μ and g are defined as:

$$\mu(\Pi) = \frac{1+\zeta(2-\zeta)Wi^2\Pi}{(1+\Gamma^2\Pi)^{(1-n)/2}} \tag{2.47}$$

$$\Pi = \frac{1}{2}tr(\dot{\gamma}_{ij}\cdot\dot{\gamma}_{ij}) \tag{2.48}$$

$$g = 1 + \frac{\varepsilon\cdot Wi}{\beta}tr(T_p) \tag{2.49}$$

n is the power-law exponent, Γ is another time constant, Π is the second invariant of the shear rate tensor, and ε is a material constant related to the behaviour of fluid in extensional flow.

In the case of steady state flow, terms containing the derivatives of the stress relative to time drop out. The general form of the constitutive equations for the six components of the stress T_p can be described as follows (subscript $_p$ has been dropped for brevity):

$$\left(g + WiA_{ij}\right)T_{ij} + Wi(u\frac{\partial T_{ij}}{\partial x} + v\frac{\partial T_{ij}}{\partial y} + w\frac{\partial T_{ij}}{\partial z}) + WiB_{ij} = \mu\beta\dot{\gamma}_{ij} \tag{2.50}$$

T_e (the elastic part of the polymer stress) is extracted from the polymer stress T_p as follows:

$$T_e = T_p - \beta\dot{\gamma} \tag{2.51}$$

And the general form of stress equations in terms of T_e is then described as

$$\left(g + Wi \cdot A_{ij}\right)T_{ij} + Wi(u\frac{\partial T_{ij}}{\partial x} + v\frac{\partial T_{ij}}{\partial y} + w\frac{\partial T_{ij}}{\partial z}) + Wi \cdot E_{ij} =$$

$$\beta\dot{\gamma}_{ij}(\mu - 1 - Wi \cdot \varepsilon \cdot tr(T) - Wi \cdot A_{ij}) - Wi \cdot \beta \cdot H_{ij} \qquad (2.52)$$

A , B, E and H coefficients for each stress component are given in Appendix B.

2.4- Decoupling of the elastic stresses

There are several methods to decouple the viscoelastic stress calculation from the calculation of the velocity field. The methods that were used by Xue et. al (1995), Debbaut et. al (1997) and the EVSS method that has been used in this study are described here.

1- In the method used by Xue et. al (1995); T_p is calculated from the constitutive equation (2.50) and is treated as a source term in the momentum equations. Therefore the momentum equations can be described as

$$Re\, V \cdot \nabla V - (1-\beta)\nabla^2 V - \nabla \cdot T_p + \nabla P = 0 \qquad (2.53)$$

2- In Debbaut et. al (1997), T_p is calculated from the constitutive equation (2.50), then T_e is calculated from equation (2.51). The creeping flow assumption has been used and therefore the momentum equations can be written as

$$-\nabla^2 V - \nabla \cdot T_e + \nabla P = 0 \qquad (2.54)$$

where T_e is treated as a source term.

3- In the method that has been used in this study, T_e was calculated directly from equation (2.52) and were used as source terms in equation (2.54).

The major difference between the methods of Xue et al. (1995), and the two methods of Debbaut et al. (1997) and this work is in mathematical nature of the momentum equation. In the latter two methods, the Stokes operator is not weighted by the solvent viscosity and therefore is not influenced by the value of β directly. Independence of the momentum equations from β also make it easier to implement multi-mode constitutive equations as follows (Debbaut et al., 1997);

$$-\nabla^2 V - \nabla \cdot T_e + \nabla P = 0 \tag{2.55}$$

$$T_e = \sum_i T_{e,i} \tag{2.56}$$

$$f(T_{e,i}) = 0 \tag{2.57}$$

where **i** refers to each mode contribution. In this study however, only the single mode MPTT constitutive equation has been used because of the ease of calculations and availability of the data.

2.5- Algorithm for the 3-D problem

The fully segregated 3-D algorithm for analysis of the viscoelastic flow using creeping flow formulation and EVSS method can be described as follows.

1- Equations for the conservation of mass and momentum are solved using the segregated method (i.e. Pressure Correction method). The elastic stresses are treated as source terms in the momentum equations and their values from previous iterations are used in the calculation, making them "known" for the present iteration. The discretized form of the momentum equations are obtained from modification of equations 3.34 to 3.36, to include decoupled stress components as the source terms.

$$K_u^* u^{i+1} = C_x p^{i+1} - Q_x T_{xx}^* - Q_y T_{xy}^* - Q_z T_{xz}^* \tag{2.58}$$

$$K_v^* v^{i+1} = C_y p^{i+1} - Q_x T_{yx}^* - Q_y T_{yy}^* - Q_z T_{yz}^* \tag{2.59}$$

$$K_w^* w^{i+1} = C_z p^{i+1} - Q_x T_{zx}^* - Q_y T_{zy}^* - Q_z T_{zz}^* \tag{2.60}$$

where K values were given in Chapter Three and Q_x, Q_y and Q_z are defined in terms of the interpolation function N as;

$$Q_x = \int_{\Omega_e} \frac{\partial N_i}{\partial x} d\Omega \tag{2.61}$$

$$Q_y = \int_{\Omega_e} \frac{\partial N_i}{\partial y} d\Omega \tag{2.62}$$

$$Q_z = \int_{\Omega_e} \frac{\partial N_i}{\partial z} d\Omega \tag{2.63}$$

2- After convergence in the first step, equations for the stress components are solved one by one, over the whole domain. Calculation of stress components continues

until the change in their values is less than a specified tolerance. The discretized form of the constitutive equations for stress components can be written as;

$$[M_1 + Wi M_2]T_{ij} = R_1 + Wi R_2 \tag{2.64}$$

where $\mathbf{M_1}$ and $\mathbf{M_2}$ and $\mathbf{R_1}$ and $\mathbf{R_2}$ are defined in terms of interpolation functions $\mathbf{N}$ as;

$$M_1 = \int_{\Omega_e} [1 + Wi(a + b_{ij})] N_i N_j \, d\Omega \tag{2.65}$$

$$M_2 = \int_{\Omega_e} N_i (u \frac{\partial N_j}{\partial x} + v \frac{\partial N_j}{\partial y} + w \frac{\partial N_j}{\partial z}) \, d\Omega \tag{2.66}$$

$$R_1 = \int_{\Omega_e} [\beta(\mu - 1) c_{ij}] N_i \, d\Omega \tag{2.67}$$

$$R_2 = \int_{\Omega_e} \{E_{ij} + [(a + b_{ij}) c_{ij} + H_{ij}]\beta\} \, d\Omega \tag{2.68}$$

Components of $\mathbf{E_{ij}}$ and $\mathbf{H_{ij}}$ are defined in Appendix B, and a, $\mathbf{b_{ij}}$, and $\mathbf{c_{ij}}$ are defined as;

$$a = \frac{\varepsilon}{\beta} tr(T^*) \tag{2.69}$$

$$b_{ij} = (\zeta - 1)\dot{\gamma}^*_{ij} \tag{2.70}$$

$$c_{ij} = \dot{\gamma}^*_{ij} \tag{2.71}$$

As a test for convergence, variation in each variable ϕ_i relative to the maximum nodal value of variables was compared against the tolerance

$$\frac{\left|\phi_i^{n+1} - \phi_i^n\right|}{\max[\phi]} < \varepsilon' \tag{2.72}$$

where ϕ_i^{n+1} is the calculated value and ϕ_i^n is the previous value at the same node, and ε' is the tolerance.

This two step process continues, until the change in the velocity field becomes insignificant.

2.6- Concluding Remarks

In this chapter, a 3-D fully segregated algorithm has been described. This algorithm is based on a creeping flow formulation, EVSS decoupling method and a single mode MPTT constitutive equation.

The segregated pressure correction (PC) method was applied to the generalized Newtonian flow. Its performance, convergence and accuracy were compared with the fully coupled method.

Segregated methods have several advantages over fully coupled formulations, including: savings in memory and a modular structure. The modular structure allows calculation of other variables like temperature to be added as a separate module. One very important advantage of the segregated method compared to fully coupled methods is breaking the problem into a solution of Poisson like equations that are very well suited for iterative solvers (Haroutunian et al., 1993). Iterative solvers are far more efficient for obtaining solutions on large meshes when compared to direct methods.

In the next chapter the study of the viscoelastic flows begins with study of secondary flows in straight ducts based on the fully developed flow assumption.

Chapter 3

Viscoelastic Flows – Fully Developed Flow Assumption

In this chapter, secondary flows of the viscoelastic fluids in straight ducts is studied based on the assumption of fully developed flow (2.5-D). The development of the 2.5-D algorithm is followed by the verification of the algorithm which includes tests and comparison with the results of Xue et al. (1995). Secondary flows are studied using particle tracking.

In the end, new results examining the effects of Wi and Re on the intensity and pattern of secondary flows are presented.

3.1- The Fully Developed Flow Assumption

There are several recent studies on secondary flows of viscoelastic fluids in ducts (Xue et al., 1995, and Debbaut et al., 1997). These analyses are all based on the assumption of fully developed flow in ducts. The assumptions are as follows.

1- Derivatives of all variables, except pressure, in the direction of the flow (x-axis) are zero, and the velocity and stress components can be described as follows;

$$V = V(y,z) \tag{3.1}$$

$$T = T(y,z) \tag{3.2}$$

2- Pressure is decoupled into a constant pressure drop in the x direction and an in-plane component that is only a function of the transverse axes (i.e. y, the width direction and z, the height direction).

$$P = x\Delta p + p(y,z) \tag{3.3}$$

Xue et al. (1995) applied these assumptions using the control volume approach. They used a grid consisting of three planes in the direction of the flow to obtain the fully developed solution. Debbaut et al. (1997) applied these assumptions using the finite element method but did not fully explain the algorithm.

3.2- 2.5-D Algorithm

The following segregated algorithm, which is based on the fully developed flow assumption, is based on the finite element discretization of a plane, where the flow reaches the fully developed condition.

1- *Calculation of elastic stress components*;

Using a previously calculated (or on the first iteration, estimated) flow domain, stress components are calculated from constitutive equations. Values of each of the six stress components are calculated one at a time. At the end of each iteration, the variation in the stress values are checked until the variation becomes less than a pre-specified tolerance. Discretized equations for the stress components are described by equations 2.64 to 2.71. Equation 2.64 is modified (by dropping the derivatives relative to x) as follows.

$$M_2 = \int_{\Omega_e} N_i (v \frac{\partial N_j}{\partial y} + w \frac{\partial N_j}{\partial z}) d\Omega \qquad (3.4)$$

2- *Calculation of transverse velocity components (v and, w) and in-plane pressure (p);*

The velocity components v, w, and, pressure p are calculated using the segregated pressure-correction method. At this stage, elastic stress components are treated as source terms in the momentum equations, with their values from the previous stage being used. Discretized continuity and momentum equations for each variable are written as;

- pressure calculation

$$\left[C_y^T C_y + C_z^T C_z\right]\Delta p^{i+1/2} = -C_y^T v^i - C_z^T w^i \tag{3.5}$$

- v calculation

$$K_v^* v^{i+1} = C_y p^{i+1} - Q_y T_{yy}^* - Q_z T_{yz}^* \tag{3.6}$$

- w calculation

$$K_w^* w^{i+1} = C_z p^{i+1} - Q_y T_{zy}^* - Q_z T_{zz}^* \tag{3.7}$$

3- *Calculation of u velocity (main flow direction) and pressure drop (Δp)*;

Using stress and velocity values from previous stages, u values and then the flow-rate in the flow direction are calculated. Δp is then adjusted so that the flow satisfies continuity. The discretized x-momentum equation can be written as follows:

$$K_u^* u^{i+1} = S\Delta p - Q_y T_{xy}^* - Q_z T_{xz}^* \tag{3.8}$$

$$S = \int_{\Omega_e} N_i d\Omega \tag{3.9}$$

and flow rate is calculated from integration of u over the cross-section.

$$q = \int_{Area} u dA \tag{3.10}$$

These steps continue until the variation in flow-rate is less than a pre-specified tolerance to ensure continuity.

3.3- Verification of The Algorithm

To verify the program and the algorithm, the program was tested for the cases where no-secondary flow was expected, then the results were tested for mesh independence. At the end, a comprehensive parametric study was performed and its results were compared against Xue et al. (1995).

3.3.1- Tests for No-Secondary Flow Cases

There are three cases (associated with three viscoelastic parameters), where no-secondary flow is expected:

a) Wi=0, where no elastic property exists.

b) ζ=0, where ψ_2 (second normal stress coefficient) is zero.

c) ε=0, which results in $\Psi_2 = k\,(\eta_p + \eta_s)$ i.e. Ψ_2 being a linear function of viscosity.

The first two cases resulted in zero transverse velocities. The third case resulted in maximum transverse velocities of the order of 10^{-6}, similar to what was reported by Xue et al. (1995) for square ducts.

3.3.2 Mesh Independence

The next step in the verification of the program and algorithm is to show that the results are mesh independent. The mesh in this study consisted of 9-node quadrilateral elements, quadratic in velocity and stress, and linear in pressure. The gridlines of a 10x10 mesh with equally spaced elements (21x21 nodes) is shown in the Figure 3-1 (the centre of the duct is at the top right corner in all figures). In Figure 3-1 each grid point represents a node with each element consisting of nine nodes. The size of each element in Figure 3-1 is 0.05x0.05 (dimensionless). Transverse velocity vectors, and the vortices, are shown in the Figures 3-2 and 3-3. The analyses were performed on a mesh representing a quarter of a square duct, taking advantage of planes of symmetry in the duct geometry.

In order to verify mesh independence of the results, results from the 10x10 element mesh were compared to a 20x20 mesh (with equally spaced elements). In this comparison, the average difference of values between the two meshes was of $O(10^{-6})$ for u velocities and 10^{-7} for v and, w. The average relative difference for v and, w was less than 3% and, the average relative difference for u was less than 0.001%. The main difference in the values of v and w was observed near the wall and specially in the corner of the duct.

Figure 3-1: 10x10 Mesh

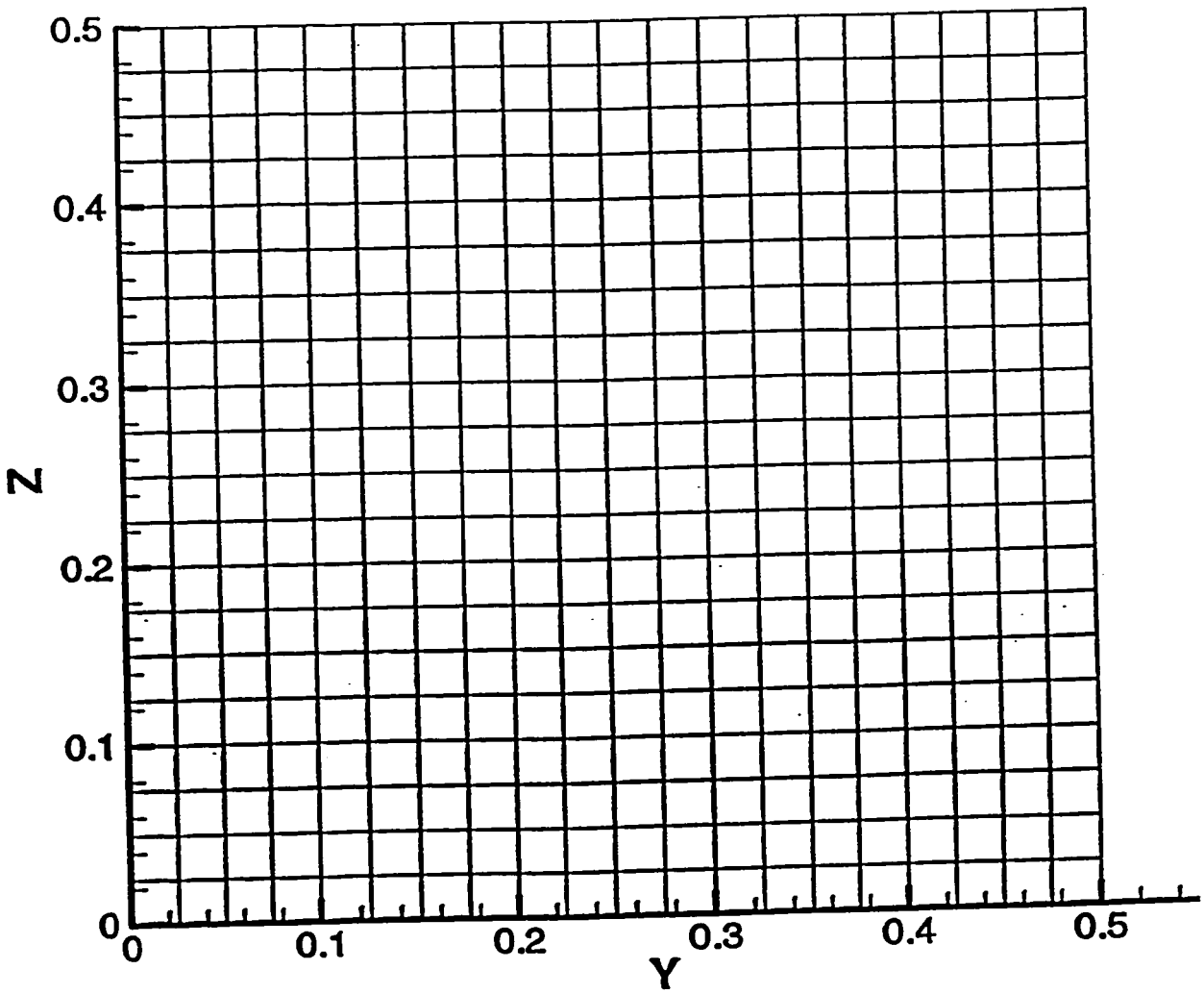

Figure 3-2: Transverse Velocity Vectors

(Wi=0.1, Γ=0.1, n=0.65, β=1.0, ζ=0.2, and ε=0.1)

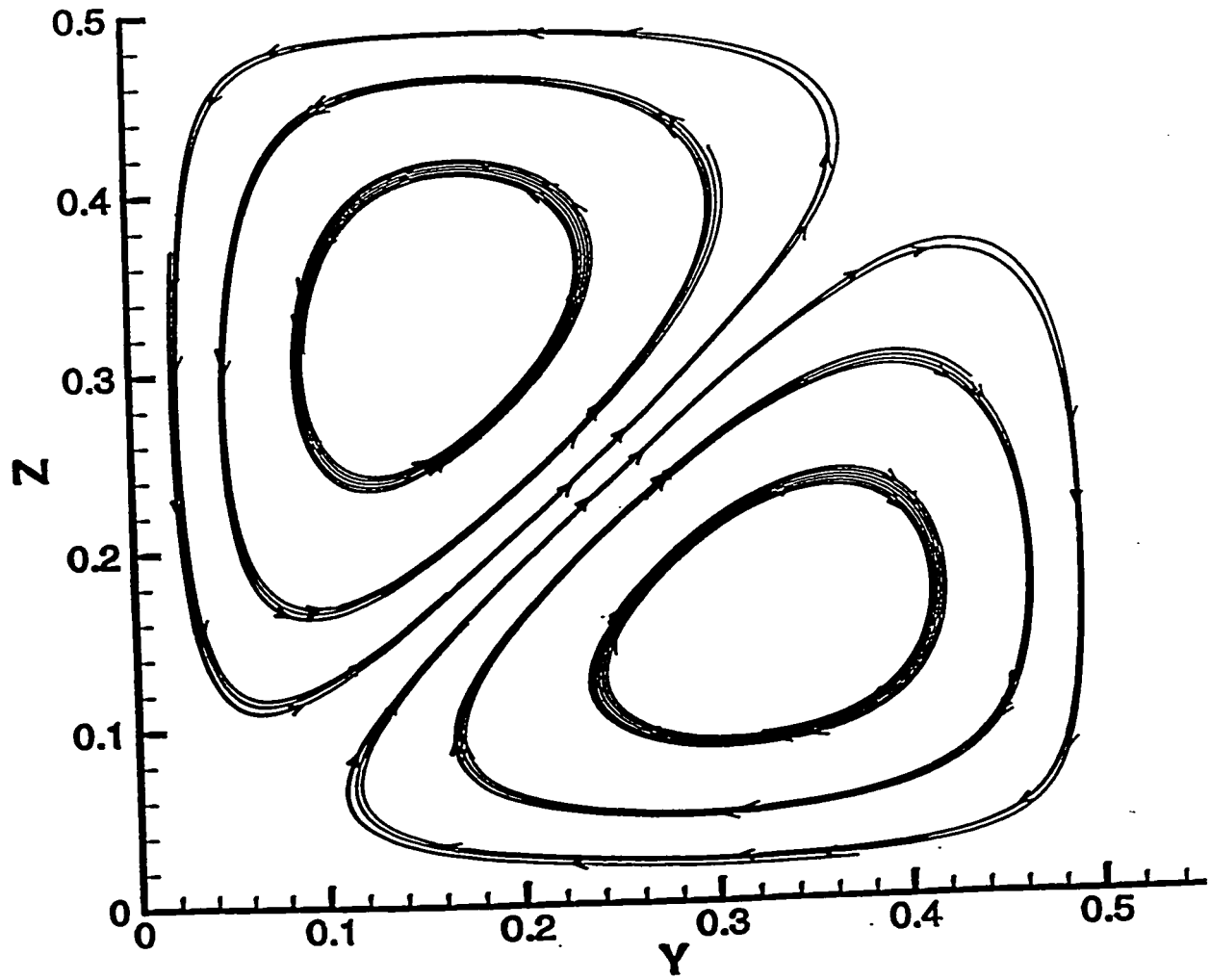

Figure 3-3: Two Vortices Pattern

(Wi=0.1, Γ=0.1, n=0.65, β=1.0, ζ=0.2, and ε=0.1)

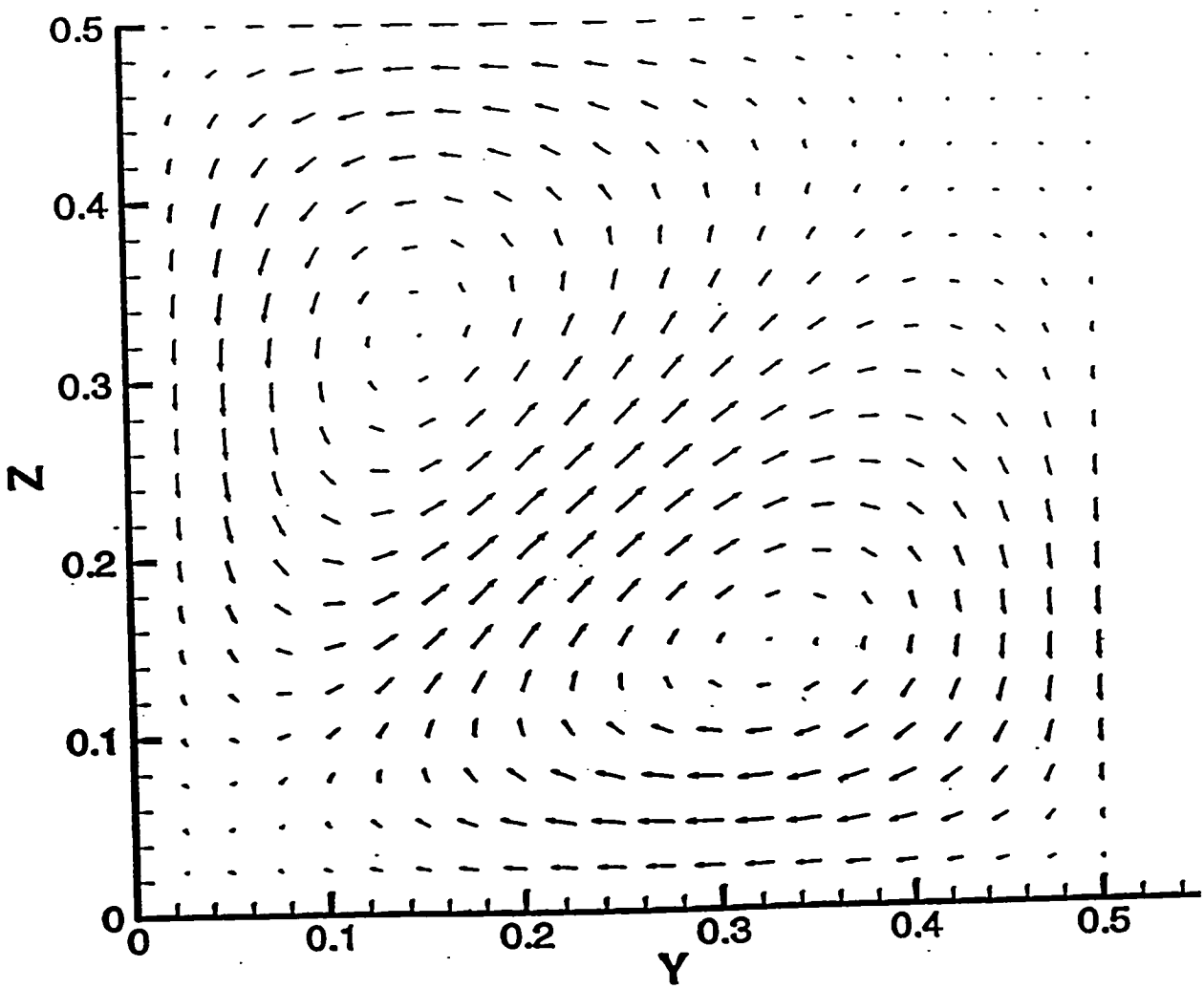

3.3.3- Parametric Study

In order to study the effects of different material properties on the secondary flows, all of the parameters Wi, Γ, n, ε, ζ and, β were varied, one at a time, around a base set of data shown in Table 3.1.

Xue et al. (1995) reported intensity of secondary flows S_{vm} defined as;

$$S_{vm} = \mathrm{Max}(\sqrt{v^2 + w^2}) \qquad (3.11)$$

where v and w are the nodal values. S_{vm} was made dimensionless for comparison by dividing by u_{av}.

Table 3.1 – Values of dimensionless parameters at base point for parametric study (Xue et al, 1995)

Parameter	Value (dimensionless)
Wi	0.135
Γ	0.135
n	0.65
ε	0.1
ζ	0.2
β	1

Typical value for ζ is 0.2 (Bird et al., 1987). For ε, reported values vary from 0.01 (White et al., 1988) to 1.87 (Kajiwara et al., 1993).

In Xue et al. (1995), time constants in the model (Γ, λ) were assumed equal. In this work, the effect of each time constant has been investigated separately. The effects of changes in n and β are also studied.

Results are obtained for the 10x10 mesh (Figure 4-1). The tolerance for the first step (stress calculation) was 10^{-12}, for the second step (for variation in pressure values) the tolerance was 10^{-6} . Tolerance for continuity was 10^{-6}.

Figure 3-4: Effects of Wi on Secondary Flow

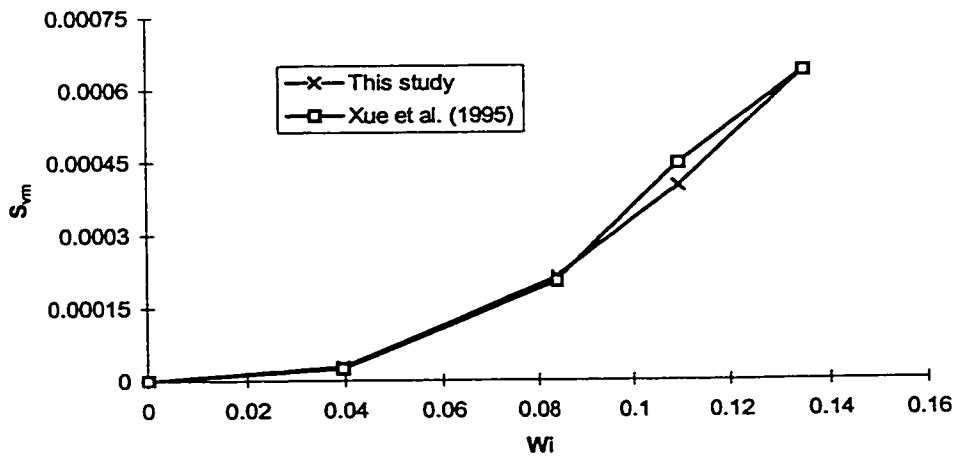

As seen in Figure 3-4, the intensity of the secondary flow strongly depends on the Wi, as expected.

Comparison with the result of Xue et al., reveals that at (Wi=0.106) there is approximately a 10% difference between the results from the two studies; otherwise there is good agreement between the rest of the results.

Figure 3-5: Effects of ζ on Secondary Flow

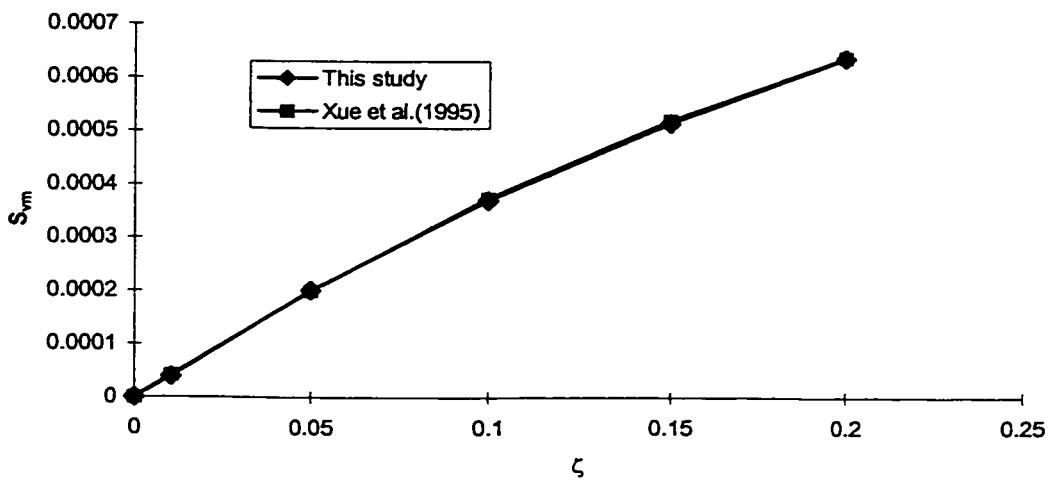

ζ is a parameter that is directly related to the intensity of secondary flows. In terms of viscometric functions, ζ can be described as

$$\zeta = 2\frac{\Psi_2}{\Psi_1} \tag{3.12}$$

Where Ψ_2 is the second normal stress coefficient and Ψ_1 is the first normal stress coefficient. The relationship between the second normal stress difference and the intensity of the secondary flow has long been established (Dodson, 1974) and, as expected, there is a direct relationship between ζ and the intensity of the secondary flows.

There is also good agreement between the results of Xue et al. (1995) and those of this study, for this set of data (Figure 3.5).

Figure 3-6: Effects of ε on Secondary Flow

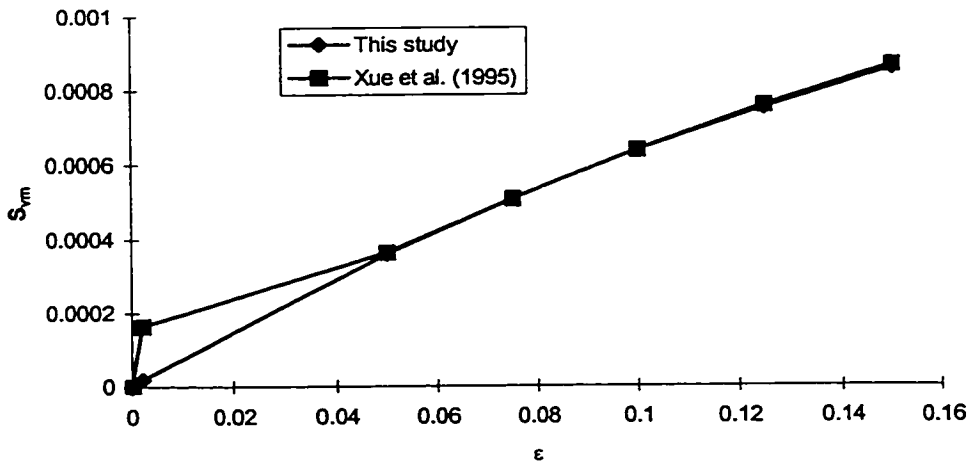

There appears to be direct relation between ε and the intensity of secondary flows. ε is a parameter that is directly related to the extensional properties of fluid. It also insures that Ψ_2 (second normal stress coefficient) is not a linear function of shear viscosity. If Ψ_2 is a linear function of shear viscosity (ε=0), there will be no secondary flow as mentioned earlier (in tests for no-secondary flow cases). No vortex pattern was observed for ε<0.002 in the tests that were done.

As shown in Figure 3-6, there is a significant unexplained difference between predictions of this study and results from Xue et al. (1995) for $\varepsilon<0.05$. For $\varepsilon>0.05$, there is good agreement between predictions of this work and results from Xue et al. (1995).

The effects of other parameters, (that is n, Γ and β) were not studied by Xue et al. (1995) and are reported here without comparison.

Figure 3-7: Effects of n on Secondary Flow

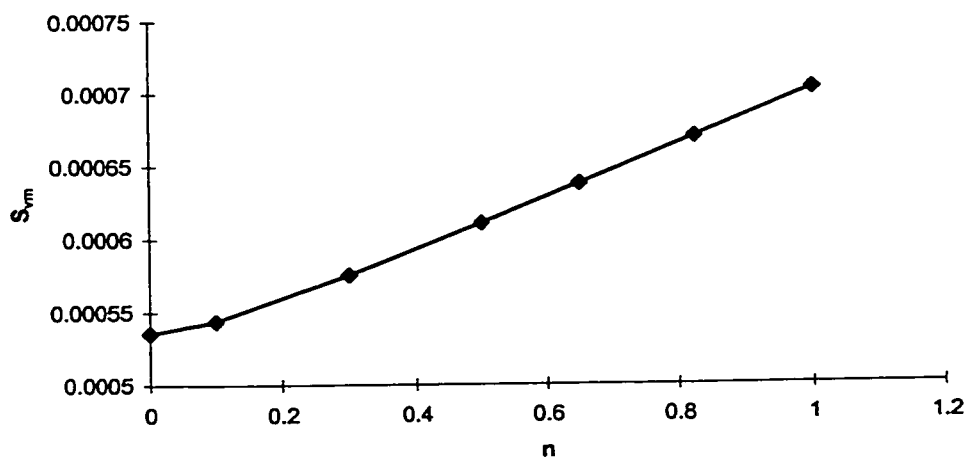

The parameters n and Γ control the shear-thinning behavior of the model. Therefore, these two extra parameters give more flexibility to the MPTT model in describing the u profile when compared to the PTT model. In the PTT model, ζ, ε and Wi are the parameters that control shear-thinning and viscoelastic properties of the fluid, which are not necessarily related.

Figures 3-7 and 3-8 show that an increase in shear-thinning behavior (either by an increase in Γ, or by a decrease in n) is associated with lower intensity of secondary flows.

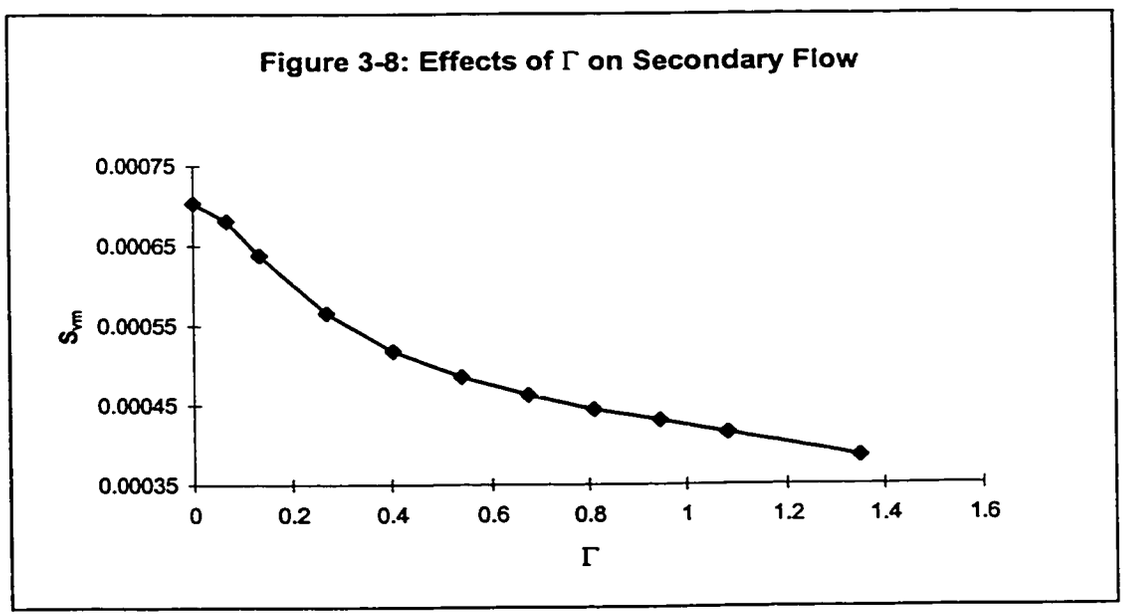

The parameter β represents the polymer contribution (versus Newtonian solvent) and Figure 3-9 shows its effect on the intensity of the secondary flow. The intensity of the secondary flow increases with an increase in β, up to 0.9 where it reaches a maximum. This effect was further investigated for the PTT model and is shown in Figure 3-10.

Figure 3-9: Effects of β on Secondary Flow

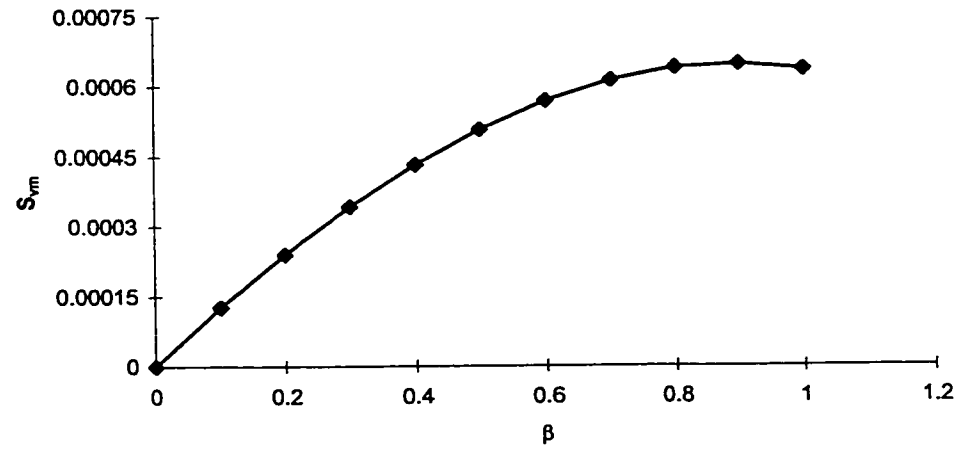

Figure 3-10: Secondary flow intensity vs. β for PTT model

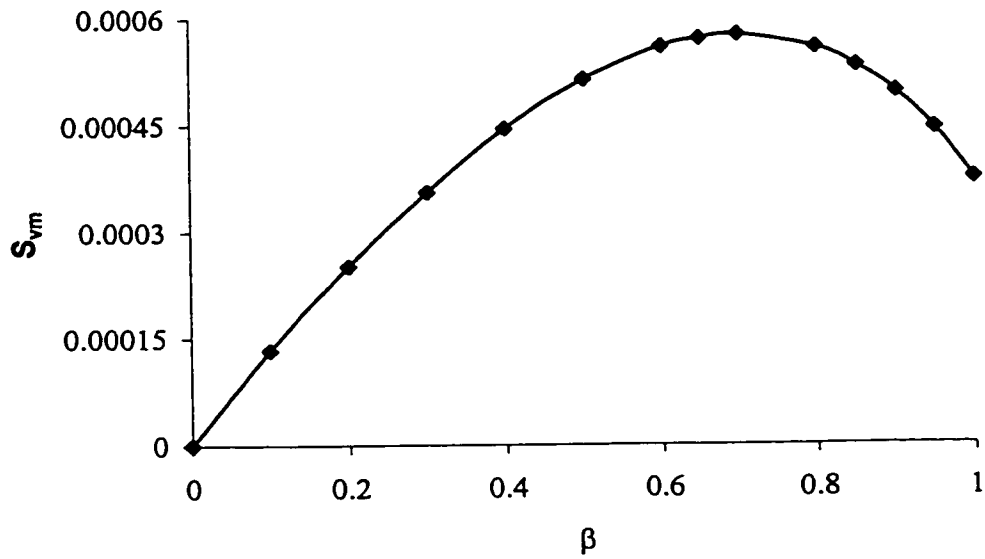

3.4- Effect of duct aspect ratio

In addition to square ducts, rectangular ducts were studied to compare the present results with those of previous studies (including Xue et al. 1995). Only two vortices were observed in each quadrant of the flow cross section as shown in Figures 3-11 and 3-12 for aspect ratios of 4:1, and 12:1. In Figures 3-11 and 3-12, the y and z axes coincides with the walls of the duct.

As the duct aspect ratio increases, the intensity of secondary flow decreases in the middle of the duct and becomes dominant near the wall.

For the case of the square duct, it was found that any small deviation from a perfect square results in a tangible effect on the symmetry of the vortex pattern. To demonstrate that sensitivity, an aspect ratio of 1:1.01 (that is 1% deviation from a perfect square) was studied. As shown in the Figure 3-13, one of the vortices tends to stretch in the direction of wider side and push the other one from the centre.

This test shows that even a 1% change in the aspect ratio triggers an asymmetric vortex pattern. For an experimental study of secondary flows it would be important to consider this sensitivity in preparation of the duct for experiments.

Figure 3-11: Vortices for aspect ratio 4:1

(Wi=0.1, Γ=0.1, n=0.65, β=1.0, ζ=0.2, and ε=0.1)

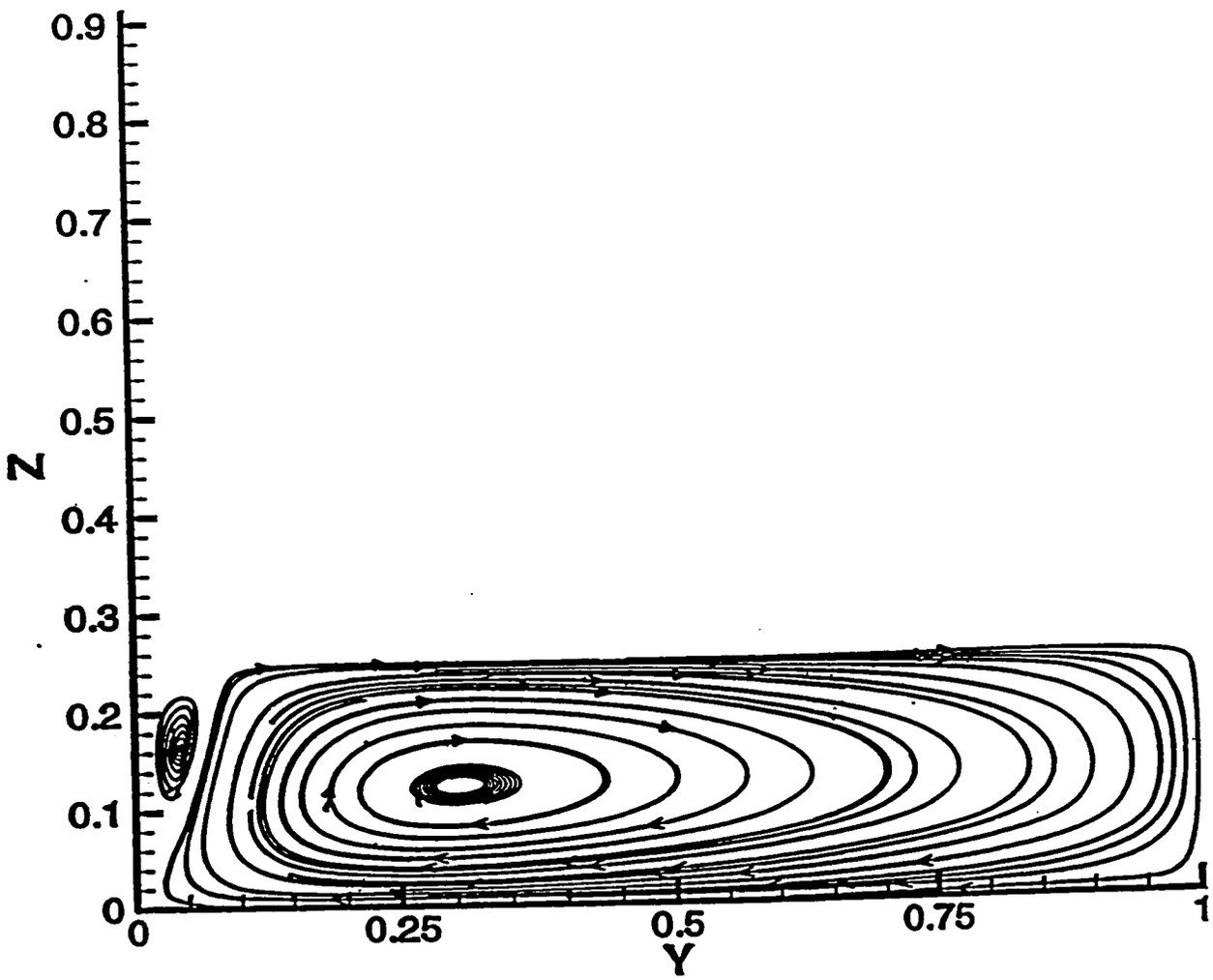

Figure 3-12: Vortices for aspect 12:1 (near the wall)

(Wi=0.1, Γ=0.1, n=0.65, β=1.0, ζ=0.2, and ε=0.1)

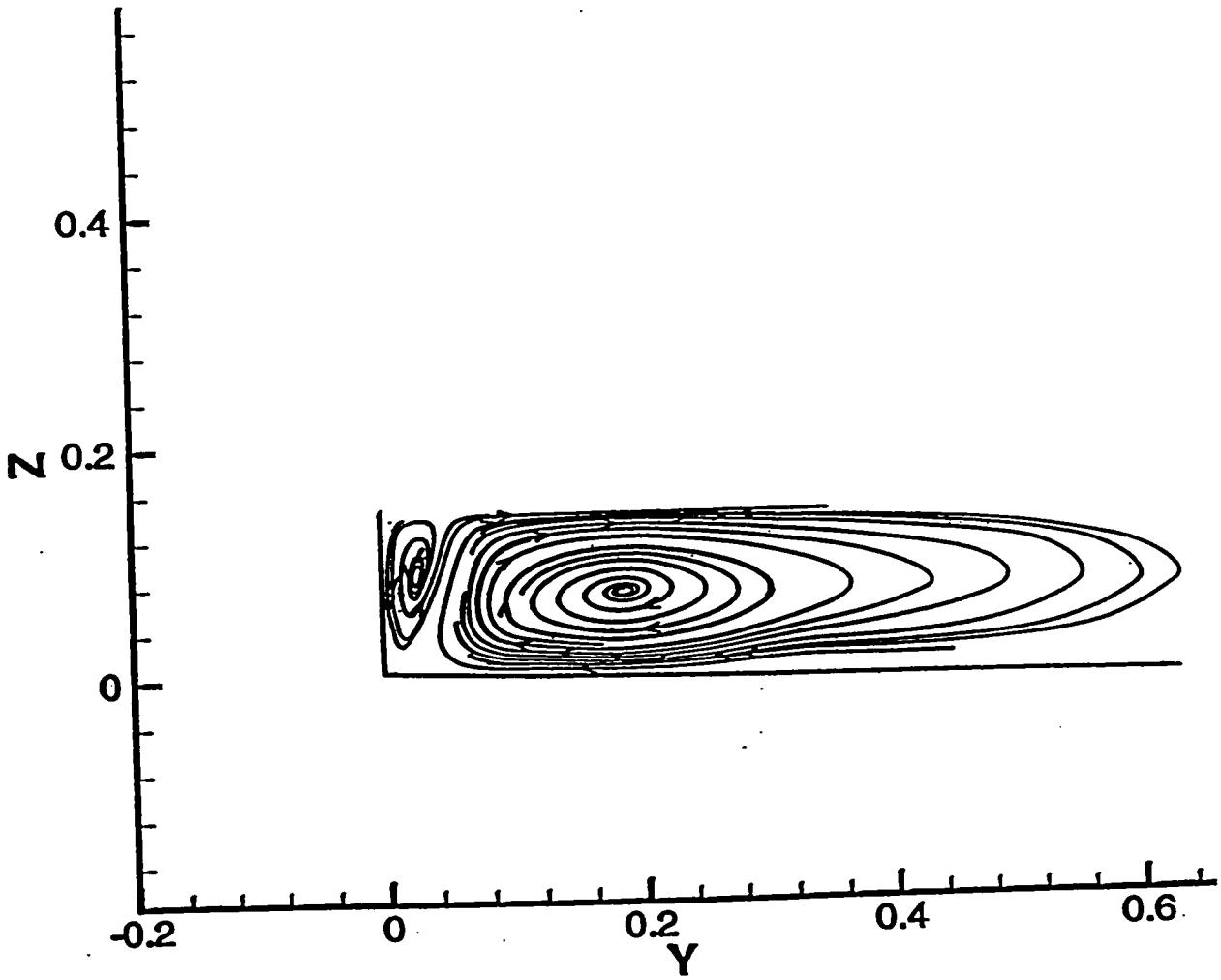

Figure 3-13: Effects of loss of symmetry in Square Duct

(Wi=0.1, Γ=0.1, n=0.65, β=1.0, ζ=0.2, and ε=0.1)

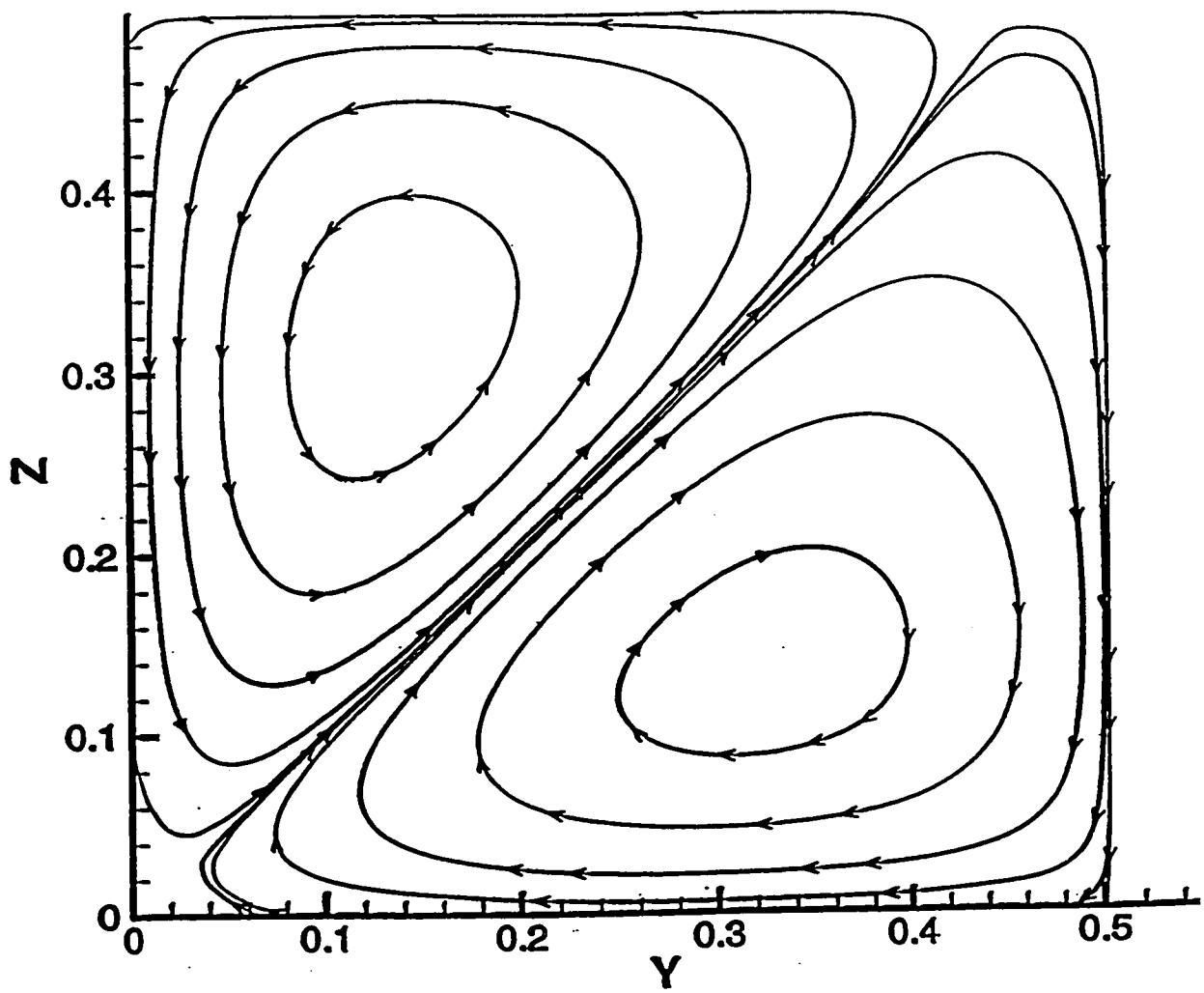

3.5- Particle tracking of the 3-D flow

Dooley and Dietsche (1996) showed the effect of viscoelasticity and specifically the effects of secondary flows on the "layer displacement". They used 165 layers of the same polymer in a multi-layer coextrusion experiment. The polymer layers had been pigmented alternatively black and white to show layer displacements due to secondary flows. Dooley and Dietsche (1996) also performed a 2.5-D numerical analysis (modeling the flow in a cross-section using a fully developed flow assumption) employing Polyflow (Polyflow Sa) and the PTT (Phan-Thien Tanner) model. They found that the estimation of the secondary flow magnitude was very dependent on the rheological parameter values extracted from the material data.

Debbaut et al. (1997) used a five-mode Giesukus model in a 2.5-D analysis to calculate the velocity field. Using the velocity field they calculated the pathlines to track material points and showed the material pathlines at several cross-sections along the channel.

Here the relationship between secondary flows and the fluid displacement is studied using particle tracking. Stream-traces of the fluid were depicted using Tecplot™ (Amtec Engineering), to trace the material point movements throughout the duct. Figures 3-14 and 3-15 show progress in the position of a line of particle tracers initially positioned at 20% of the height of the die inlet (z =0.2), and at 1000, and 3000D. Values

of the model parameters for these cases (Figures 3-14 and 3-15) were Wi=0.1, Γ=0.1, β=1.0, ζ=0.2, and ε=0.1. Figure 3-16 represents particle displacement starting for higher Wi at Wi=1.0, and at 300D.

Since the secondary flows have different direction and intensity at different heights in the duct, they result in different kinds of displacement depending on their starting position. Figure 3-17 shows the particle movements starting from different initial heights (z =constant) for the case where Wi=0.1, Γ=0.1, β=1.0, ζ=0.2, and ε=0.1, at 1000D. Figure 3-18 shows the particle movement starting at the same position as the Figure 3-17 when Wi=1.0 and at 100D.

Figure 3-14: Particle positions at 1000D, starting at z=0.2

(Wi=0.1, Γ=0.1, β=1.0, ζ=0.2, and ε=0.1)

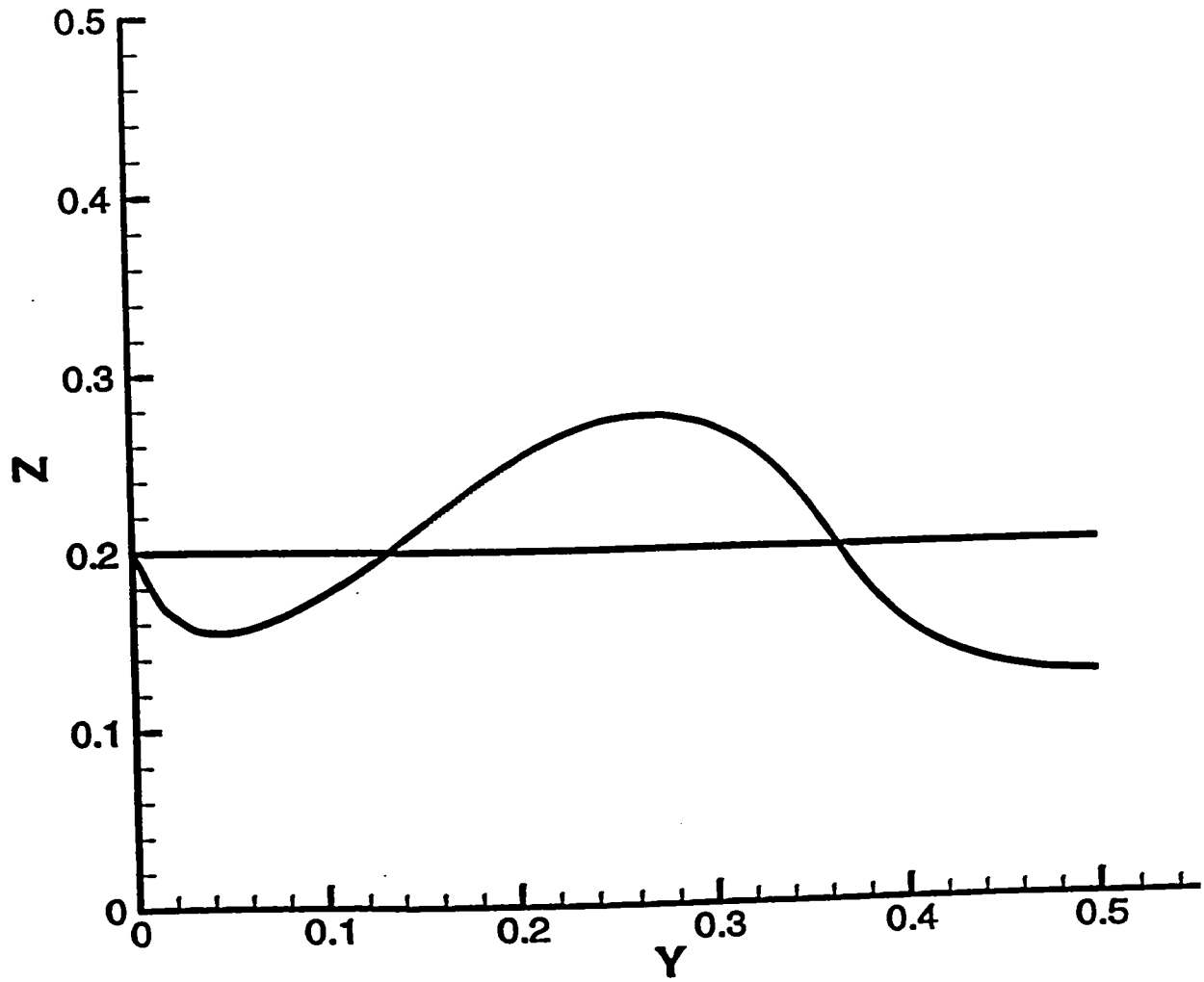

Figure 3-15: Particle positions at 3000D, starting at z=0.2

(Wi=0.1, Γ=0.1, β=1.0, ζ=0.2, and ε=0.1)

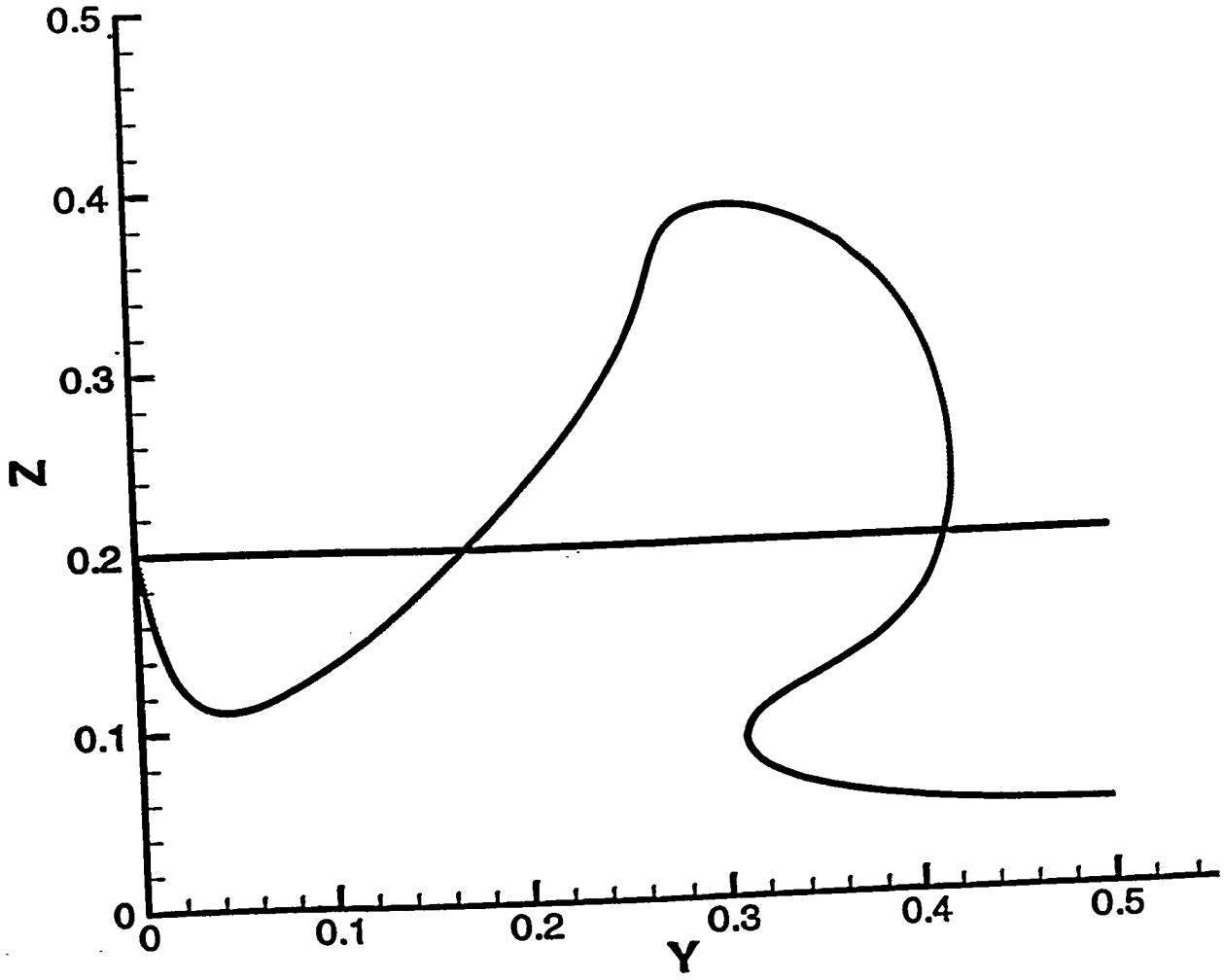

Figure 3-16: Particle positions at 300D, starting at z=0.2

(Wi=1.0, Γ=0.1, β=1.0, ζ=0.2, and ε=0.1)

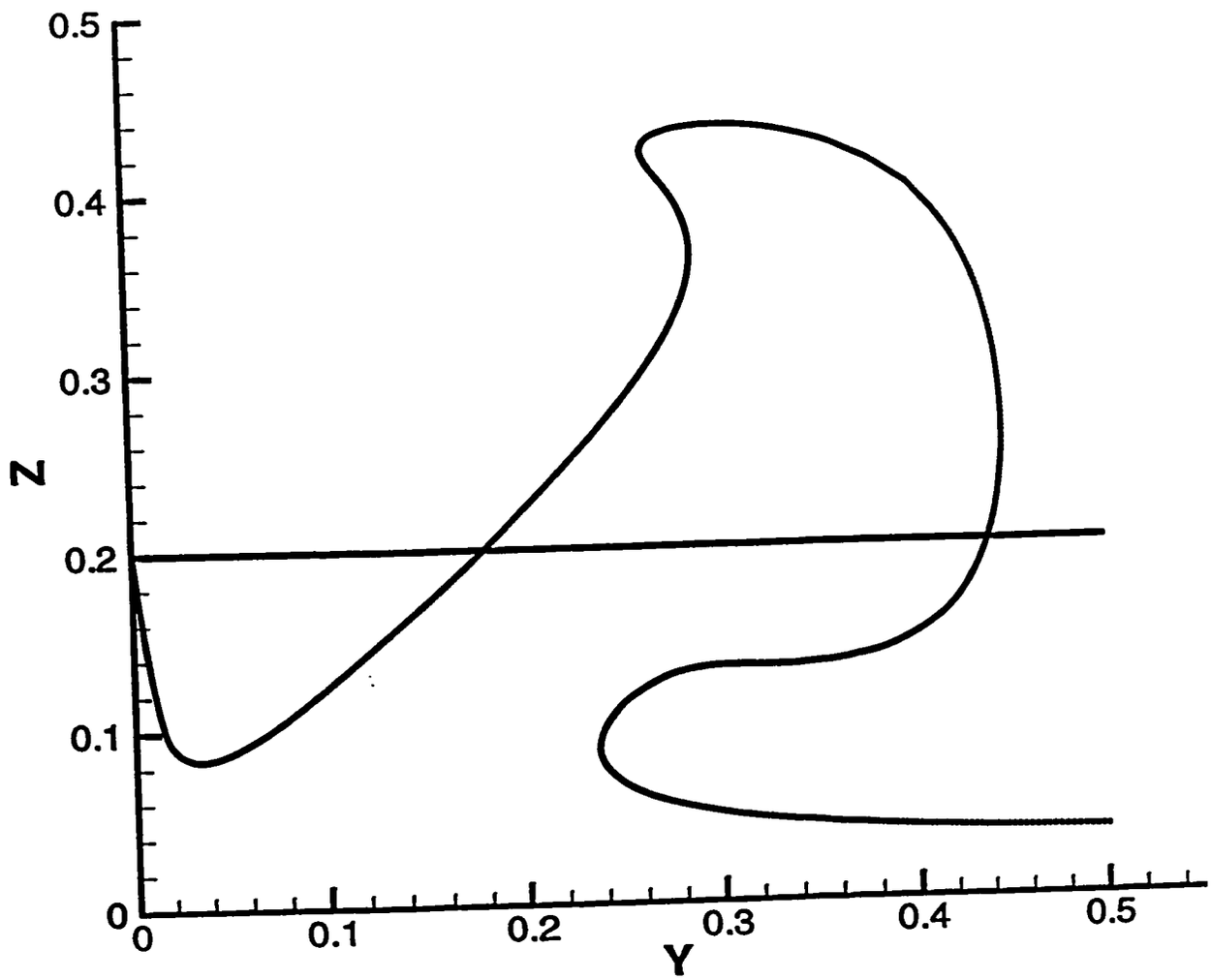

Figure 3-17: Particle positions at 1000D, starting at different z

(Wi=0.1, Γ=0.1, β=1.0, ζ=0.2, and ε=0.1)

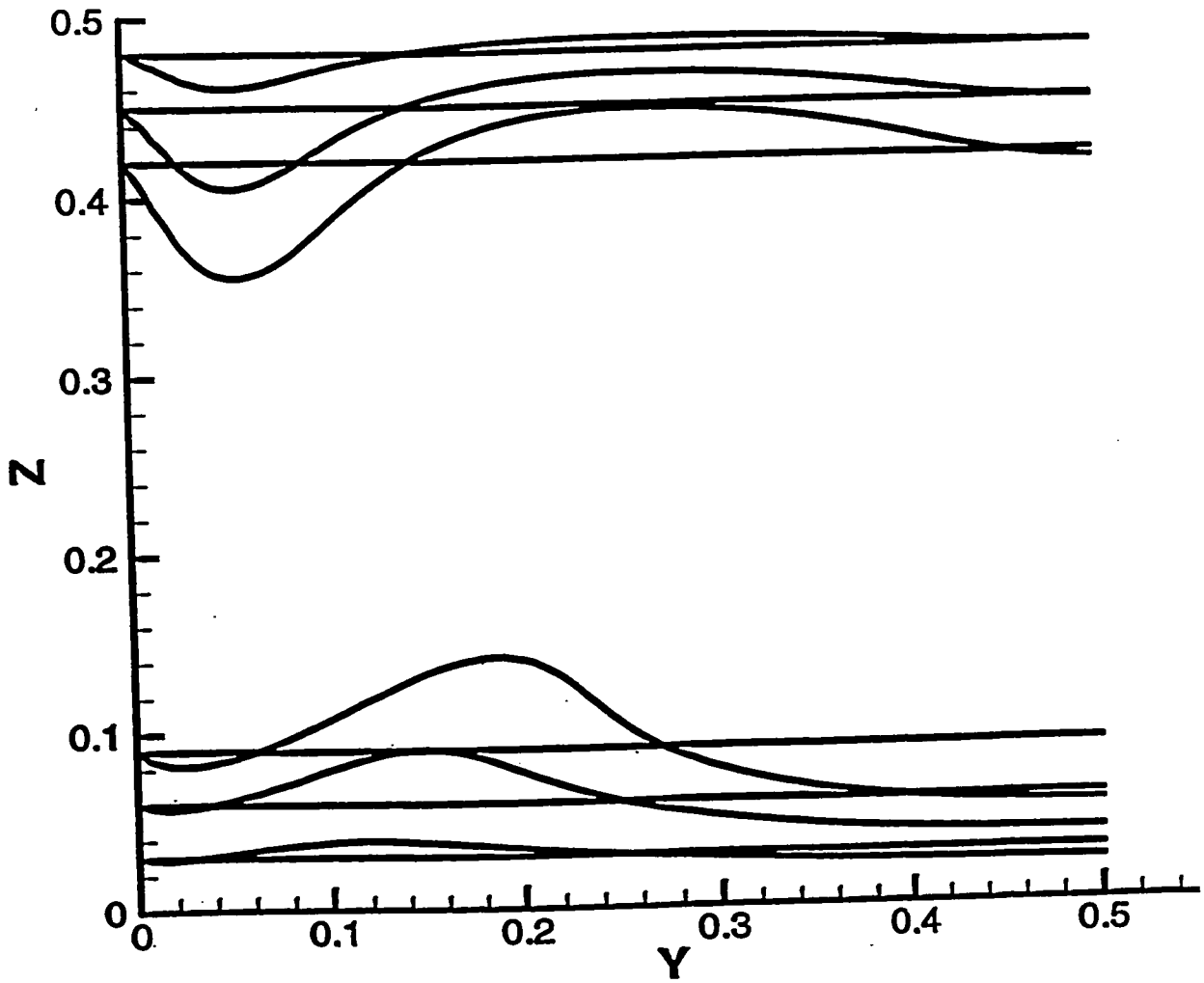

Figure 3-18: Particle positions at 100D, starting at different z

(Wi=1.0, Γ=0.1, β=1.0, ζ=0.2, and ε=0.1)

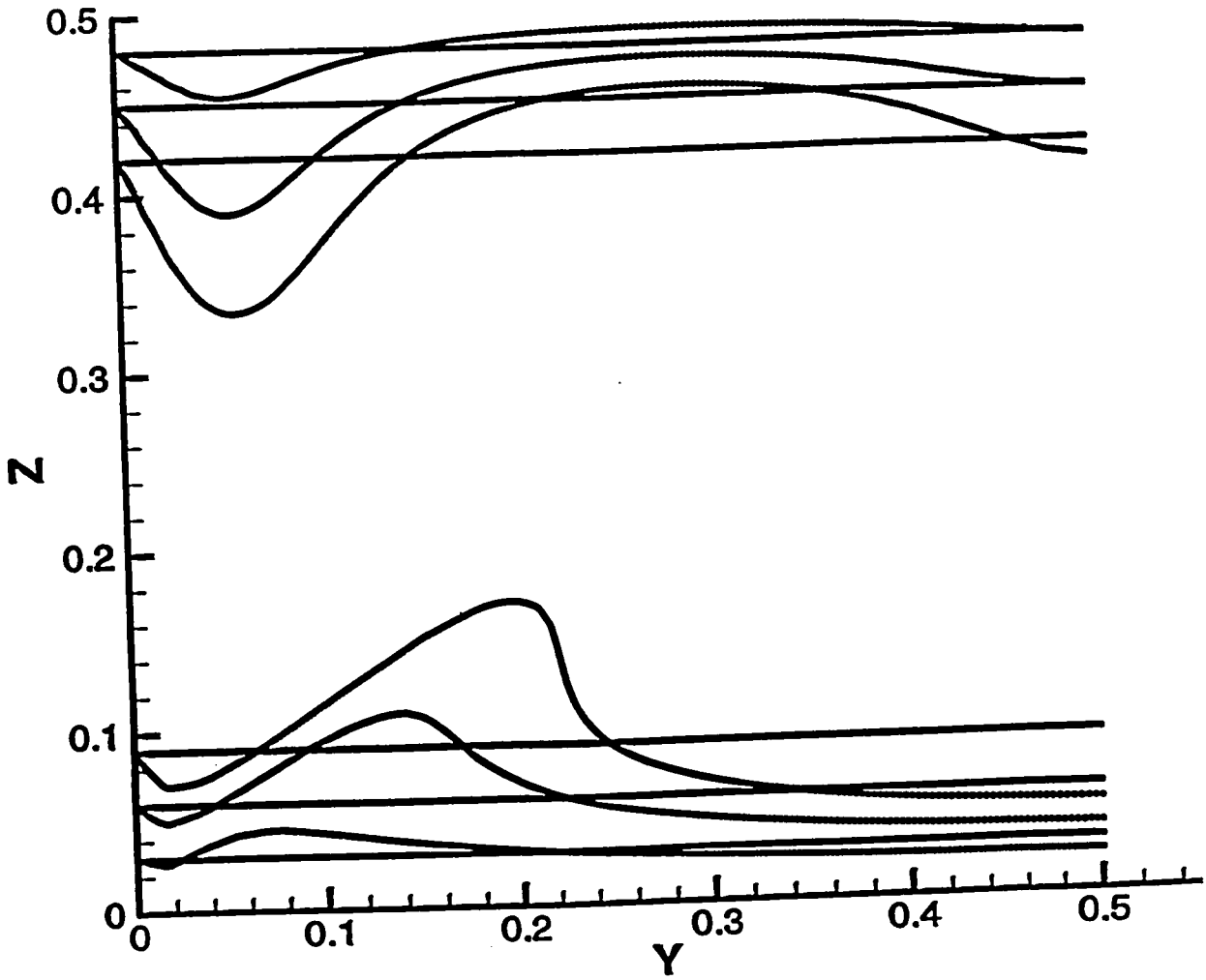

3.6- Effect of error in u-velocity profile on calculation of elastic stresses causing secondary flows

In order to study the effect of u-velocity profile on the magnitude of the stresses that are associated with the secondary flows (T_{yy}, T_{yz} and T_{zz}), CEF constitutive equation that is explicit in terms of stress is studied. For the slowly varying flows CEF model has been used to predict the secondary flows. Extra stress terms for CEF can be written as follows;

$$T = \eta\dot{\gamma} + \frac{1}{2}\Psi_1 \overset{\nabla}{\dot{\gamma}} + \Psi_2 \dot{\gamma}\cdot\dot{\gamma} \tag{3.13}$$

where η, Ψ_1, Ψ_2 are shear rate dependent. T_{yy}, T_{yz} and T_{zz} can be stated as follows.

$$T_{yy} = 2\eta\frac{\partial v}{\partial y} + \Psi_2\left(\frac{\partial u}{\partial y}\right)^2 \tag{3.14}$$

$$T_{yz} = \eta\left(\frac{\partial v}{\partial z} + \frac{\partial w}{\partial y}\right) + \Psi_2\frac{\partial u}{\partial y}\frac{\partial u}{\partial z} \tag{3.15}$$

$$T_{zz} = 2\eta\left(\frac{\partial w}{\partial z}\right) + \Psi_2\left(\frac{\partial u}{\partial z}\right)^2 \tag{3.16}$$

To examine the importance of the terms $\frac{\partial v}{\partial y}, \frac{\partial v}{\partial z}, \frac{\partial w}{\partial y}$, and $\frac{\partial w}{\partial z}$ a test was performed by eliminating these terms in calculation of elastic stress components (T_e), to evaluate their effect on the S_{vm} through comparison. For the case (Wi=0.135, Γ=0.135, ζ=0.2, ε=0.1, β=1.0, and n=0.65), elimination of the terms $\frac{\partial v}{\partial y}, \frac{\partial v}{\partial z}, \frac{\partial w}{\partial y}$, and $\frac{\partial w}{\partial z}$ resulted

in a 4% reduction in the predicted values of S_{vm}. However, at higher Wi (Wi=0.5) the difference was about 33%. Therefore for flow at low Wi (Wi<0.135), the terms $\frac{\partial v}{\partial y}, \frac{\partial v}{\partial z}, \frac{\partial w}{\partial y}$, and $\frac{\partial w}{\partial z}$ can be neglected and equations (3.14 to 3.16) can be stated as;

$$T_{yy} = \Psi_2 (\frac{\partial u}{\partial y})^2 \tag{3.17}$$

$$T_{yz} = \Psi_2 \frac{\partial u}{\partial y} \frac{\partial u}{\partial z} \tag{3.18}$$

$$T_{zz} = \Psi_2 (\frac{\partial u}{\partial z})^2 \tag{3.19}$$

showing that terms $\frac{\partial u}{\partial y}$ and $\frac{\partial u}{\partial z}$, are also important in the calculation of elastic stresses causing secondary flows. Equations 3.17 to 3.19 shows any error in calculation of u-velocity profile at the cross section (i.e. u(y,z)) has a significant effect in estimation of elastic stresses causing secondary flows. Therefore apart from having the correct estimate of Ψ_2 (or model parameters that are related to it) it is essential to have an accurate prediction of the u-velocity profile to obtain an accurate estimates of the intensity of the secondary flows.

3.7- Secondary flows at high Weissenberg number

Flows of polymer melt in industrial applications occur at Weissenberg numbers higher than 0.1. Therefore cases of the flow with Wi as high as 20 were studied.

Intensity of secondary flows (S_{vm}) in such flows were of the order of 10^{-3} (one order of magnitude higher than what was predicted in low Wi (~0.1)). Therefore, secondary flows that are predicted for high Wi are in the range that can be measured more readily in experiments. Gervang et al. (1991) have employed laser velocimetry to measure the secondary flows in polymer solutions and their measurements were in the range of 10^{-3} to 10^{-2} (dimensionless).

By increasing the Weissenberg number (Wi>1) several interesting phenomena were observed and are summarized below.

a) As Wi increases, it was found that for $n \neq 0$ (n is the shear thinning exponent), u_c (the main velocity component at the centre of the duct) was higher than what was predicted for a Newtonian fluid, which is not expected for polymers (as polymers have a shear thinning behavior that results in a lower u_c than a Newtonian fluid). Therefore, n=0 was selected for all cases of high Wi flows.

Figure 3-19 : Secondary flows intensity at high Wi

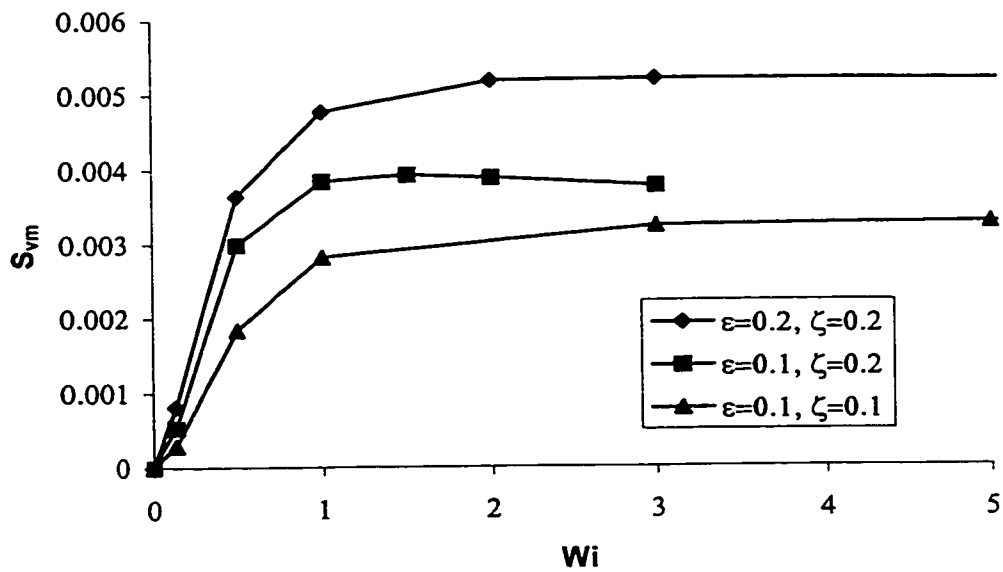

b) Figure 3-19 shows several interesting phenomena. First, the intensity of secondary flows reaches a maximum and plateaus so that an increase in Wi no longer has any effect on S_{vm}. As seen in Figure 3-19, there is a sharp increase in S_{vm} in low Wi (as reported in Figure 3-4) but at higher Wi (Wi>1) the intensity of the secondary flows reaches a plateau. From this observation, it is expected in an experiment with the same fluid at different flow rates, the intensity of secondary flows will depend linearly on the flow rate as the flow rate increases, therefore it can be examined experimentally.

c) Figure 3-19 also shows results for a different set of (ζ, ε) indicating that reaching a plateau does not depend on the value of other parameters. However, the maximum

value does depend on these parameters. It also shows how changes in values of (ζ, ε) affect the maximum value.

It is necessary to have a finer mesh near the wall because of shear thinning and large changes in u near the wall. It is also important to have a consistent element size in the domain to minimize the errors in calculation of v and w. In the study of high Wi, a mesh of 11x11 elements was used which was similar to 10x10 mesh with refinement near the wall.

3.8- Effect of Re on the secondary flows

To study Re effects on the intensity of secondary flows for MPTT fluid, the momentum equations were modified to include convective terms. In this case the momentum equations can be written as;

$$\mathrm{Re}\, V \cdot \nabla V - \nabla^2 V - \nabla \cdot T_e + \nabla P = 0 \tag{3.20}$$

The discretized form of the momentum equations can be written as;

$$(K_u^* + O)\, u^{i+1} = S\Delta p - Q_y T_{xy}^* - Q_z T_{xz}^* \tag{3.21}$$

$$(K_v^* + O)\, v^{i+1} = C_y p^{i+1} - Q_y T_{yy}^* - Q_z T_{yz}^* \tag{3.22}$$

$$(K_w^* + O)\, w^{i+1} = C_z p^{i+1} - Q_y T_{zy}^* - Q_z T_{zz}^* \tag{3.23}$$

where

$$O = \int_{\Omega_e} Re N_i (v^* \frac{\partial N_j}{\partial y} + w^* \frac{\partial N_j}{\partial z}) d\Omega \qquad (3.24)$$

and S is defined by equation 3.9.

Figure 3-20 : Effect of Re on secondary flows intensity

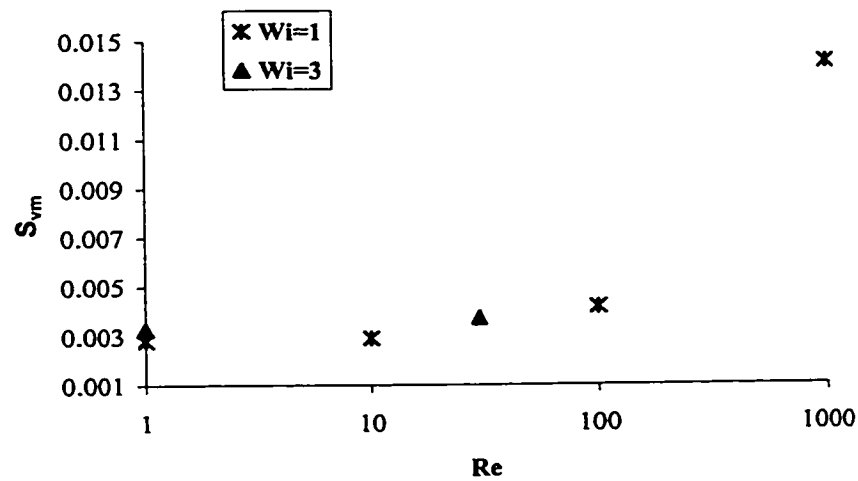

The effect of Re is more important, for polymer solutions than for melts. Due to the high viscosity, Re is less than 1 for polymer melt flow, and the Re effect on secondary flows becomes important when it is higher than 10 as shown in Figure (3-20). The significance of Re effects depends on the magnitude of v and w as well.

Mesh independence of the results was investigated by comparing the solution from an 11x11 mesh with that of a 22x22 mesh. Flow and fluid parameters for this case

were; Wi=1.0, β=1.0, ζ=0.1, ε=0.1, Γ=1.0, n=0 and Re=1000. The average relative difference of comparable nodal values for u for the two meshes was less than 0.7% and for transverse velocity components it was less than 6%.

As shown in the Figure 3-21, the combination of high Re and high Wi results in a dramatic change in the pattern of vortices. The number of vortices increases from two to eight. There are two vortices that are encompassed by a larger one, and there is also an isolated one in each half of the domain (quarter of the duct).

The change in pattern of vortices begins with a gradual shift in the centre of vortices toward the centre of the duct, as shown in Figure 3-22. In this case, the same model parameters as the previous case (Wi=1.0, β=1.0, ζ=0.1, ε=0.1, Γ=1.0, n=0) have been used for Re=450 .

By increasing Re, it can be observed that streamlines near the walls begin to bend inward, as shown in Figure 3-23. Figure 3-23 shows the vortices at Re=550. A further increase in Re results in more complicated patterns as shown in Figure 3-21 (for Re=1000).

Figure 3-21: Pattern of secondary flows in Re=1000,

(Wi=1.0, β=1.0, ζ=0.1, ε=0.1, Γ=1.0, n=0)

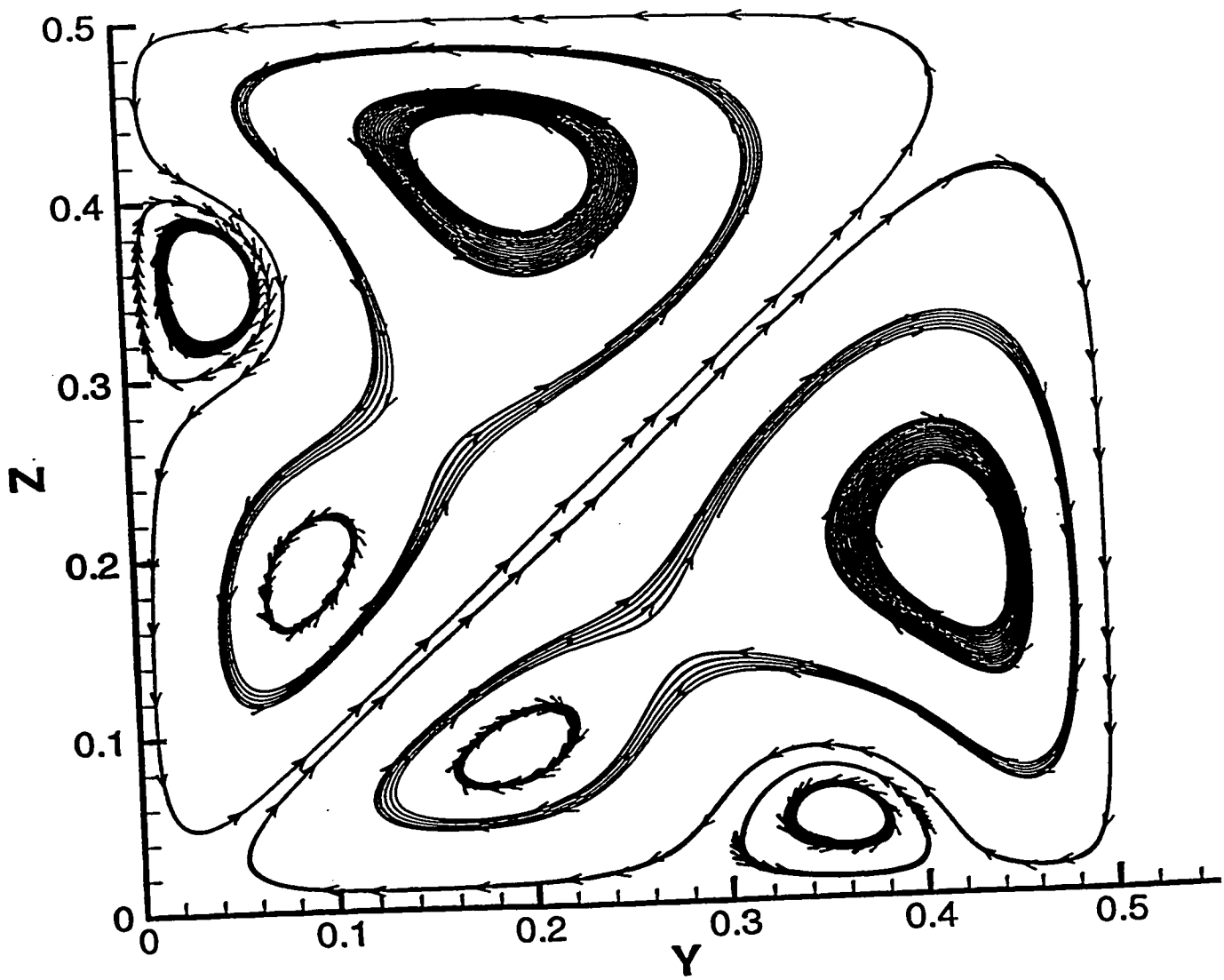

Figure 3-22: Pattern of secondary flows in Re=450

(Wi=1.0, β=1.0, ζ=0.1, ε=0.1, Γ=1.0, n=0)

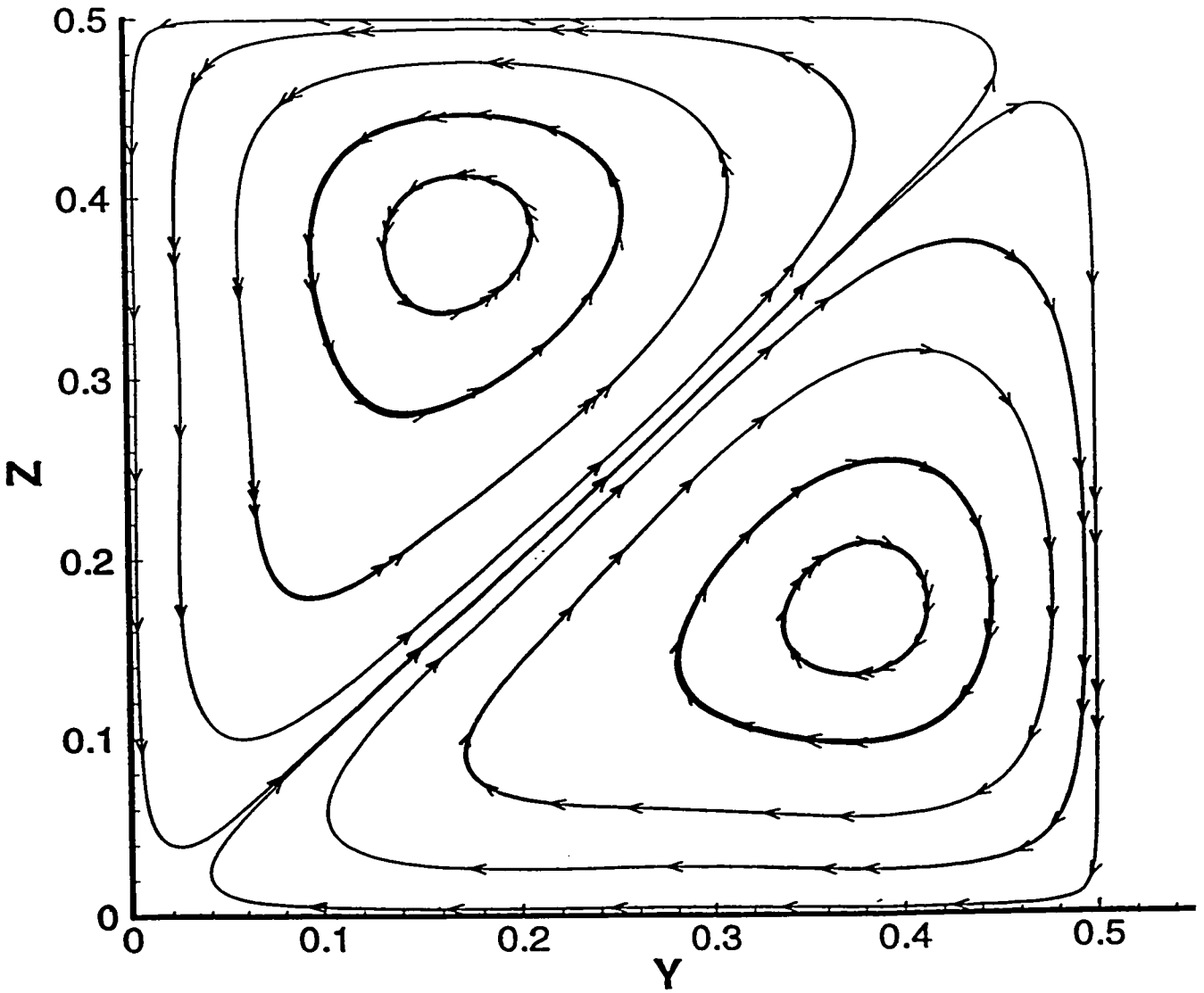

Figure 3-23: Pattern of secondary flows in Re=550

(Wi=1.0, β=1.0, ζ=0.1, ε=0.1, Γ=1.0, n=0)

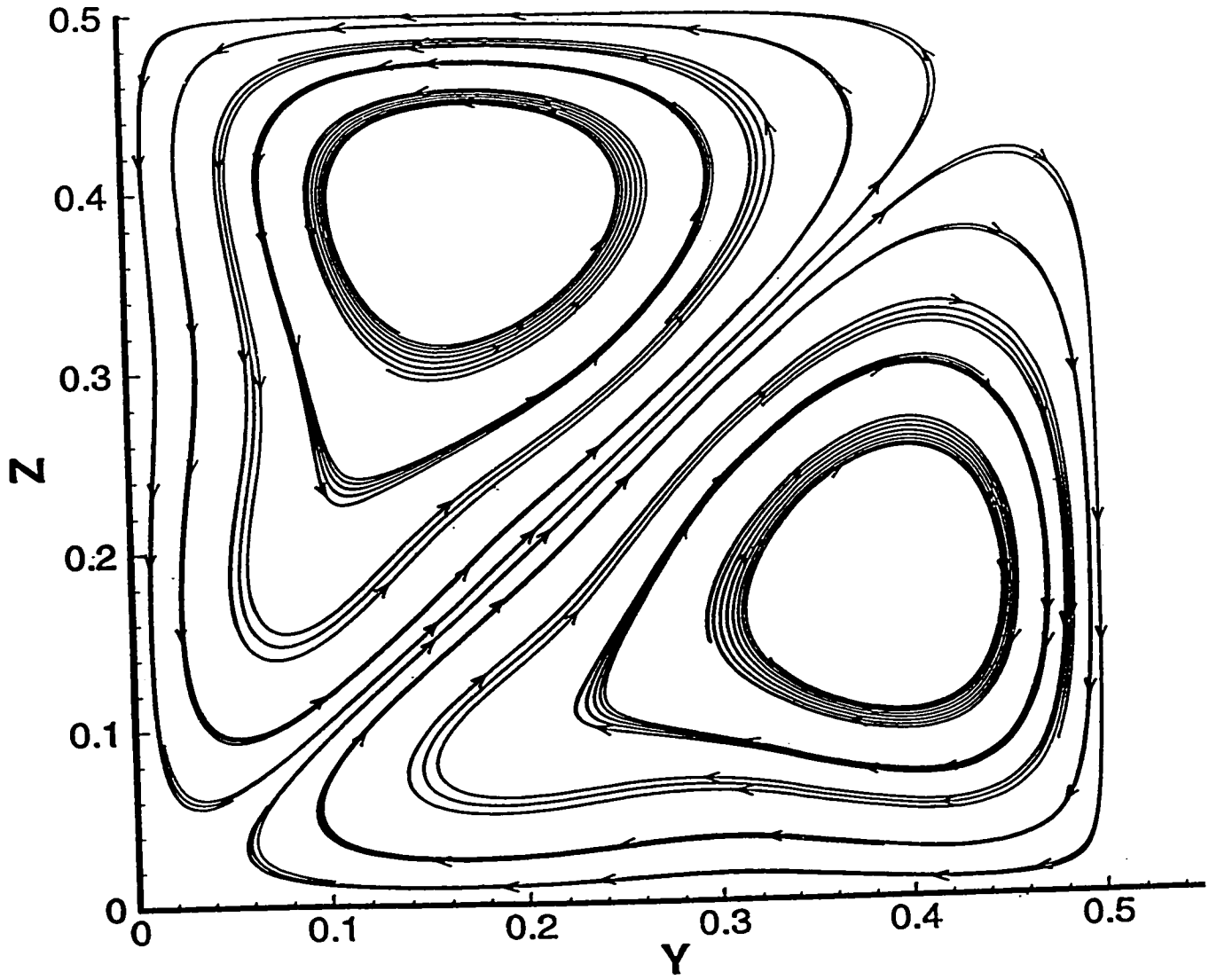

Figure 3-24: Pattern of secondary flows in Re=2000 for a rectangular duct

(Wi=1.0, β=1.0, ζ=0.1, ε=0.1, Γ=1.0, n=0)

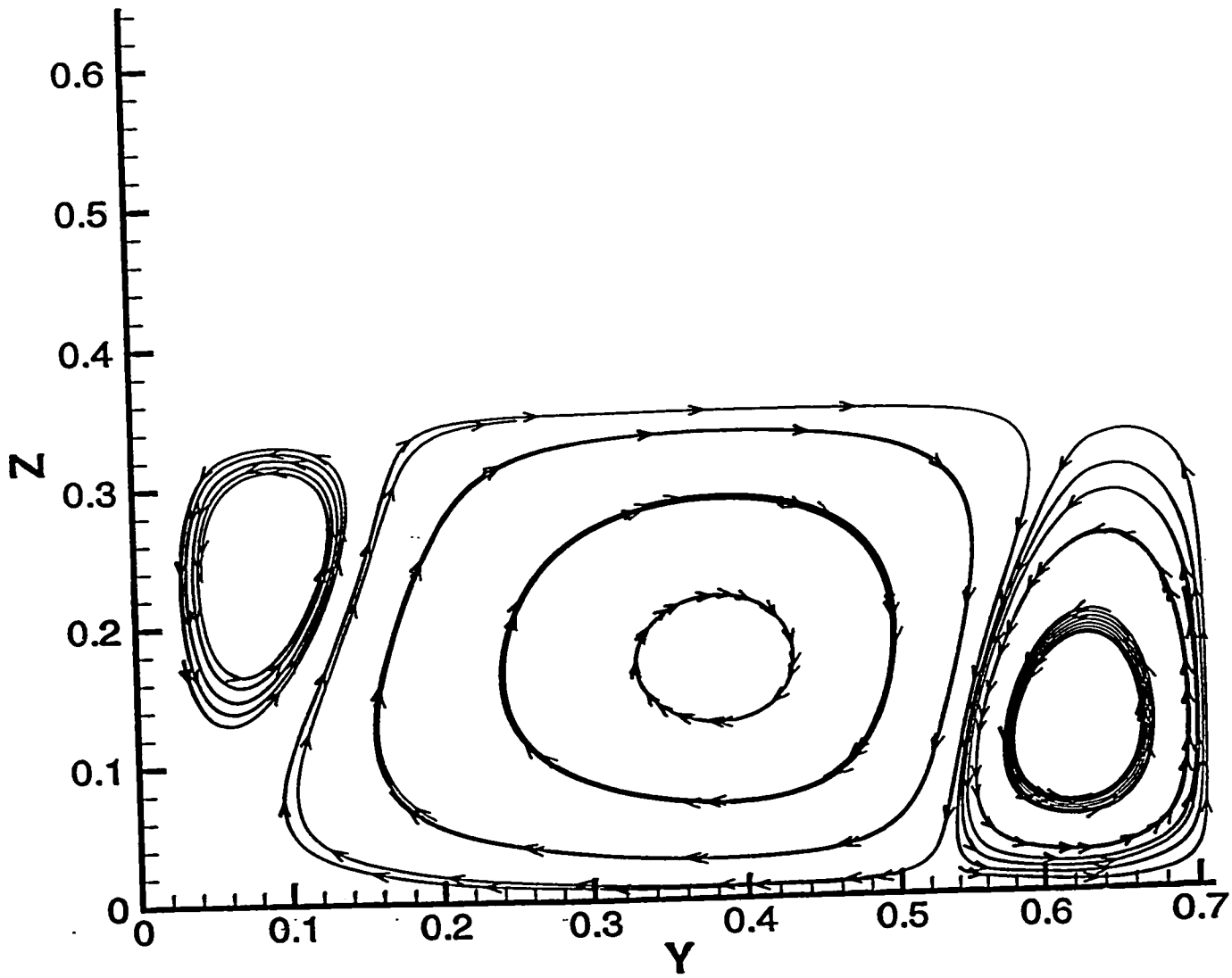

Interestingly, an increase in Re results in a very different pattern for rectangular ducts. As shown in Figure 3-24, three vortices appear for the case of (Wi=0.1, β=1.0, ζ=0.1, ε=0.1, Γ=1.0, n=0), and Re=2000. The presence of such vortices in the flow of polymer solutions changes the heat transfer and mixing properties in such flows and deserves further studies.

3.9- A 2.5-D algorithm based on Carreau-MPTT constitutive equation

Generalized Newtonian fluid (GNF) models can be used to describe the u-profile in the ducts accurately. However, due to the lack of an elastic component in such models they cannot be used to predict the secondary flows. Since it was understood that prediction of secondary flows depends on an accurate account of the u-velocity profile, the following algorithm is proposed to take advantage of the capability of GNF models for u-velocity profile in predicting secondary flows.

1- Using the u-momentum equation and integral continuity equation, obtain Δp and the u-profile. For the u-momentum equation the Carreau model is used. The shear viscosity data of the polymer may also be used to obtain an accurate prediction of the u-profile.

$$K_u^* u^{i+1} = C_x p^{i+1} \tag{3.25}$$

where K_u is calculated using Carreau model as follows.

$$K_u = \int_{\Omega_e} \eta(\dot{\gamma}) \frac{\partial N_i}{\partial x} \frac{\partial N_j}{\partial x} d\Omega \qquad (3.26)$$

2- In the second step a viscoelastic constitutive equation is used to calculate all the elastic stress components, based on the u-profile (as done in the 2.5 D algorithm that was used in the section 3.2).

3- The transverse velocity components are obtained from a solution of v and w momentum equations and differential continuity equation (i.e. equations 3.5 to 3.7). In this step the EVSS method is used and elastic stresses are introduced in the momentum equations as the source terms.

Steps 2, and 3 are repeated until the variation in the v and w values are less than a prescribed tolerance. The difference between this method and the one that was described earlier in section 3.2 is in the calculation of the u-velocity profile. In this method, the u-velocity profile is calculated independently at the beginning and the steps 2 and 3 are iterated to calculate v and w components. In the original 2.5-D algorithm calculation of u is part of the iteration, and the viscoelastic constitutive equation is used to obtain the u-velocity profile.

The advantage of this method is in establishing a direct link between S_{vm} and the viscoelastic parameters. In the 2.5-D algorithm that was described previously, the polymer has to be tested in different viscoelastic tests to obtain all the constitutive

equation parameters. These tests include tests for N_2, which is difficult to perform and also some elongational tests are also required to obtain ε. Then if there is a disagreement between calculated S_{vm} values and experimental values there is no easy way for correction to the parameters. Any change, in viscoelastic parameters has an effect on the u-profile and S_{vm}. Based on this method, empirical values for such viscoelstic parameters can be found that at least make an accurate prediction of the secondary flows, even if they are not an accurate or complete description of the viscoelastic fluid behavior.

By applying the semi-empirical method, a complex problems is broken into two separate and less complex problems. Prediction of the u-profile with GNF is usually an easy step. Establishing a link between S_{vm} and viscoelastic parameters seems practical although it requires experimental effort.

The proposed method was tested for the case of a low density polyethylene (Kajiwara et al., 1993) that its PTT and Carreau parameters were available. For the PTT model, the parameters were reported as λ=1 s, ξ=0.22, ε=1.87, β=0.9333 (Kajiwara et al., 1993) and for the Carreau model λ=3 s and n=0.43 (Matsunaga et al.,1995).

The results were obtained both from new and previous (section 3.2) algorithms. For Wi =0.668 the difference in S_{vm} was less than 2% (S_{vm} was 3.93×10^{-3} and 3.86×10^{-3} from the new and old methods respectively).

This method was proposed and tested to reinforce the idea that obtaining a correct u-velocity profile, plays a major role in accurate prediction of the intensity of the secondary flows. In this method the effect of secondary flows on the u-velocity profile has been neglected and it is only acceptable for creeping flow. As Re increases, effect of v and w on u-velocity profile becomes significant and this method is no longer applicable.

3.10- Concluding Remarks

In this chapter, the fully segregated algorithm for 2.5-D finite element analysis of secondary flows of viscoelastic fluids in non-circular straight ducts was described. The algorithm was implemented and tested for mesh independence. A comprehensive parametric study was performed and effects of model parameters were discussed. Comparison of the results from the parametric study for the cases similar to the cases studied by Xue et. al (1995) demonstrated close agreement. The effect of secondary flow on the particle trajectories in flow of a viscoelastic fluid was also discussed.

The performance of the algorithm was tested for high Wi to the point where an increase in Wi no longer had any effects on intensity of the secondary flows. For high Wi (Wi>1), the intensity of secondary flow was one order of magnitude higher than what was obtained in the range of Wi=0.1.

The effects of Re were investigated by modifying the momentum equations to include convective terms. The intensity of the secondary flows was shown to increase with Re. For the first time it was shown that the number and pattern of vortices in duct flows changes dramatically depending on the geometry and other material and flow parameters. The presence of such patterns of the flow may result in a better understanding of heat transfer and mixing of the polymer solutions.

It is very important that parameters of the model are selected (fitted) in a way that ensures accurate prediction of the u-velocity profile. Any error in prediction u-velocity profile has an adverse effect on predicting the elastic stresses that are causing the secondary flows. Also, a new method was proposed based on a separate estimation of the u-velocity profile from the calculation of secondary flows, resulting in a direct correlation between viscoelastic parameters and intensity of the secondary flows.

In the next chapter, secondary flows of viscoelastic fluids in straight ducts will be studied using a full 3-D analysis. Several cases of boundary conditions are studied and the results are presented and compared to the solutions from the 2.5-D algorithm.

Chapter 4

Viscoelastic Flow – 3-D Analysis of Secondary Flows

The 3-D pressure corrected segregated algorithm was described in Chapter Two. In this chapter it is applied to the analysis of viscoelastic flow in the straight ducts. Results for different boundary conditions at the inlet and outlet planes are presented and discussed.

Secondary flows are the focus of our study in this chapter since they are caused by the viscoelastic nature of the flow. The difference between 3-D analysis and 2.5-D analysis (used in the previous chapter) is in the assumptions and formulation of the problem. In 2.5-D analysis it was presumed that there is a fully developed profile of all velocity components. Therefore, it was assumed that at a plane where flow is fully developed, all variables (except pressure) are independent of the x-direction (direction of the primary flow). All equations were solved at that plane neglecting derivatives relative to x (except pressure). The pressure was decoupled to two components; a constant

pressure drop in the x direction and in-plane pressure p(y,z). In 3-D analysis, all momentum equations and continuity are solved together without dropping any terms or making any assumption regarding the pressure. Inlet and outlet boundary conditions are applied to a 3-D duct at the inlet and outlet planes and their effects are studied.

There have been several studies on 3-D flow of viscoleastic fluids. In works by Tran-Cong et al. (1988) and Shiojima et al. (1990) secondary flows were neglected by assuming model parameters that result in a zero second normal stress coefficient. They justified their assumption by considering the secondary flows to be weak and insignificant in the case they studied. Naturally, in these cases, v and w (transverse components of velocity) have been considered zero at the outlet plane.

In studies by Takase et al. (1998), and Sizaire and Legat (1998), secondary flows and their effect on coextrusion layer displacement of polymer have been the main subject of analysis. However, they also chose vanishing transverse velocities as the boundary condition at the outlet. Obviously, assuming zero transverse velocities at the outlet plane does not result in a fully developed flow that involves secondary flows. Therefore, a question arises as what is the correct boundary condition for a fully developed flow of viscoelastic fluid that involves secondary flow. The second question is if fully developed flow involving secondary flows cannot be obtained from 3-D analysis, what is the meaning of the solution that is obtained from 2.5-D analysis. If the results from 2.5-D

analysis are right and meaningful, then why secondary flows have been neglected at the outlet even in the cases where secondary flows were main issues.

In this chapter the emphasis is on applying Neumann boundary conditions for all velocity components (gradients of velocity components in flow direction is set zero) at the outlet to obtain a fully developed solution, and to compare it with the solution from 2.5-D analysis.

Results for different cases of boundary conditions are described. The problem that arises at the boundary using an elliptical formulation of momentum equations along with EVSS method, is shown and described. Several tests has been done to find the source of the problem. After understanding the source of the problem, modifications are suggested to circumvent the problem of deviating from fully developed solution.

4.1- Verification of The Computer Program

The 3-D algorithm and governing equations were described in section 2.5 . 27-node brick elements were used throughout this study while velocity and stress components were interpolated by tri-quadratic Lagrangian polynomials and pressure was interpolated by tri-linear polynomials (Reddy, 1984). The fully segregated 3-D algorithm and its implementation have to be tested in two separate stages:

1- Test of the module that calculates pressure and velocity components

2- Test of the module that calculates elastic stress components

In Chapter Three the implementation of first part of the algorithm involving calculation of the kinematics of the flow (solving continuity and momentum equations without source terms) was tested and verified.

In order to verify stress calculations, values of the velocity components from 2.5-D analysis were imposed on all cross sections of a 3-D mesh as known quantities to calculate the stress values. In this case u, v, and w are constant relative to x, and stress calculations in 3-D code should yield results similar to the calculations from 2.5-D algorithm.

4.2- Study of Different Boundary Conditions

Several cases of boundary conditions were studied and are described below. Results for the u-velocity on the centre line (u_c) and S_{vm} are presented for each case. The MPTT model parameters that are used throughout this chapter are β= 0.1, Wi=0.1, ε= 0.1, ξ=0.2, Γ=0.1, unless stated otherwise.

It was difficult to obtain a vortex pattern in any duct shorter than L=2D, and at least 10 elements in the axial direction (x-direction) were required. A minimum of (4x4) elements were required at each cross-section to capture the vortex pattern.

An important boundary condition that had a crucial role in satisfying continuity was to put zero pressure only at one point in the outlet plane. For the cases studied here the mass loss was less than 0.01%. Tolerance for the maximum pressure variation from iteration to iteration was less than $2x10^{-6}$ and for the stresses it was less $1x10^{-10}$.

A) The first set of boundary conditions was the imposition of a fully developed flow solution of primary flow (obtained from fully developed flow assumption) at the inlet with no transverse velocity components. Neumann boundary conditions (equations 4.2) are imposed for all velocity components at the outlet.

Inlet:

$$\begin{aligned} u &= u(y,z) \\ v &= 0 \\ w &= 0 \end{aligned} \qquad (4.1)$$

Outlet:

$$\begin{aligned} du/dx &= 0 \\ dv/dx &= 0 \\ dw/dx &= 0 \end{aligned} \qquad (4.2)$$

The flow domain is divided into three separate sections. In the first section, the secondary flows are forming. In the second section, there is a stable secondary flow with an intensity close to that of the fully developed flow solution. In the last section, the pattern of secondary flows converts from a vortex pattern to one of transverse velocities toward the centre as shown in Figure 4-1 (note that only ¼ of the duct is shown).

The maximum intensity of the secondary flows (S_{vm}) occurs at y=0.225 and z=0.225, and intensity of the secondary flows at this point as a function of position along the duct is shown in Figure 4-2. Figure 4-2 shows the formation of secondary flows by an increase in S_{vm} from zero to a plateau that approaches to a value close to the one obtained assuming fully developed flow. In the second zone it stays at a stable value. In the final section, as the pattern of secondary flows changes, the intensity of secondary flows increases. Deviation of S_{vm} from the stable value was associated with the change in pattern of secondary flows.

Figure 4-1 : Pattern of transverse velocity components at the outlet

(Wi=0.1, β=0.1, ε=0.1, ζ=0.2, Γ=0.1, n=0.65)

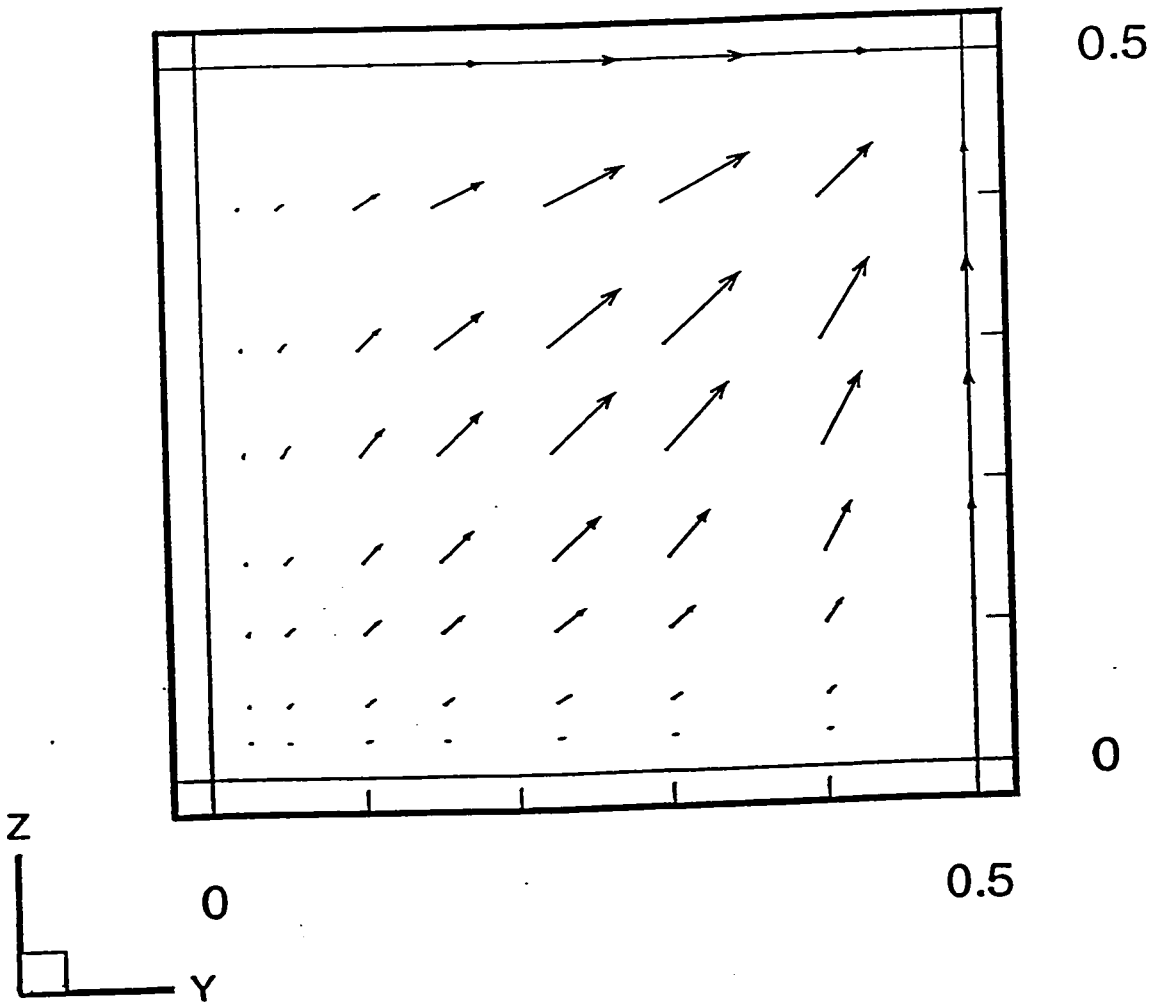

Figure 4-2: S_{vm} progress Throughout a Square Duct

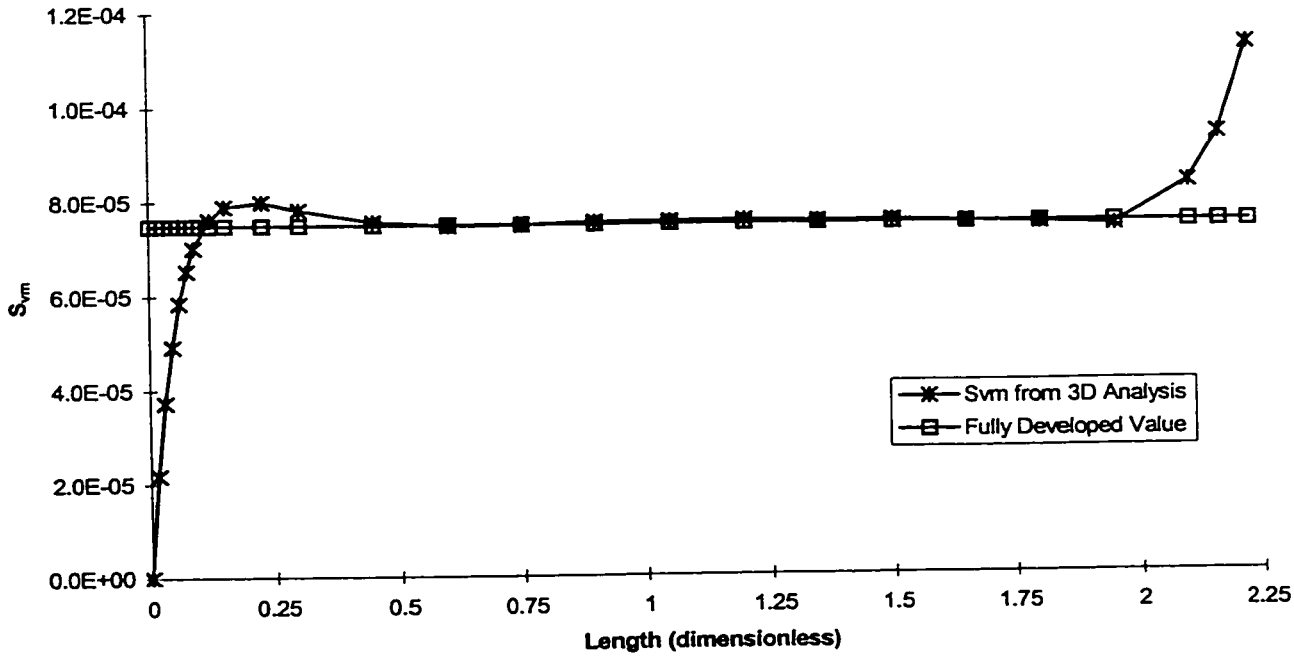

The results shown in Figure 4-2 were obtained from a mesh of (LxWxH)17x4x4, with L=3D. Progress of axial velocity on the centre line (u_c) is shown in Figure 4-3. u_c maintains its fully developed value until near the end of the duct where the vortex pattern breaks down and u_c increases.

Figure 4-3: Axial Velocity at The Center of The Duct

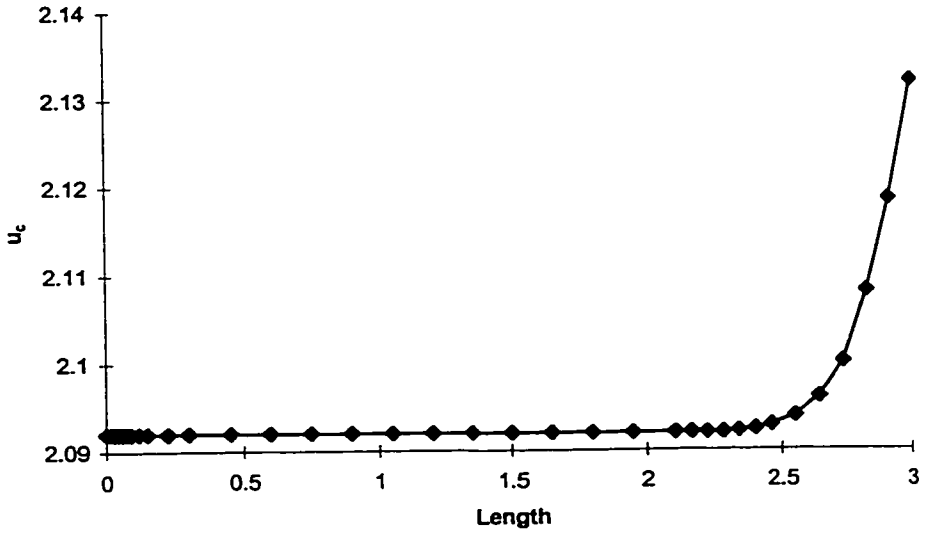

It was important to have three to four elements in the last section of the mesh (approximately 1D from the outlet). If there are not enough elements or the duct is shorter than 2D, the pattern of vortices will not appear. If the duct is sufficiently long but the number of elements is less than 4 in the last section, the breakdown of the vortex pattern travels further upstream.

In case A the fully developed solution from 2.5-D analysis was imposed as the initial boundary condition. The next case, is based on the imposition of flat velocity profile at the inlet (developing flow).

B) The second case of boundary conditions, (and the most difficult case to converge) is the imposition of a flat velocity profile at the inlet with zero transverse

velocity components. Neumann boundary conditions are imposed on the velocity components at the outlet (Equations 4.4).

Inlet:

$$\begin{aligned} u &= 1.0 \\ v &= 0 \\ w &= 0 \end{aligned} \tag{4.3}$$

Outlet:

$$\begin{aligned} du/dx &= 0 \\ dv/dx &= 0 \\ dw/dx &= 0 \end{aligned} \tag{4.4}$$

The MPTT model parameters for this case were β=0.1, Wi=0.1, ε=0.5, ξ=0.2 and Γ=0.1. The progress of u_c and S_{vm} are shown in Figures 4-4 and 4-5.

It is interesting to note that behavior of the solutions for the 3-D analysis in cases A and B are very similar. In the middle zone S_{vm} approaches the fully developed value (where the vortex pattern appears) and at the end solutions behave similarly as well.

Figure 4-4: Progress of u_c along the duct

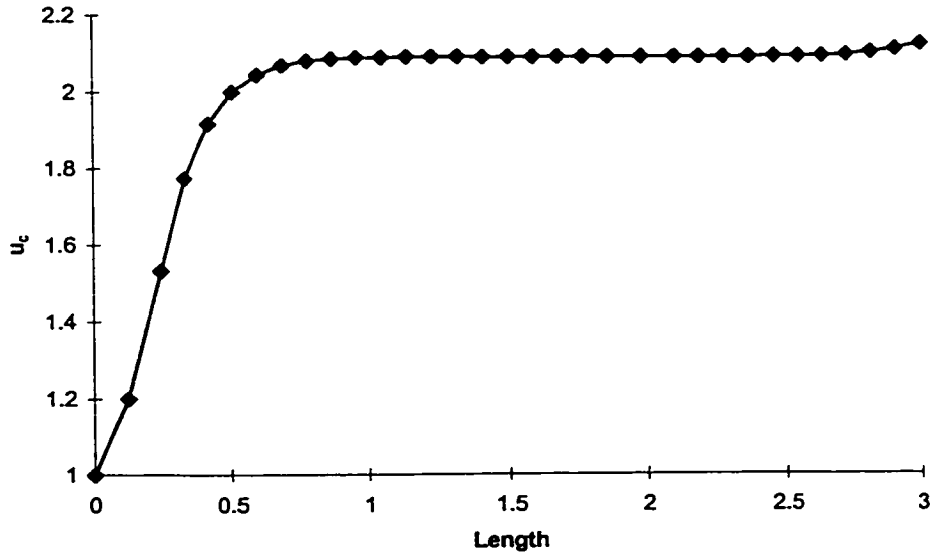

Figure 4-5: Comparison of S_{vm} between cases A & B

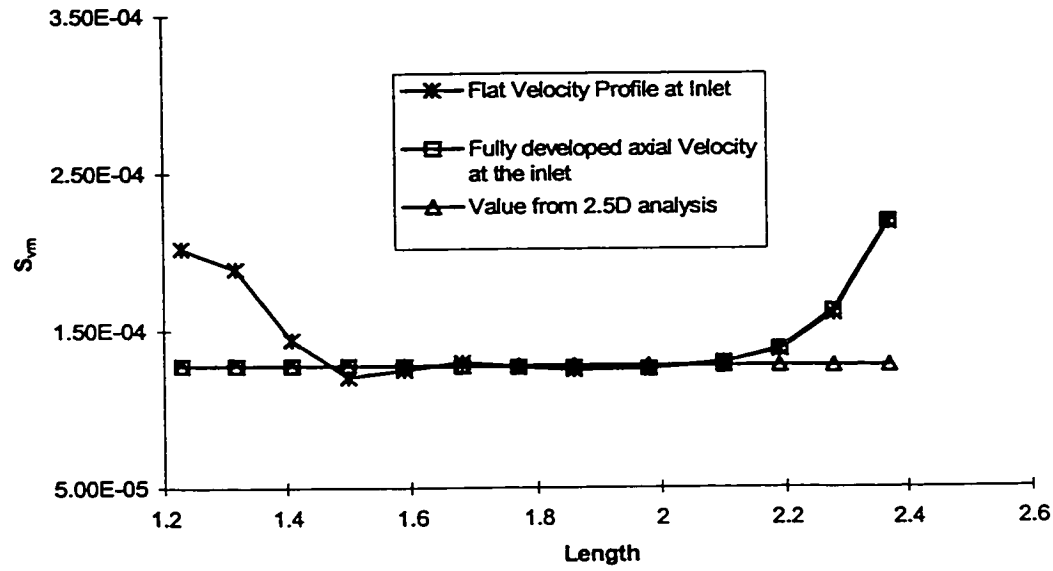

To ensure the validity of the results, case A was also studied for a denser mesh (13x6x6). Results from each cross-section of two meshes (13x4x4 and, 13x6x6) were compared with the fully developed solution for 4x4 and 6x6 meshes. The axial pattern of both meshes were similar. The axial pattern of gridlines is shown in Figure 4-6. Cross-sections of the meshes with the velocity vectors depicting the vortices pattern are shown in Figures 4-7 and 4-8.

In the study of secondary flows based on the fully developed flow assumption, results were found to be mesh independent. However, fine meshes (10x10 mesh vs. 20x20) were required to show small differences (e.g. less than 3% on average) in transverse velocity values (as reported in Chapter Three).

The average difference between results from the 3-D analysis and the fully developed solution are defined as following.

$$\Delta_{av} = \frac{\sum_{i=1}^{NN} \left| \frac{\phi_{3,i} - \phi_{2,i}}{\phi_{2,i}} \right|}{NN} \tag{4.5}$$

where NN is the number nodes in each cross-sectional plane (normal to the direction of the flow), ϕ_3 is the calculated value of the variable ϕ, at each node from 3-D analysis, and ϕ_2 is the corresponding value from 2.5-D analysis.

Figure 4-6 : Axial pattern of the meshes

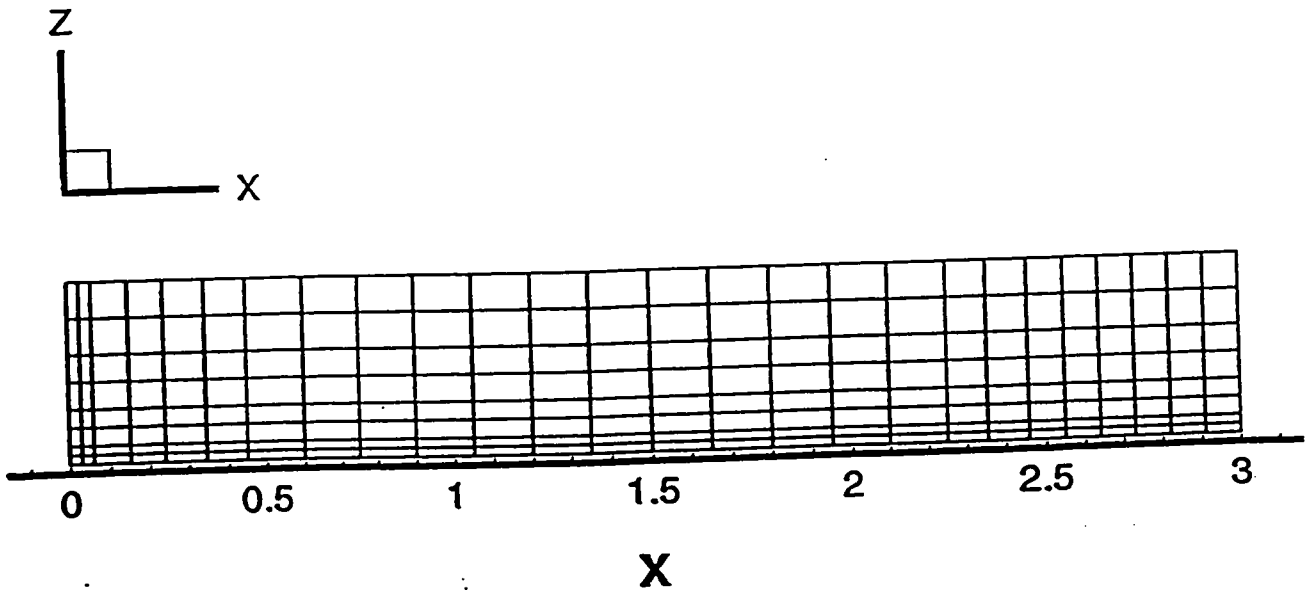

Figure 4-7: Transverse velocity vectors for a mesh with 4x4 elements at cross-section (x=1.5D)

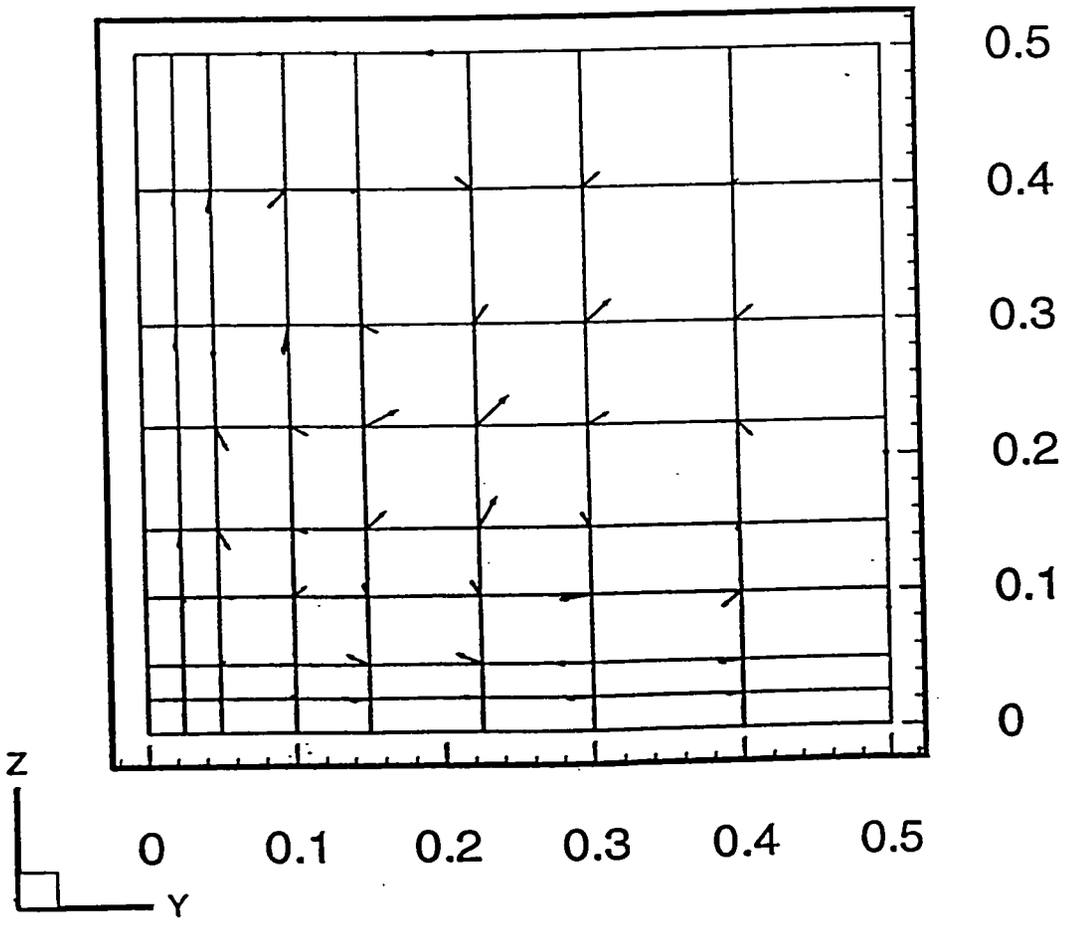

Figure 4-8: Transverse velocity vectors for a mesh with 6x6 elements at cross-section (x=1.5D)

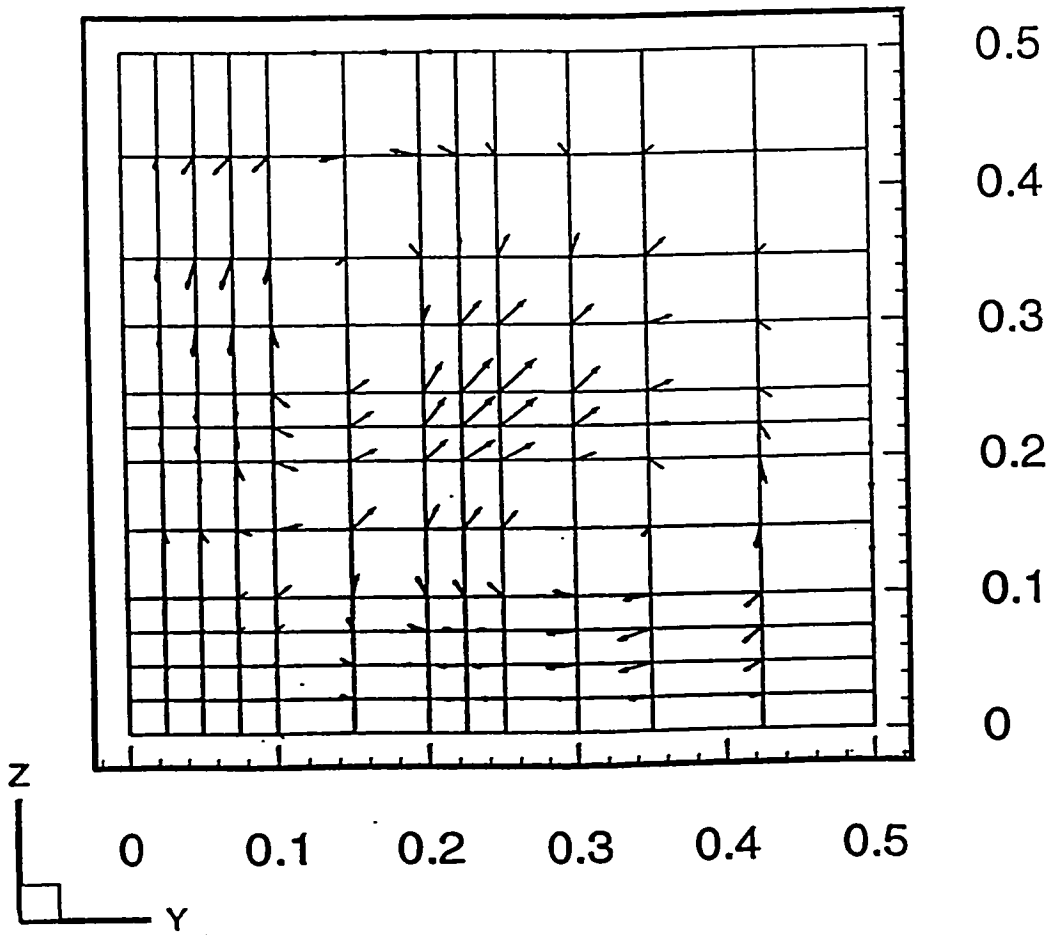

The average difference (Δ_{av}) for velocity components is shown in Figures 4-9 and 4-10 for the two meshes.

Figure 4-9: Comparison between fully developed and 3D solutions (4x4 mesh)

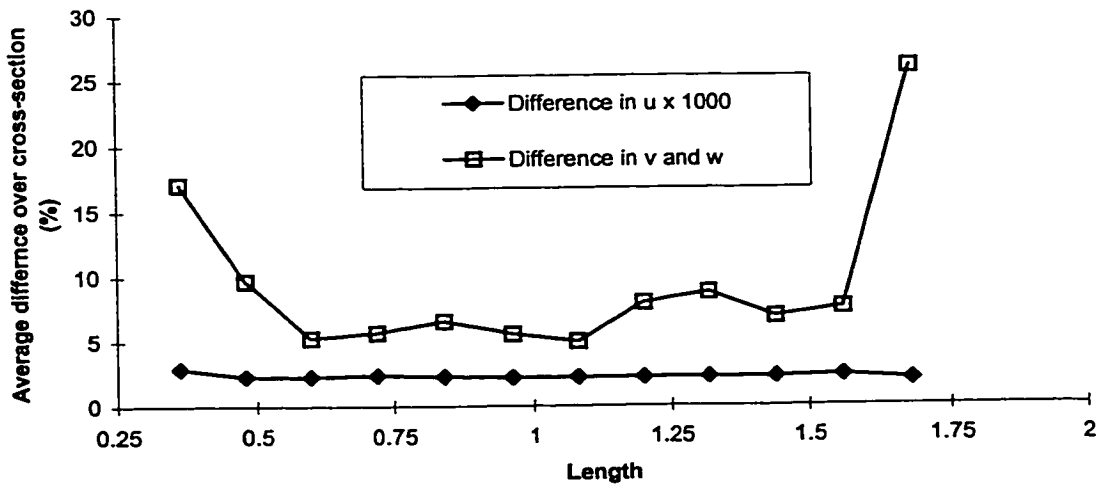

There is a very good consistency between results for the u (axial velocity). There was even better consistency for the denser mesh (6x6). The average difference in u velocity at the exit plane from 3-D analysis was 0.014% for the two meshes. The average difference for v and w was 4.2%.

As seen in Figure 5-11, the average difference between the solution from the two analyses (2.5-D analysis and 3-D analysis) is between 5 and 10%. The average absolute error defined as;

$$\Delta_{|av|} = \frac{\sum_{i=1}^{NN} \left| \phi_{3,i} - \phi_{2,i} \right|}{NN} \tag{4.6}$$

was of order of 10^{-7}.

Figure 4-10: Comparison Between Fully developed and 3D Solutions (6x6 mesh)

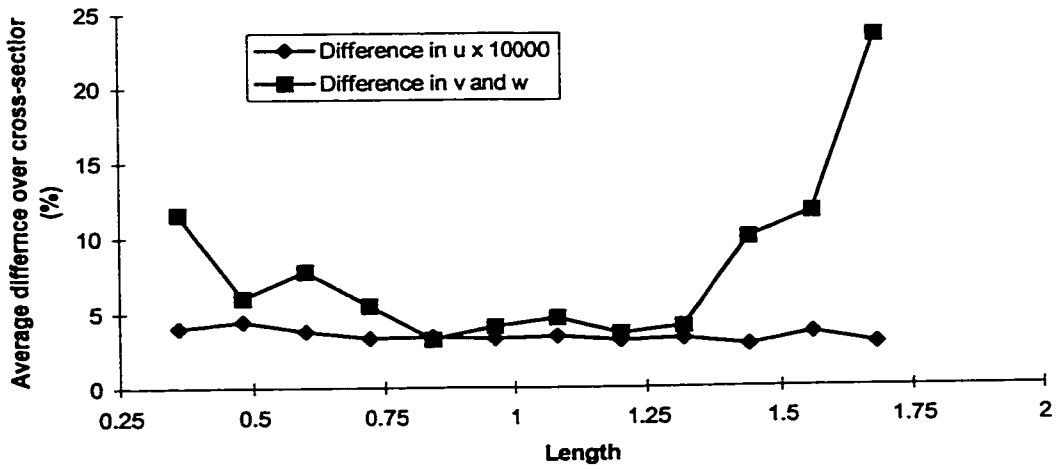

In the case of the second mesh (13x6x6) there were points ((0.025, 0.35) ,(0.025, 0.425), (0.35, 0.025), (0.425, 0.025)) where there were significant differences between the values of v and w. These have been neglected in Figure 4-10. Inclusion of those points would have increased the average error two to four fold.

An interesting observation was the comparison of the pressure values between the 3-D and the fully developed flow solution. The pressure drop in the axial direction calculated from the fully developed solution was 28.187 (dimensionless) and pressure drop based on the difference of average pressure at each cross-section from the 3-D analysis was 28.186. Therefore the assumption to decouple pressure into an axial gradient and an in-plane function did not result in a significant error in the prediction of

pressure drop in the flow direction. Comparison of the in-plane pressure difference between the two methods of analysis showed an average of 6.7% difference.

4.3- Further tests on the solution behavior

To find out the reason for the destruction of vortices and subsequent increase in u velocity some further numerical tests were performed applying case A boundary conditions. One of these sets of tests was to examine effect of viscoelasticity on the behavior of the solution. Cases of no secondary flow were also examined. The other test was to drop the x-derivatives of the stress.

To investigate effect of viscoelasticity two cases with higher elasticity were studied. In one case β was increased from 0.1 to 0.3. In the second case Weissenberg number was increased from 0.1 to 0.3. Results for both cases are compared with the solution using the fully developed assumption as shown in Figure 4-11.

Essentially the same pattern of behavior for S_{vm} (Figure 4-2) involving an overshoot, a plateau and final increase was observed for the two cases. In the case of Wi=0.3 there was a higher overshoot in S_{vm}, near the inlet where it increases from zero to its fully developed value.

Figure 4-11: S_{vm} Progress along the duct (effect of higher elasticity

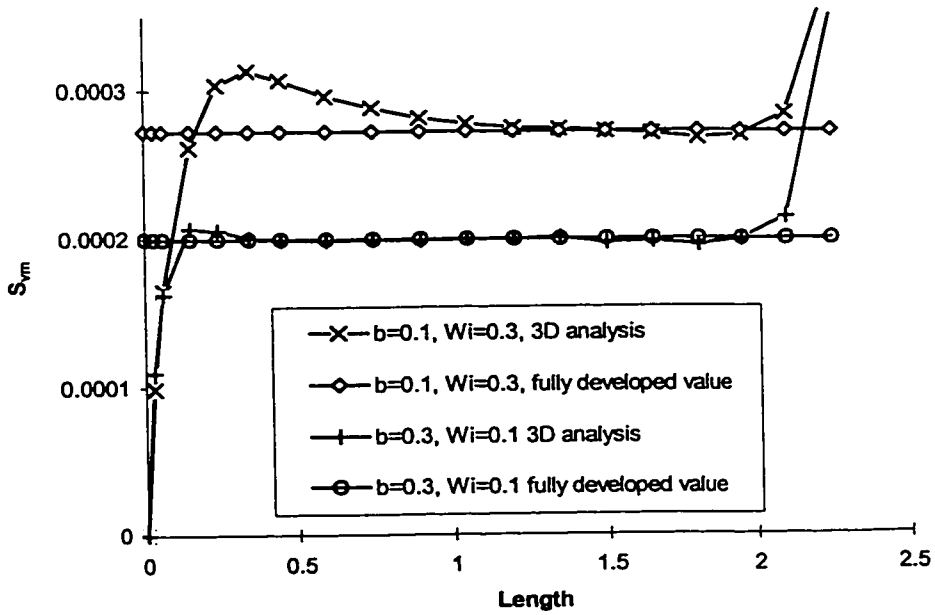

The second test (to evaluate the effect of elasticity) was to eliminate its effect by making Wi=0. For the case Wi=0, $n \leq 1$ and $\Gamma \neq 0$, the MPTT model reduces to the Carreau model. The prediction of the u-profile at the beginning of the duct was consistent with the solution using the Carreau model (using the direct implementation and without decoupling of the stresses). However, a deviation from the fully developed flow profile still occurred at the end section of the duct. There was no pattern of vortices anywhere in the duct, however a similar pattern of secondary flows toward the center (Figure 4-1), was observed at the end of the duct.

Other cases of no-secondary flows were also tested (i.e. ζ=0 and ε=0). For these cases, it is expected that the Neumann boundary conditions at the outlet work. There was no pattern of vortices; however, the same pattern (Figure 4-1) was observed at the end of the duct. It was concluded that neither viscoelastic nature of the fluid nor the presence of secondary flows are responsible for the behavior of the solution at the end of the duct as it occurred even in the absence of second normal stress differences.

Since the pattern of Figure 4-1 was observed even when the MPTT model was reduced to the Carreau model, the presence of source terms was considered as the possible cause of the problem, since this problem was not observed in the solution when Carreau model was implemented directly. This idea was further investigated and discussed in the next section.

Another test was to drop the derivatives of stress components with respect to x (axial direction). Equations 2.58 to 2.60 were modified to the following to see if the derivatives of the stress components in x direction are responsible for the deviation of the solution near the end of the duct .

$$K_u^{\bullet} u^{i+1} = C_x p^{i+1} - Q_y T_{xy}^{\bullet} - Q_z T_{xz}^{\bullet} \tag{4.7}$$

$$K_v^{\bullet} v^{i+1} = C_y p^{i+1} - Q_y T_{yy}^{\bullet} - Q_z T_{yz}^{\bullet} \tag{4.8}$$

$$K_w^{\bullet} w^{i+1} = C_z p^{i+1} - Q_y T_{zy}^{\bullet} - Q_z T_{zz}^{\bullet} \tag{4.9}$$

As shown in Figure 4-12, the middle zone (where the vortex pattern is observed) was extended without any change in the value of S_{vm}. The value of u_c at the outlet was reduced from 2.1322 (with derivatives of stress included) to 2.098 (without derivatives of stress) while the fully developed value was 2.092 (Wi=0.1, Γ=0.1, β=0.1, ε=0.1, and ξ=0.2). Basically, this assumption reduced the magnitude of deviation from the fully developed solution that occurs at the end part of the duct but did not eliminate it. However, the test reinforced the idea that source terms in momentum equations are responsible for the deviation from the fully developed solution because any increase or decrease in the value of the source terms had a direct impact on the magnitude of the deviation from the fully developed flow solution.

Figure 4-12: S_{vm} Progress along the duct (neglecting stress terms in the direction of the flow)

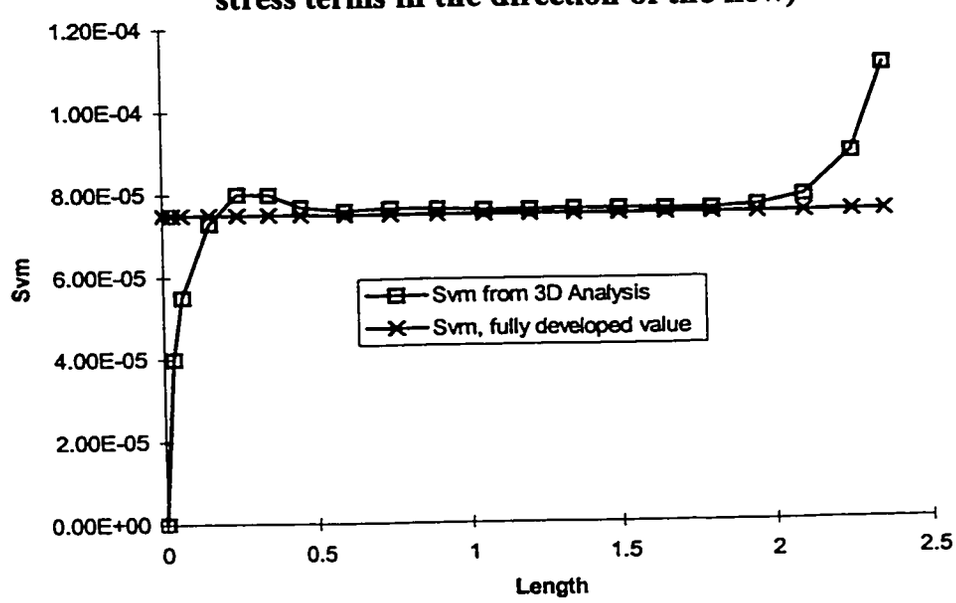

4.4- Discussion of the Results

Reviewing the results of the 3-D analysis, two questions arise:

1. Is there a fully developed solution for viscoelastic flow in a straight duct?

2. If there exists a fully developed solution for the viscoelastic case, why does 3-D analysis deviate from that near the outlet? What is the source of the deviation from the fully developed flow that appears in the middle of the duct?

From observations that were made during the test cases it can be stated that:

1- The fully developed solution is a solution for at least part of the domain, and in that part of the domain, u, v and, w do reach values that are independent of x (direction of the flow).

2- The problem of destruction of the vortices and subsequent increase in u velocity is not because of the viscoelastic nature of the flow, or presence of the secondary flows, as it happened even when Wi=0.

3- The problem is somehow related to the presence of source terms in the momentum equations since it does not occur with the direct implementation of the Carreau model and does occur when it is implemented through the EVSS method.

Sizaire and Legat (1998) have analyzed coextrusion of viscoelastic materials in tubes. While they had success with Reiner-Rivlin model (Macosko, 1994) they report problems of convergence with the Geisekus model (Geisekus, 1982), even at low Wi. The Geisekus model was implemented using source terms in the momentum equations while Reiner-Rivlin model was directly applied to the momentum equations (because stress components are explicit in terms of velocity gradients in Reiner-Rivlin model). This indicates (as it has been concluded here) that viscoelasticity or the presence of secondary flows are not responsible (since the Reiner–Rivlin model works) and perhaps the application of source terms is causing numerical divergence.

On the other hand, decoupling of elastic stresses and introducing them as source terms in the momentum equations has been successfully applied in many cases including 2.5-D analysis that was used in the previous chapter. Therefore, the difference between 3-D analysis and 2.5-D analysis in this regard needs to be explained.

In a fully developed flow, flow variables are independent of their position in the direction of the flow. When there is no source term in the momentum equation, applying boundary conditions at the proper length ensures that from that point on, the u profile is

not a function of x. Having source terms in the momentum equations, however, suppresses having a fully developed flow. For example, consider a flow with a heat source where the temperature is rising in the flow direction without reaching any fully developed value. Forcing the temperature by boundary conditions (such as $T=T_o$ or $dT/dx=0$) at any point, results in non-realistic and artificial results. Now in the case of solving the equations of motion where stresses are decoupled and treated as source terms they result in artificial results when they are forced by the boundary conditions requiring fully developed flow.

Behavior of the solution in the middle zone shows that when the equations are not under the influence of imposed boundary conditions the solution is similar to fully developed solution, and deviation from the fully developed flow occurs near the outlet where boundary conditions are applied. Therefore, it was hypothesised that combination of the presence of the source terms and forced boundary condition results in non-realistic solutions at the end of the duct. To investigate this hypothesis the following tests were carried out.

The first test was to eliminate source terms from the u momentum equation. A case was selected such that the parameters for Carreau model and PTT model were known to produce similar u velocity profiles (Matsunaga et al., 1995, Kajiwara et al., 1993). The Carreau model was used in the x momentum equation directly eliminating the need for considering source terms in u momentum equation.

$$K_u^* u^{i+1} = C_x p^{i+1} \tag{4.10}$$

where K_u is calculated using Carreau model as follows.

$$K_u = \int_{\Omega_e} \eta(\dot{\gamma}) \frac{\partial N_i}{\partial x} \frac{\partial N_j}{\partial x} d\Omega \tag{4.11}$$

Since derivatives of the stress in the x direction are forced to zero in the fully developed flow, T_{xx} is not present in the x-momentum equation. Therefore it is not important that the Carreau model does not predict T_{xx} as far as the x-momentum equation is concerned. For the y and z momentum equations, the EVSS method was used, with stresses calculated from the PTT constitutive equation.

$$K_v^* v^{i+1} = C_y p^{i+1} - Q_x T_{yx}^* - Q_y T_{yy}^* - Q_z T_{yz}^* \tag{4.12}$$

$$K_w^* w^{i+1} = C_z p^{i+1} - Q_x T_{zx}^* - Q_y T_{zy}^* - Q_z T_{zz}^* \tag{4.13}$$

The result was a reduction in final u velocity. The calculated u_c at the outlet was 2.066 compared to 2.15 before the modification (u_c was calculated as 2.042 from 2.5-D analysis). The increase in u_c was of course associated with break up of the vortices pattern. Therefore, the modification although it proved effective to some extent was not yet sufficient.

While the source terms in u momentum equations were eliminated, they were still present in the y and z momentum equations and boundary conditions in x direction had their effect. Pressure is the only variable that connects these equations and hence transfers the problem from the y and z momentum equations to the x momentum

equation. Therefore, to suppress effects of y and z momentum equations on the u calculation, a constant Δp was imposed in x momentum equation and p was calculated as a function of y and z only. The problem of the deviation from the fully developed solution was then completely eliminated.

After decoupling the pressure it was no longer necessary to use the Carreau model. Decoupling the pressure for the PTT and MPTT models resulted in a fully developed solution without any deviation. The vortex structure continued until the end of the duct and the same u velocity profile was maintained. These vortices form a spiral form in 3-D duct as they are not closed streamlines (as appears in the 2-D plots). 3-D visualization of the spiral form vortices is depicted in Figure 4-13.

It is important to note that applying vanishing transverse velocities as boundary conditions at the outlet, as carried out in Sizare and Legat (1998) and Takase et al. (1998) does not eliminate the problem. Applying this type of boundary condition reduces the intensity of the deviation in the solution near the end of the duct. As elasticity and intensity of the secondary flows increases, deviation at the boundary becomes more important and could result in divergence of the solution.

Figure 4-13: 3-D visualization of the spiral form vortices

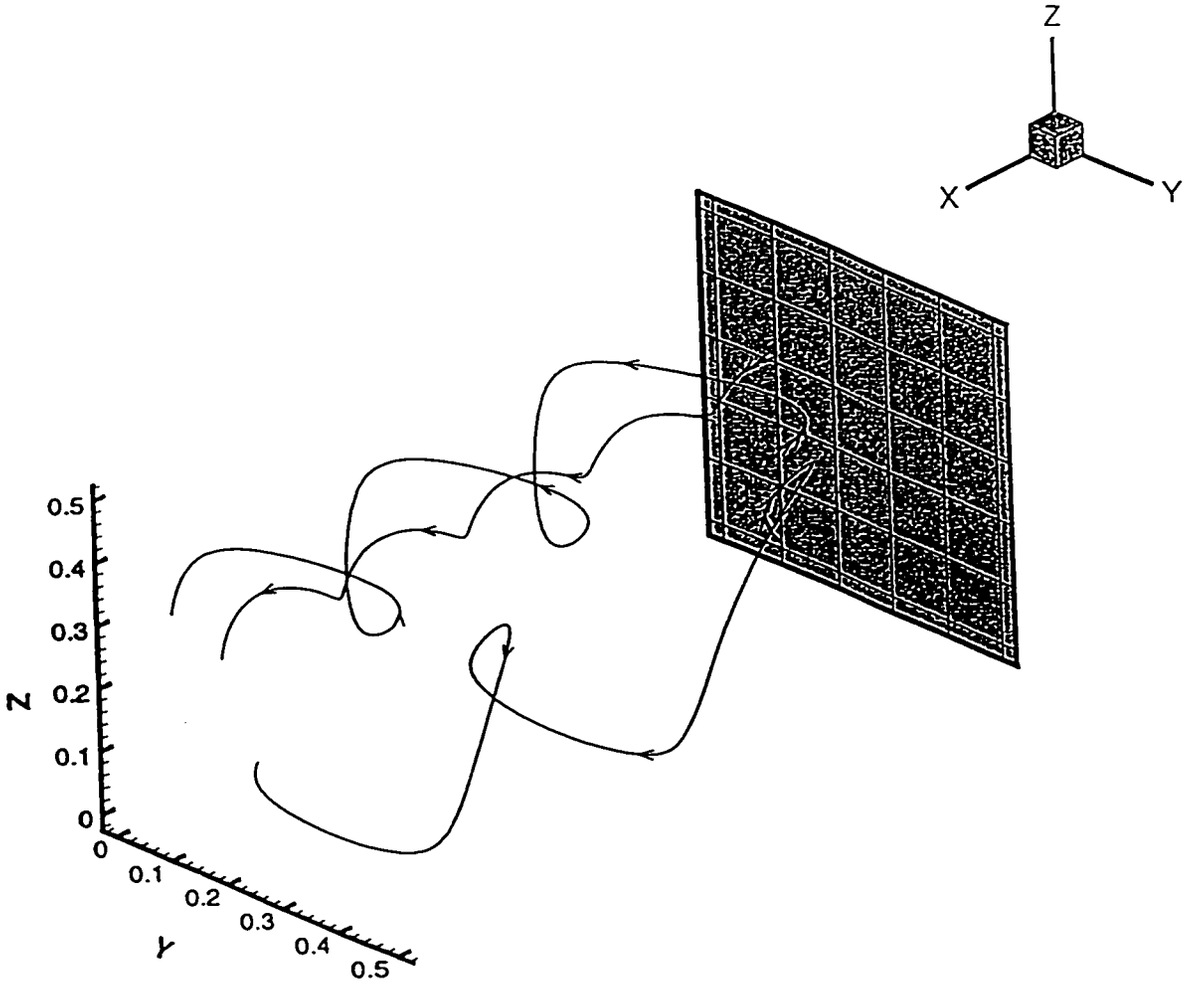

By clarifying the problem of deviation in the solution near the duct outlet three important conclusions can be drawn:

1- The fully developed flow of viscoelastic fluid does exist and it is a valid solution to the 3-D equations of the flow. The solution is consistent with the solution obtained from 2.5-D analysis.

2- An explanation was offered regarding the deviation from the fully developed solution near the outlet boundary as it is due to the presence of the source terms in momentum equations. The problem is not caused by the viscoelastic nature of the flow.

3- The problem is not eliminated by forcing the secondary flows to zero at the outlet boundary (i.e. $v=0$, $w=0$). Applying Dirichlet boundary conditions for v and w at outlet can result in divergence as the magnitude of source terms increase.

It is important to develop a formulation that can be used for the general 3-D problem where Δp is not necessarily constant. The following methods were tested for overcoming the problem of deviating solutions near the outlet boundary without restricting pressure in the whole domain.

1- Adding 1D to the length of the duct to assure a fully developed solution and decoupling the pressure for that added part only as it was observed that 1D was a sufficient length to obtain fully developed solution. For the rest of the domain pressure remains in its general form.

2- Introducing pressure in formulation in the following form;

$$p = \Delta p + p'(x, y, z)$$

and to assure fully developed flow at the end of the duct, it is necessary to force the $dp'(x, y, z)/dx = 0$ throughout the length over which fully developed flow is expected and not only at the exit plane. Therefore the criteria for any formulation to produce fully developed solutions can be restated so that any formulation that ensures $dp'/dx = 0$ over a certain length (1D) of the duct will result in a fully developed solution. The pressure drop (per unit length) can be obtained from 2.5-D analysis.

4.5- Concluding Remarks

In this chapter, the fully segregated 3-D creeping flow formulation that was described in Chapter Two was examined and verified. Formation of the secondary flows from different initial conditions was studied. It was shown that, although the fully developed solution is obtained in part of the domain, there is a problem (destruction of

the vortices) near the outlet that is related to the boundary condition , as the problem persisted even by changing the mesh or the length of the duct.

Several numerical experiments were done to show that the problem (destruction of vortices and a subsequent increase in u) arises from a conflict between introduction of source terms in momentum equations and the boundary conditions that forces a unidimensional solution that is not physically consistent with the rest of the domain. The most crucial test was implementing the Carreau model both directly and indirectly (using EVSS method) which showed similar problem. It showed that the problem is not the viscoelastic nature of the flow. The problem was attributed to the inconsistency of fully developed boundary conditions with the presence of the source terms in the differential equations that are being solved for the kinematics of the flow. It was also established that fully developed solution for the viscoelastic flow obtained from 2.5-D algorithm is consistent with the solution from 3-D analysis.

3-D analysis also showed the effect of different initial conditions. 3-D analysis of different boundary conditions showed that secondary flows appear soon after the primary flow velocity (u) reaches its fully developed state.

As the last step in assessment of the proposed method, its performance will be examined in cases of flow in complex geometries, in the next chapter.

Chapter 5

Viscoelastic Flow in Complex Geometries

Modelling of polymer flow in complex geometries is very important for industrial applications. During processing, polymers often flow through geometries involving sudden contractions or expansions or through ducts with converging and diverging zones. Due to the complex nature of polymeric behaviour in such flow domains, it becomes increasingly important to be able to predict polymer flow behaviour. It is important to predict flow variables such as pressure, velocity and stress components, to be able to properly design tools (e.g. dies) and obtain desirable properties and physical characteristics in the final products.

Flow of polymers in complex geometries is also important from an analytical point of view. Regardless of the industrial application, analysis of flows in such geometries constitutes a good test for the performance of a numerical method, or a

constitutive equation. Therefore, there have been numerous papers in this area, especially in the study of flow through sudden contractions. However, most have concentrated on two-dimensional modelling of such flows, due to the enormous memory and run times required by the 3-D analysis of such flows.

The presence of secondary flows suggests that the flow of viscoelastic fluids, even in a straight duct, has a three dimensional aspect. Apart from that, any complexity in the geometry results in a more complex flow field involving transverse velocities with higher intensities. Ignoring the three dimensionality of the flow can be misleading, or a poor representation of the flow at least.

The purpose of this chapter is to demonstrate that the algorithm that has been developed in Chapter Two and tested in Chapter Four, is capable of modelling the flow in complex geometries. In order to evaluate the algorithm, two test cases; one involving a converging duct and another involving a sudden contraction, were selected from the literature for comparison. Model parameters were extracted from literature where 2-D analyses for those experimental cases were performed.

A 2-D version of the segregated algorithm is also developed to model planar flow in two-dimensional complex geometries for further comparison. Results of 2-D and 3-D analyses were also compared.

In the first section, the converging duct is analysed and discussed. This is followed by an analysis of a duct with a sudden contraction in the next section. In the study of straight ducts, the most important viscoelastic aspects of the flow were the presence and magnitude of the secondary flows, which are related to the elastic stresses in cross sections normal to the flow. In the study of flow in complex geometries; however, the focus will be on estimation of the stresses. Stress values are directly related to the elastic nature of the fluid, and depend –among other things- on the performance of the constitutive equation and accuracy of its parameters.

5.1- Converging Duct

One of the comprehensive experimental studies on flow of a polymer melt in the converging duct was conducted by Kajiwara et al. (1993). The polymer used was a low density polyethylene (Novatec F155, M.I.= 2.0), for which the material properties are reported in Kajiwara et al. (1993). The geometry consisted of a converging duct with a 60° angle of convergence resulting in a 4:1 reduction in height from upstream to downstream. The cross section of the duct is a rectangle with an aspect ratio of 2:1 in upstream, increasing to 8:1 downstream.

Three types of analyses were performed: 3-D and 2-D analyses of the complex geometry and 2.5-D analysis of the rectangular cross-section (normal to the flow) in the downstream.

The 3-D mesh (nodes are placed at the intersection of the gridlines) for the converging duct used for three-dimensional analysis is shown in Figure 5-1. It consists of 13x5x5 elements in the x, y, and z directions. A side view (x-z plane) of the mesh is shown in Figure 5-2. The meshes at the inlet and outlet of the duct (y-z plane) are shown in Figures 5-3 and 5-4.

A typical mesh that has been used for 2-D analysis (planar flow) of the converging duct is shown in Figure 5-5 representing the x-z plane. In Figure 5-6, the mesh that has been used to obtain a solution for fully developed flow at the outlet is shown. It consists of 6x5 elements in y and z directions.

Neumann boundary conditions for velocities were applied at outlet of the duct (case A in Chapter Four) and the length of the duct was several d (where d is the depth of the duct in the downstream section) to ensure fully developed flow in downstream of the contraction. Fully developed flow was applied at the inlet, for 3-D analysis. The fully developed solution was obtained from 2.5-D analysis. In 2-D planar analysis, a flat velocity profile was imposed at the inlet of the duct.

Kajiwara et al. (1993) used following PTT model parameters in their 2-D analysis. The parameters are shown in the following table.

Table 5-1: PTT parameters (Kajiwara et al., 1993)

η_o (Pa.s)	19500
λ (s)	1.0
β	0.9333
ε	1.87
ξ	0.22

The flow rate in the experiments was 0.75 cm^3/sec and the entrance cross-section was 4x2 cm^2 (width and depth respectively). In the next section the results for 2-D analysis are discussed followed by the results for the 3-D analysis.

Figure 5-1: 3-D Mesh of converging duct

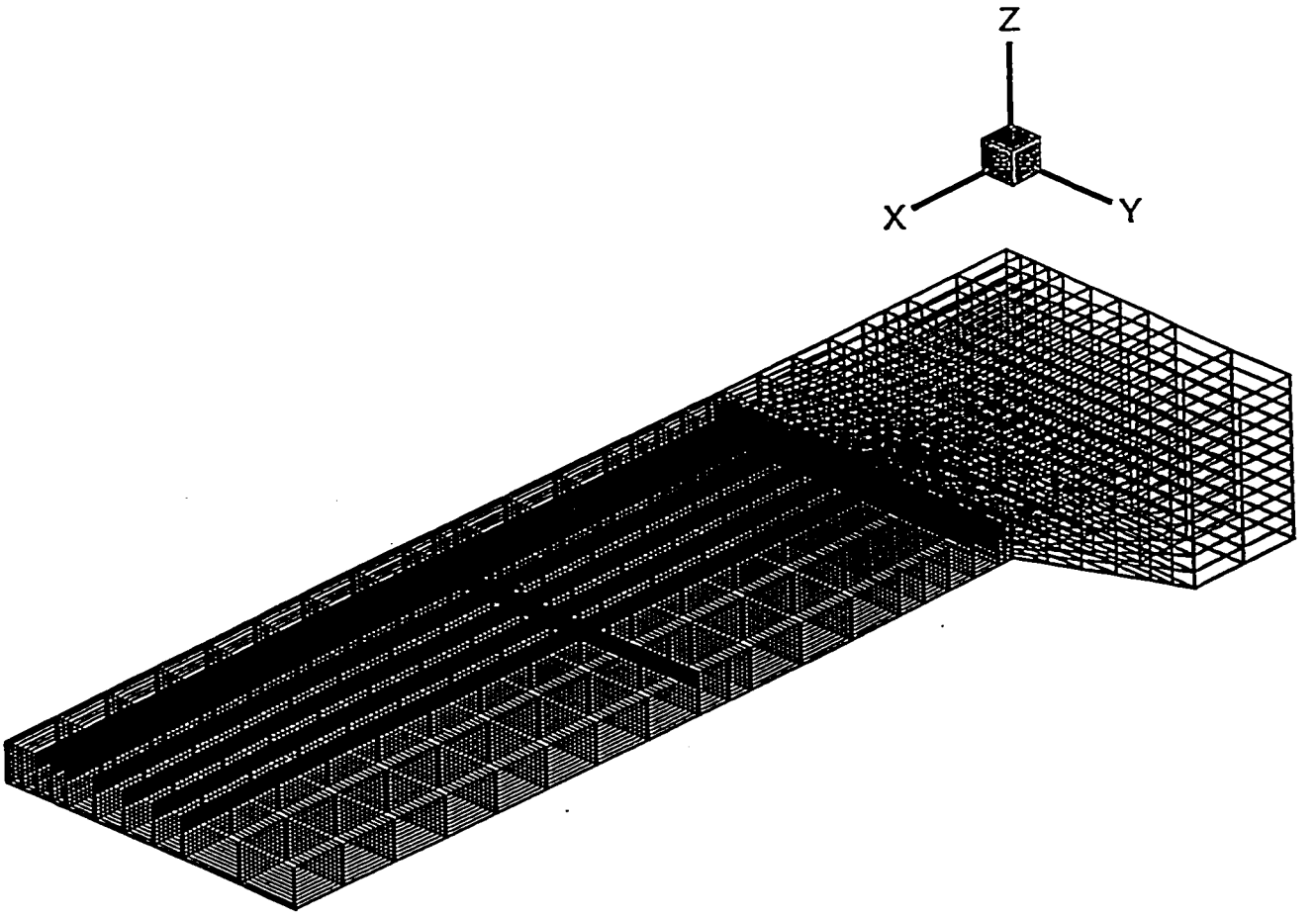

Figure 5-2: Side view of 3-D mesh for converging duct (x-z plane)

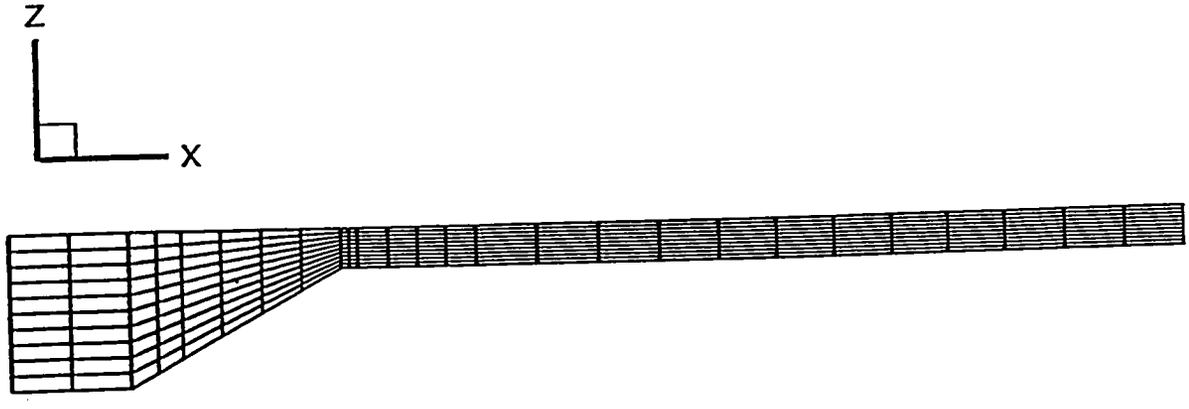

Figure 5-3: Inlet for 3-D mesh of converging duct (y-z plane in upstream)

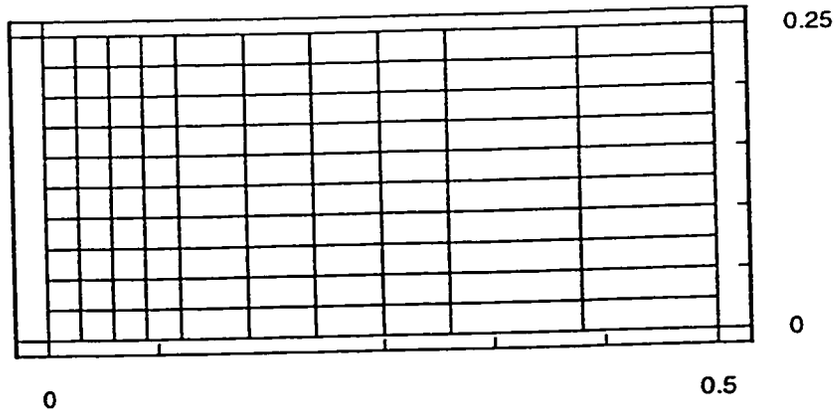

Figure 5-4: Outlet for 3-D mesh of converging duct (y-z plane in downstream)

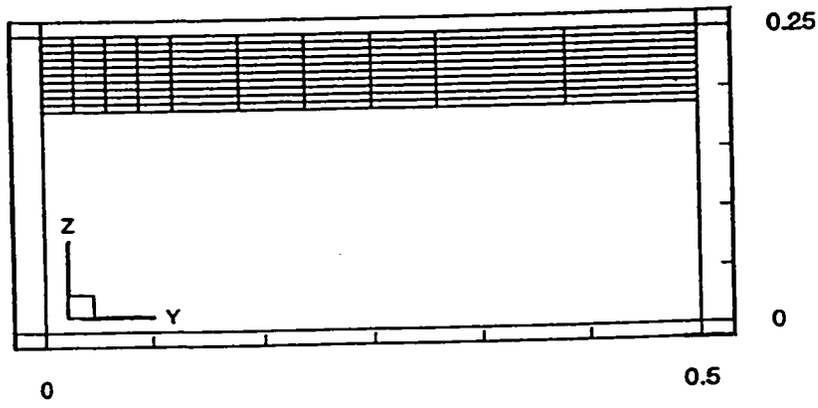

Figure 5-5: 2-D mesh for planar flow analysis of converging duct (x-z plane)

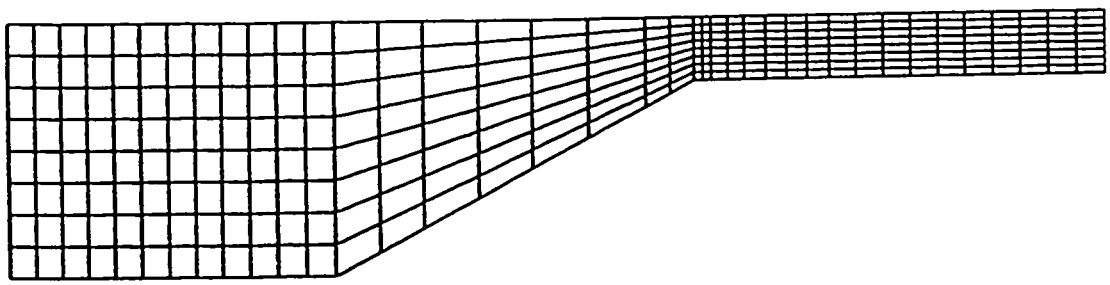

Figure 5-6: 2-D mesh for analysis of fully developed flow at downstream of the duct (y-z plane)

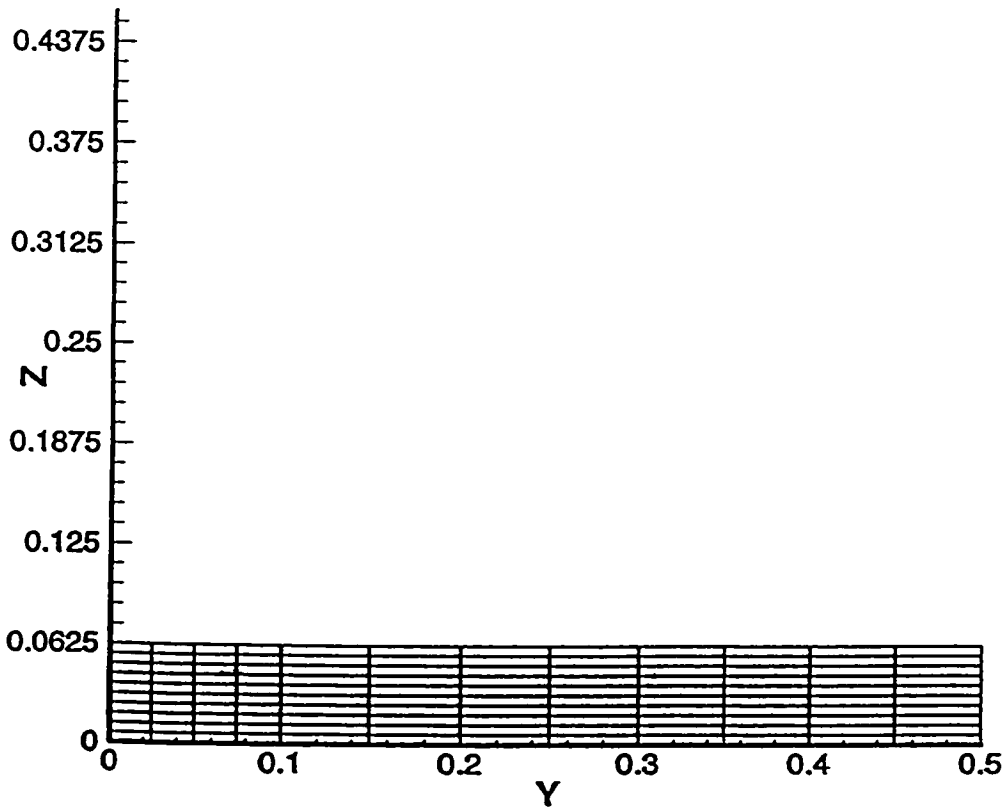

5.1.1- Results of analysis of the flow in the converging duct

As a first step in evaluating the results, stress components were compared at the downstream section where fully developed flow is achieved. Figure 5-7 shows the results for T_{xz}, obtained from 2-D (planar flow) analysis (x-z plane) in the fully developed region, and from 2-D analysis of the y-z plane based on fully developed assumption. Results for the stress in the y-z plane have been averaged over the width and are reported for each z, as Kajiwara et al. (1993) reported experimental results. They mention that this average value may correspond to the experimental value which contains the side wall effect. Results of the analysis of the fully developed solution is referred to as 2-D rectangular as it is performed for the rectangular outlet of the duct.

Figure 5-7: Comparison of Txz from 2-D analysis and Kajiwara's experiment Wi=24

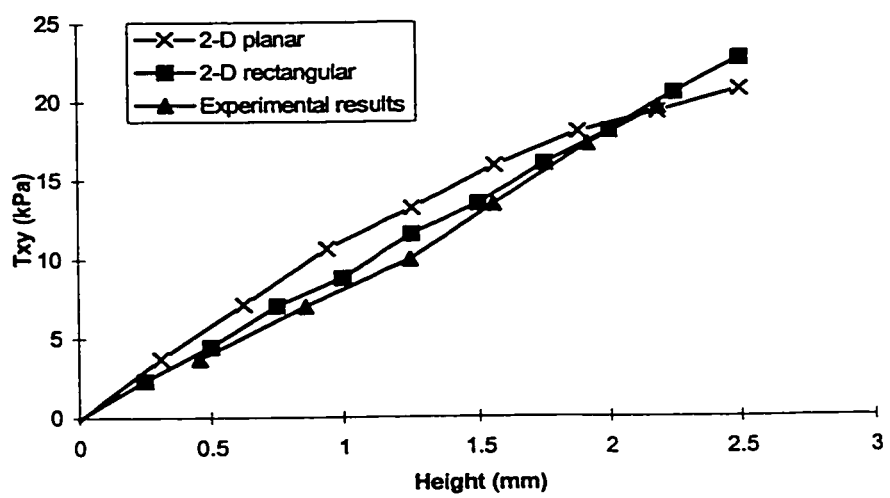

Results for the normal stress difference (T_{xx}- T_{zz}) are reported in Figure 5-8. As can be seen from Figures 5-7 and 5-8, good agreement is observed between the experimental results and computational results. There is also good consistency between results from the two types of analysis, noting that two different algorithms have been used to obtain them. The 2-D analysis in the x-z plane is based on the algorithm that is used for 3-D analysis while the 2-D rectangular results are based on the fully developed flow assumption. Results from the solution of the fully developed flow (y-z plane) are in better agreement with the experimental values.

Figure 5-8: Comparison of Txx-Tzz from 2-D analysis and Kajiwara's experiments Wi=24

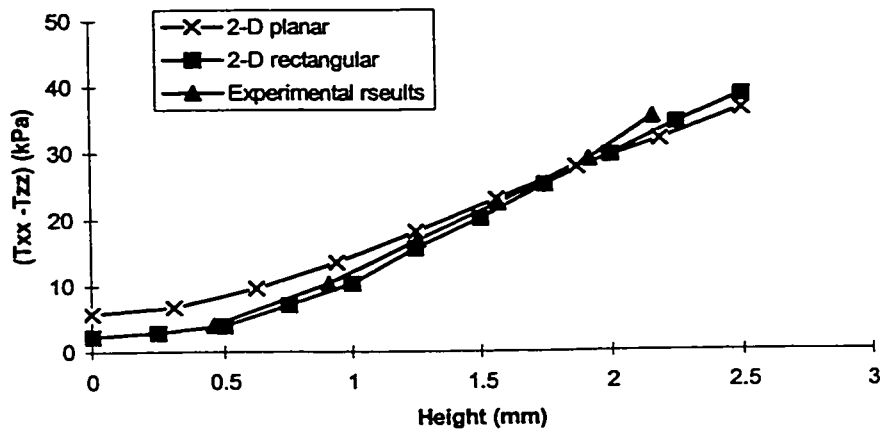

Kajiwara et al. (1993) used a mixed finite element approach to solve continuity, momentum, and constitutive equations simultaneously to obtain pressure and components of velocities and stresses. They also made the assumption of creeping flow. They used

9-node quadrilateral elements. Similar to this study, velocity and stress components were interpolated by bi-quadratic Lagrangian polynomials while bi-linear polynomials were used to interpolate pressure.

Results from Kajiwara's work and this 2-D analysis using the segregated algorithm for x-z plane and y-z plane are compared in Figures 5-9 and 5-10 for the converging zone. The results are reported at x=8.21 mm from the beginning of the converging section while the converging zone extends to x=13 mm. Results are given in Figure 5-9 for the shear stress T_{xz}, and in Figure 5-10 results are given for the normal stress differences (T_{xx}-T_{zz}).

Figure 5-9: Comparsion between 2-D analysis and experiments (Kajiwara) in converging zone Wi=24

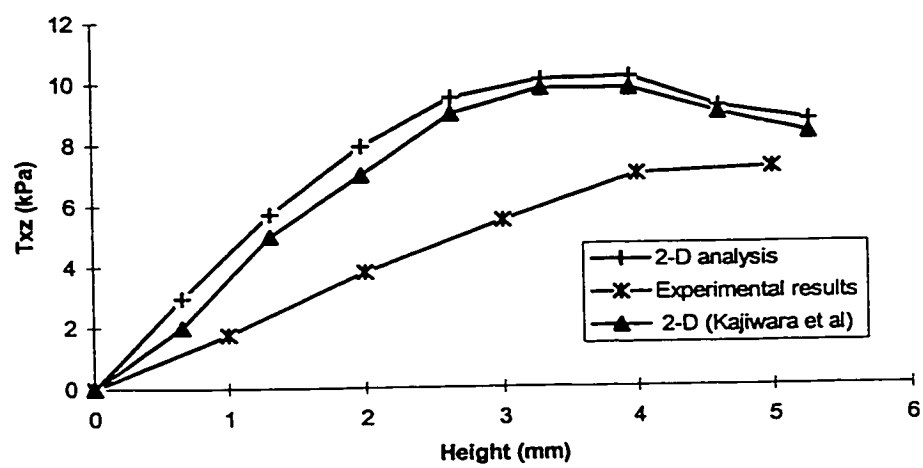

Figure 5-10: Comparison of Txx-Tzz between 2-D analysis and experiments in the converging zone Wi=24

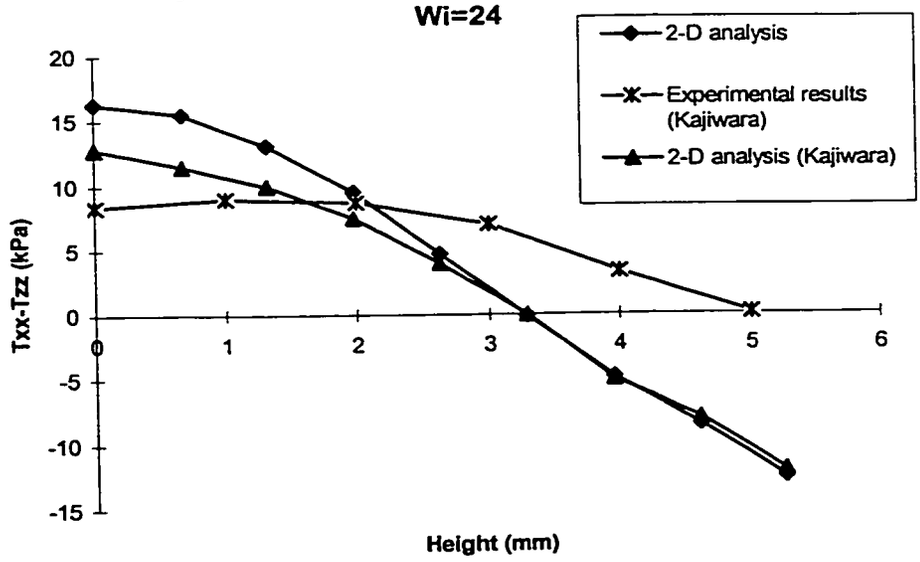

Although the agreement between results of this study and Kajiwara's work is good, the difference between experimental results and analysis is quite substantial. From an analytical point of view there are several reasons for errors in the prediction of the stresses. One important reason is that only a single mode viscoelastic constitutive equation has been used. Flows in complex geometries involve a broad range of shear-rates in the flow domain and this certainly needs a model that can properly describe the polymer behaviour in a broad range of shear-rates, such as multi-mode constitutive equations. The accuracy of model parameters, especially ε, is in doubt since it was not reported that any experiments involving extensional properties were done to obtain ε.

The 3-D simulation of the flow was conducted for the flow rate of 0.75 cm^3/sec, using material parameter from Table 5-1. However, a converged solution was never found for Wi=24 (based on u_{av} and height of the duct in downstream). Different meshes, large relaxation factors and continuation methods (starting from smaller Wi to get the solution and then proceeding to higher Wi) failed to produce a converged solution. The highest Wi that was achieved was 17.92 for the mesh shown in Figure 5-1.

Results obtained from 3-D analysis, were compared to the results from 2-D analysis for Wi=17.92. Figures 5-11 and 5-12 present the comparison in shear stress T_{xz} and normal stress difference $T_{xx} - T_{zz}$. The 2-D analysis was based on the assumption of fully developed flow.

Figure 5-11: Comparison of Txz for 2-D & 3-D cases (fully developed flow at outlet) Wi=17.92

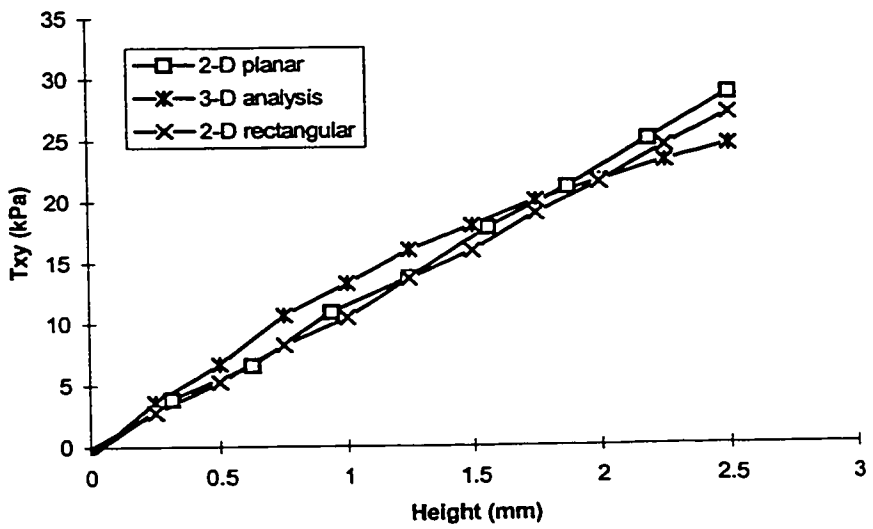

Figure 5-12: Comparison of Txx-Tzz for 2-D & 3-D cases (fully developed flow at outlet) Wi=17.92

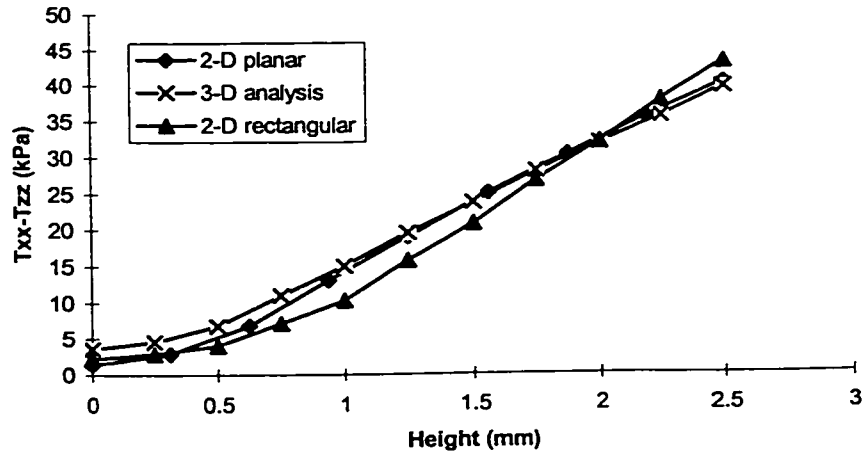

Results for shear stress and normal stress difference were also compared in the converging region. Figures 5-13 and 5-14 show results for the comparison between 2-D analysis (planar flow) and 3-D analysis in the converging zone at x=8.13 mm from the beginning of the converging zone (almost two thirds through the converging zone).

Figure 5-13: Comparison of Txz from 2-D & 3-D analysis in converging zone Wi=17.92

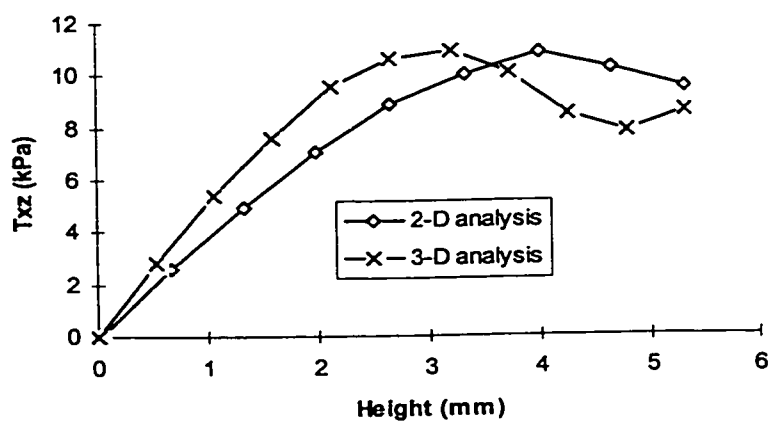

Figure 5-14: Comparison of Txx-Tzz from 2-D &3-D analysis in converging zone Wi=17.92

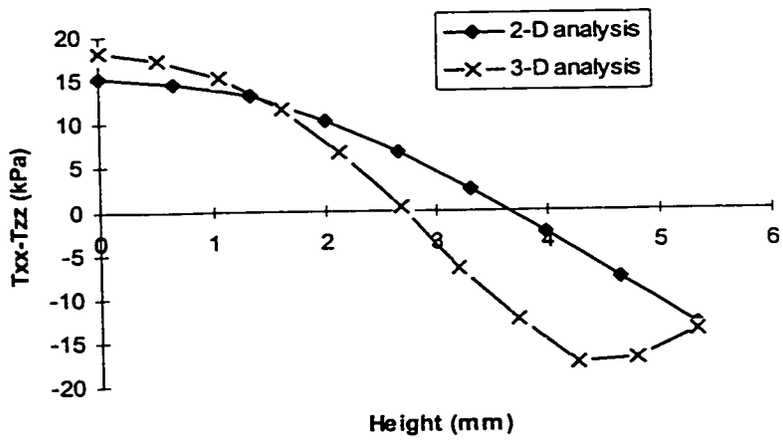

The difference between 2-D and 3-D results can be explained as follows. In the 2-D analysis, the flow is assumed planar, and there is no out of plane velocity components and therefore all the shear rate components associated with it are ignored. However, out of plane velocity components do exist in the converging zone.

Matsunaga et al. (1995) proposed two practical approximate simulation methods for three-dimensional analysis of the viscoelastic flow in a converging duct. These methods were based on obtaining the velocity field by employing a pure-viscous non-Newtonian model and using a viscoelastic model to estimate the stress field. In one of the methods White-Metzner constitutive equation was used, and in the second method stress field was obtained using streamwise integration and the numerical results were compared with experimental values.

Recently Kihara et al. (1998) analysed the flow in a converging duct (similar to the one studied here) using a streamwise integration method. Stress calculations are decoupled from the calculation of kinematics of the flow and are done by integrating the constitutive equation along the duct. The difference between the method that is used in this study and that of Kihara et al. (1998) is in the calculation of the stress and the segregated nature of the method that is used here. As mentioned earlier (Chapter One), it is unlikely that streamwise integration method can be used in modelling general complex 3-D geometries, including those involving longitudinal vortices (Keunings, 1989).

5.2- Duct With a Sudden Contraction

In this section, experimental work by Quinzani et al. (1994) on a duct with a sudden contraction is considered. The geometry, consists of a rectangular duct with a sudden contraction ratio of 3.97:1, and an aspect ratio of 10:1 in upstream. Quinzani et al. (1994) measured velocity and stress fields for several flow-rates. The experimental run with a downstream velocity u_{av} =2.14 cm/sec is considered in this study for comparison (Wi=0.0642). In this case Re=0.08 and therefore applying the creeping flow formulation is justifiable.

The PTT parameters (except ξ) were taken from the paper by Azaiez et al. (1996) and are shown in Table 5-2. A value of ξ=0.2 was selected as a typical estimate for polymers.

Table 5-2: PTT parameters for the polymer solution from Azaiez et al. (1996)

η_o (Pa.s)	1.424
λ (s)	0.03
β	1.0
ε	0.25
ξ	0.2

Similar to the previous section, a 2-D analysis based on the assumption of planar flow is also conducted to compare the results with the experimental values. The 2-D

Figure 5-15: 2-D mesh for a duct with 3.97:1 contraction

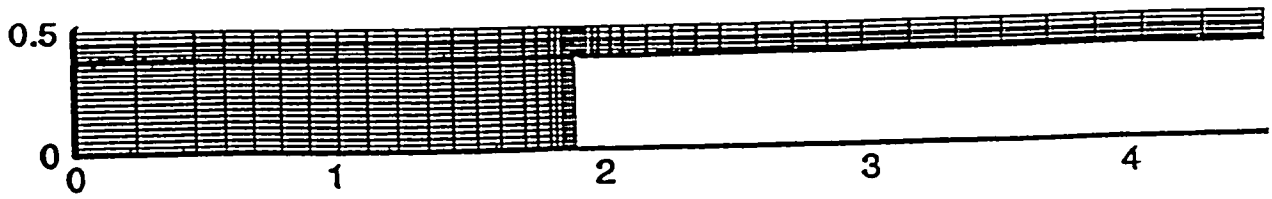

Figure 5-16: Close up of the 2-D mesh near the re-entrant corner

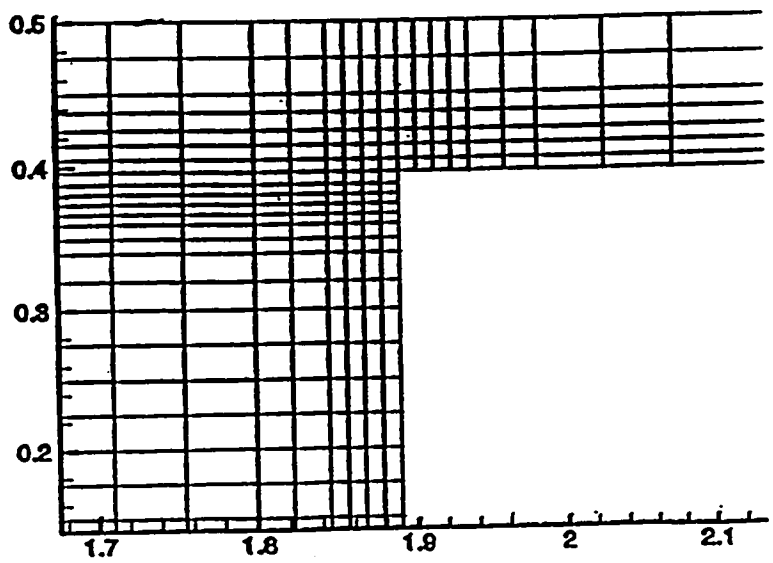

gridline (x-z plane) is shown in Figure 5-15 and a close up view of the gridline near the sudden contraction is shown in Figure 5-16. Intersections at gridlines represent the nodes and each element is consisted of nine nodes.

As a first step, a 2-D analysis of the planar flow was done. At the outlet, gradients of velocity components in x direction was set to zero and at the inlet, a flat velocity profile (with no transverse velocity) was applied. The length of the duct was at least 1D (as shown in Figure 5-15) to ensure fully developed flow both before and after the contraction. In the following figures the results for the u-profile, shear stress (T_{xz}) and normal stress difference (T_{xx}-T_{zz}) are shown for flow upstream of the contraction similar to Quinzani et al. (1994). In the figures below, d represents the distance from the contraction plane (cm) in the upstream section and h represents the height as measured from the centreline (in cm) as shown in Figure 5-17.

Figure 5-17: Schematic view of a duct with sudden contraction

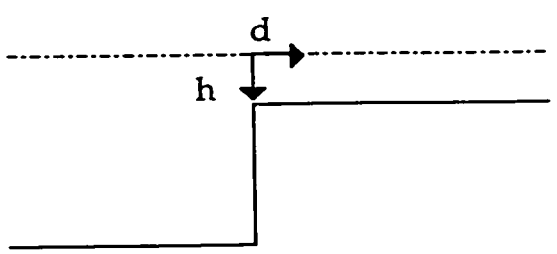

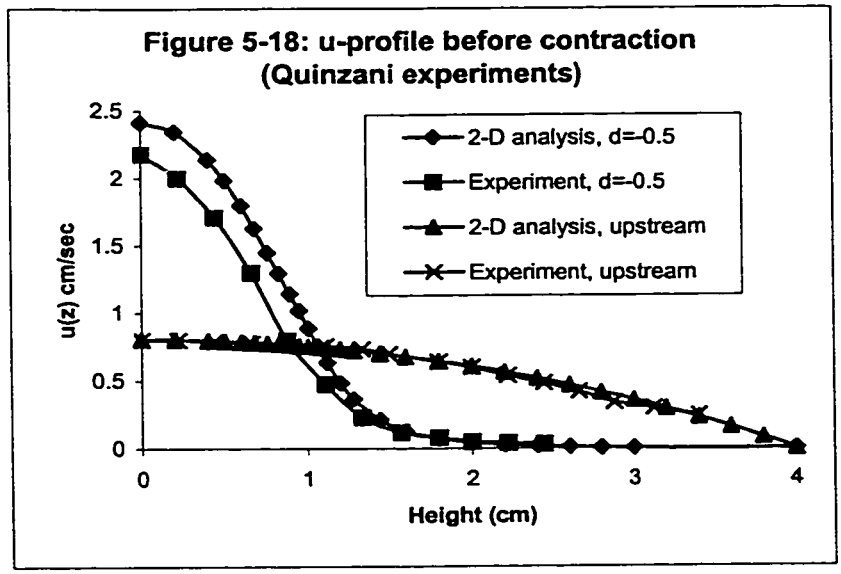

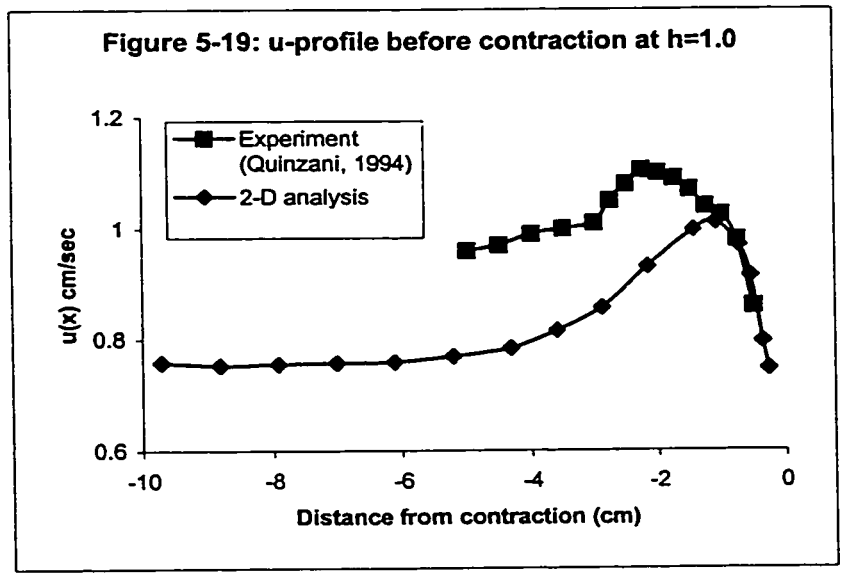

Figure 5-18 shows a good agreement between the experimental and analytical results upstream of the contraction both quantitatively and qualitatively. However, the 2-D analysis predicts values that are 15% higher than experimental values near the

contraction. In Figure 5-19, although both curves follow the same pattern, there is a 20% difference in the results.

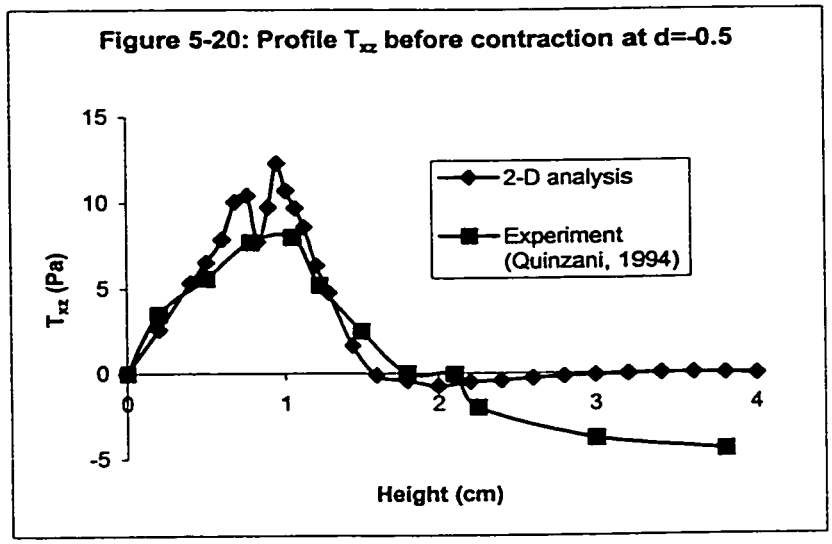

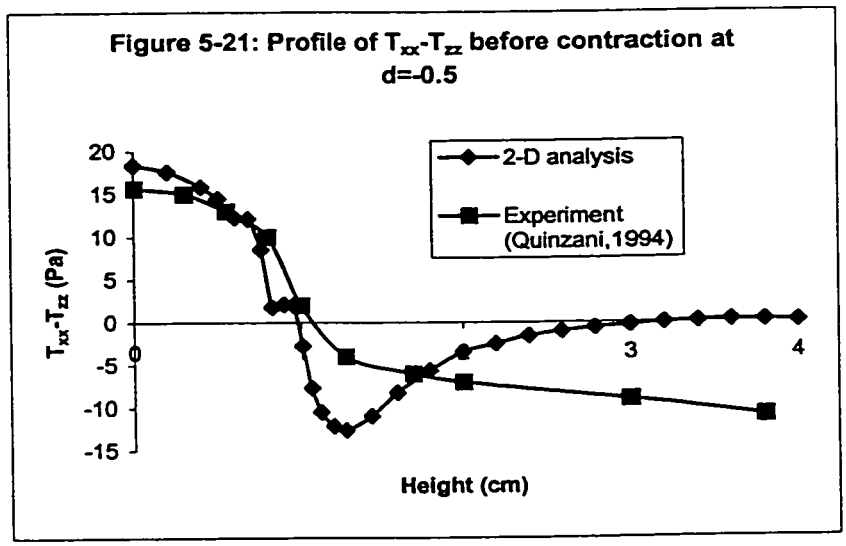

Figure 5-20 shows that 2-D analysis overpredicts T_{xz} in the vicinity of the re-entrant corner and there are also wiggles in the stress predictions. The local minimum

that has been observed in results of 2-D analysis in Figure 5-21 is also observed experimentally (by Quinzani et al., 1994) at higher Wi.

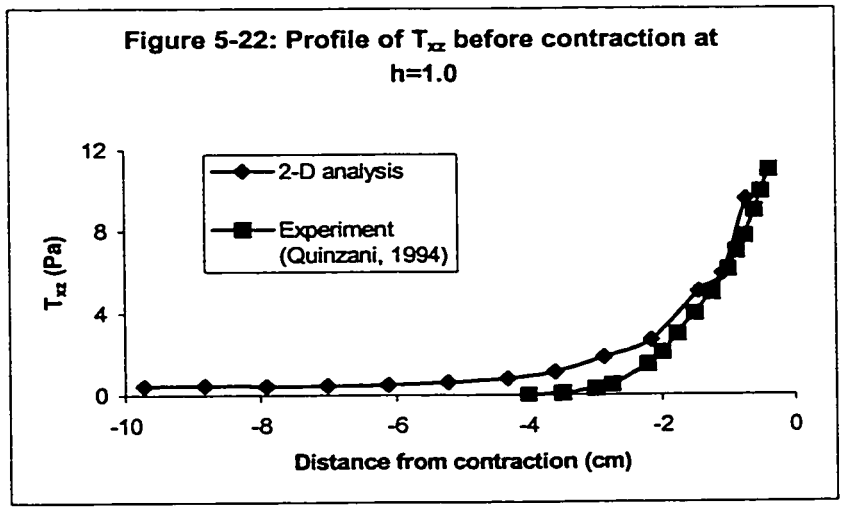

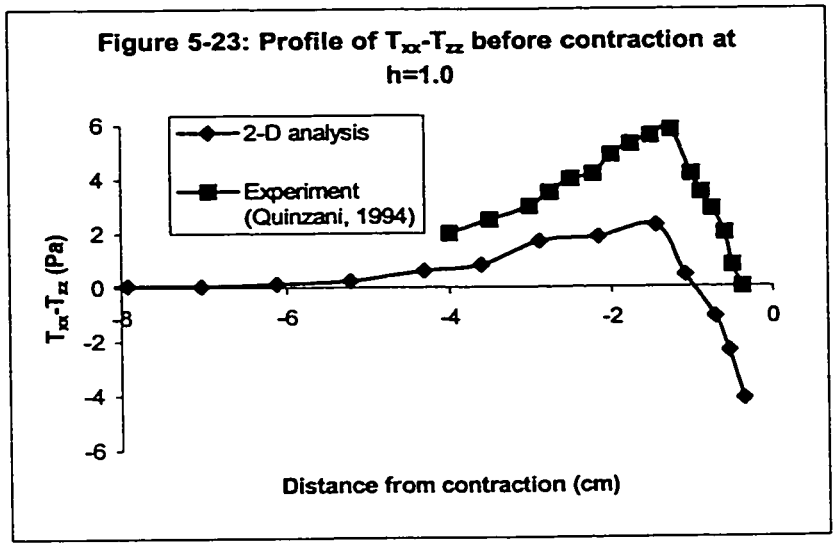

Figure 5-22 shows good agreement in the prediction of the shear stress values between experimental measurements and computational predictions. Figure 5-23 shows a similar pattern for normal stress difference with about a 50% difference in magnitude.

Comparing to the experimental results, there seems to be a good qualitative agreement in the prediction of velocity and stress profiles. The presence of the singular point at re-entrant corner (due to the singularity of the stress) seems to affect the local stress profiles.

The problem of a singular point in the flow through a sudden contraction has been extensively studied in the literature. Several methods have been suggested to overcome the numerical problems that the singular point causes. Some of these methods are based on eliminating the singularity by changing the sharp corner to a curved one, or introducing a slip boundary condition at the re-entrant corner (Brown et al., 1986). Other approaches are based on improving the stability of the numerical method. These include using upwinding methods (Hughes et al., 1982) in the calculation of stresses or in the calculation of both velocity and stress components (Keunings, 1989). As mentioned earlier, the purpose of this study was evaluating the algorithm that was developed in Chapter Two in analysis of the flow in complex geometries, further modifications are required for thorough analysis of the flow in a duct with a sudden contraction.

After the study of the planar geometry using the 2-D segregated method, a 3-D analysis of a square duct with a sudden contraction (3.97:1) was performed. The average velocity at the mid-plane (y=0.5) of square duct is higher than the average velocity in a rectangle with infinite width, therefore u_{av} was reduced and Wi was selected accordingly.

The issue of the difference in u_{av} between 2-D and 3-D geometries has been addressed thoroughly by Xue et al. (1998).

The 3-D mesh consists of 4x4x12 elements in the x, y and z directions before the contraction, and 5x4x5 elements downstream of the contraction. The gridlines are shown in Figure 5-24. A side-view of the gridlines and close up of the gridline near the contraction are shown in Figures 5-25 and 5-26. The view of the duct inlet is shown in Figure 5-27.

Gradients of the velocity components in flow directions were set zero at the outlet and a fully developed flow profile was applied at the inlet. The fully developed profile was obtained using the 2.5-D algorithm that has been described in Chapter Four. The length of the duct was at least 3l (l being the depth of the channel in downstream) to ensure that fully developed flow is obtained before the end of the duct.

To the best of author's knowledge, there is no 3-D finite element analysis on the flow of viscoelastic fluid in the duct with a sudden contraction; however, there are two recent studies by Mompean et al. (1997) and Xue et al. (1998) employing finite volume methods. Mompean et al. (1997) analyzed the flow of an Oldroyd-B fluid in both a 2-D and 3-D (square duct with 4:1 contraction) geometries. Their study also involved steady and unsteady cases. Xue et al. (1998) used a PTT fluid in their study. They performed an extensive study on the 2-D geometry and also studied the 3-D sudden contraction

Figure 5-24: 3-D mesh of square duct with 3.97 :1 contraction

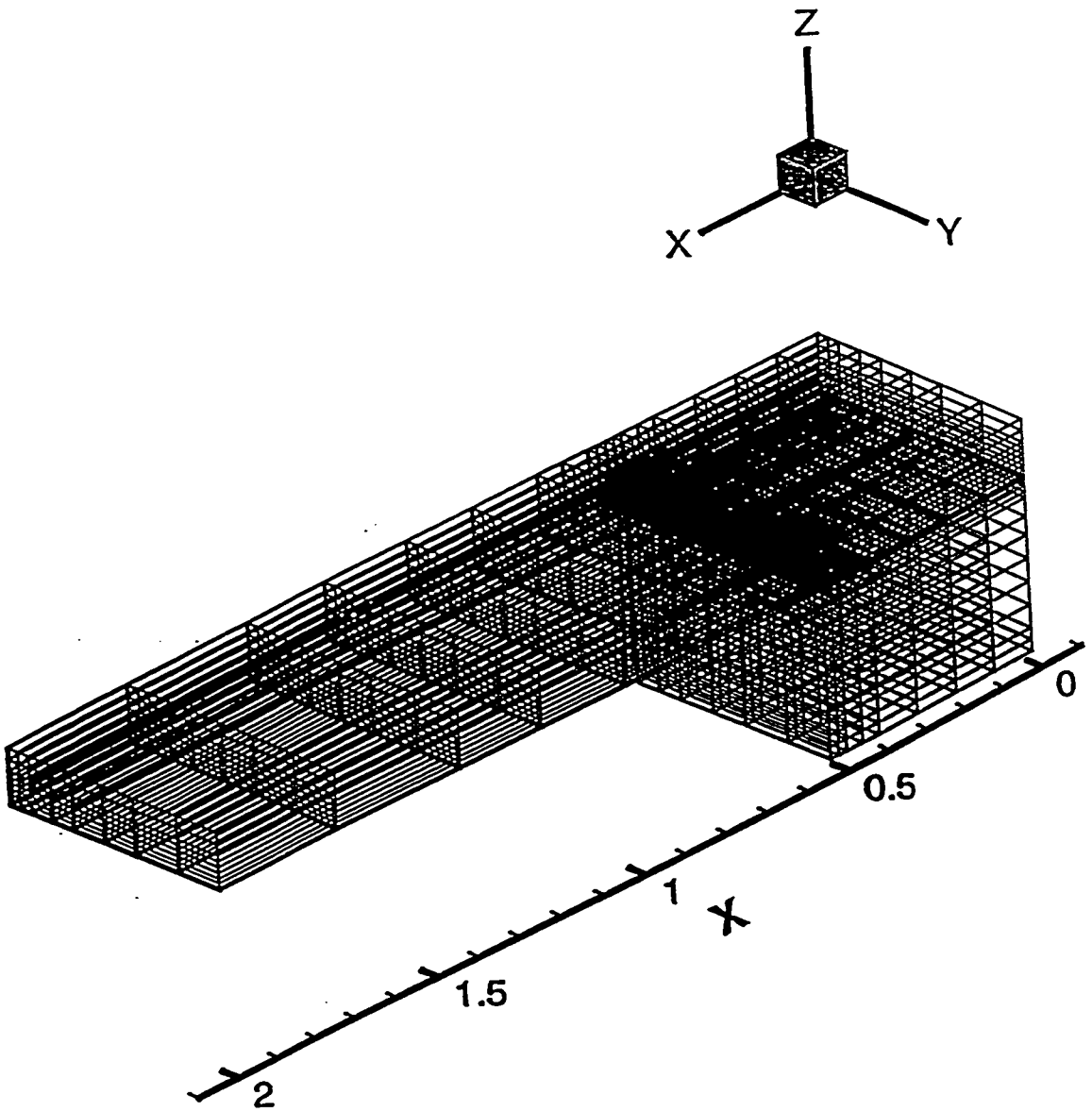

Figure 5-25: Side view of the square duct with 3.97:1 contraction (x-z plane)

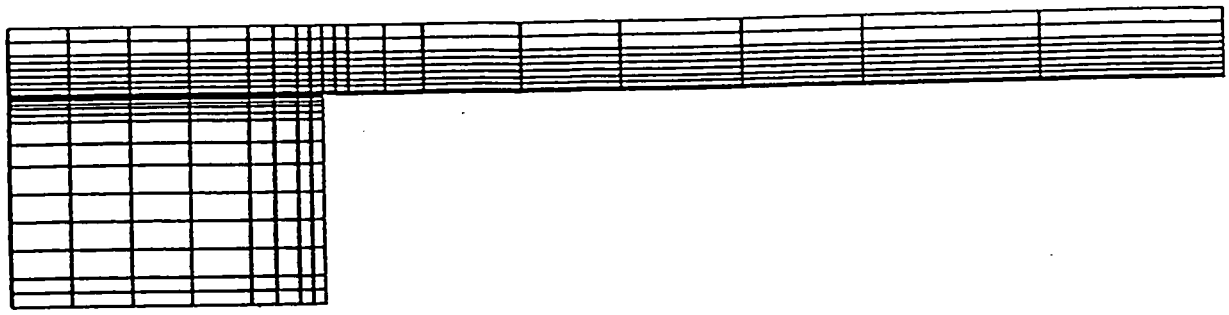

Figure 5-26: Side view of 3-D mesh (close up near the re-entrant corner)

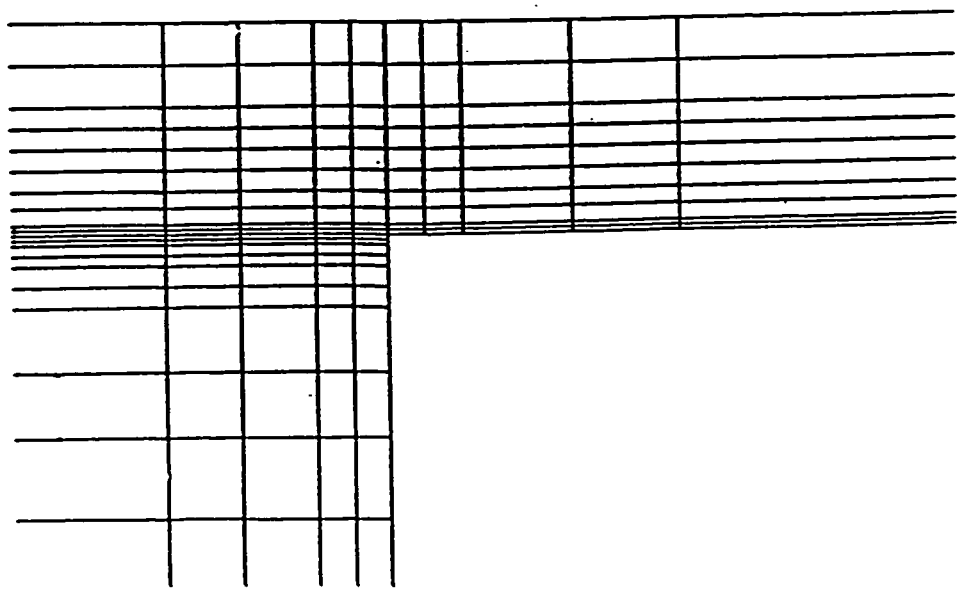

Figure 5-27: Inlet for the 3-D mesh of square duct with a sudden contraction (y-z plane)

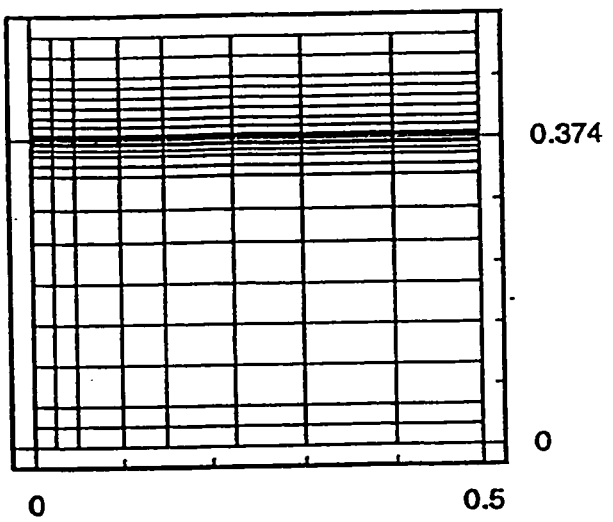

(3.97:1) of a rectangular duct (with an aspect ratio of 10:1 in upstream) and compared it with Quinzani et. al (1994) experiments, they found a good agreement between their numerical predictions and experimental results.

Results from this study are reported and compared with the experimental results from Quinzani et al. (1994). Figure 5-28, shows the u-profile at different distances from the contraction plane. Figure 5-29 shows the u-profile at different heights from the centreline before the contraction. Figure 5-30, shows profiles of shear stress (T_{xz}) at different distances from the contraction plane. Figure 5-31 shows profiles of shear stress (T_{xz}) at different heights from the centreline before the contraction. Figure 5-32 shows how the normal stress differences vary along the z-direction, at different distances from the contraction plane. Figure 5-33 shows profiles of the normal stress differences in different heights from the centreline. These figures are obtained for the mid-plane in 3-D mesh and are reported in positions similar to their 2-D counterparts that were reported earlier.

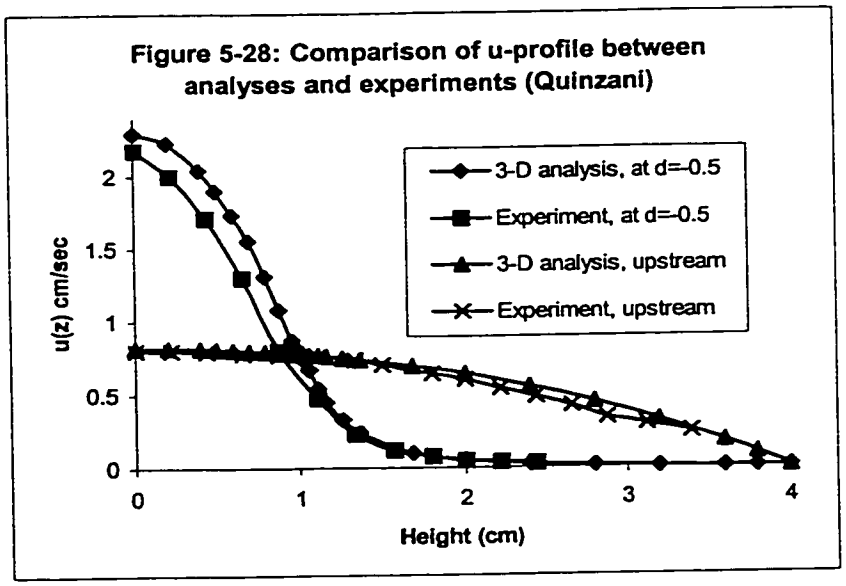

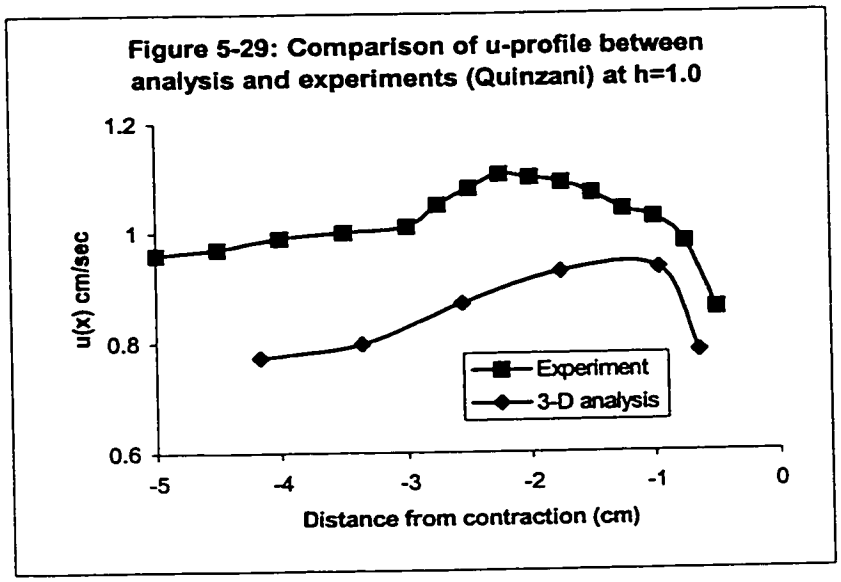

Figure 5-28, shows a very good agreement between experimental and numerical results upstream of the contraction. Near the contraction, the 3-D analysis overestimates the velocities by 10%, which is relatively better than 2-D analysis (with 15% error).

There is a similarity in the pattern for the velocity results shown in Figure 5-29 and results are about 20% different quantitatively.

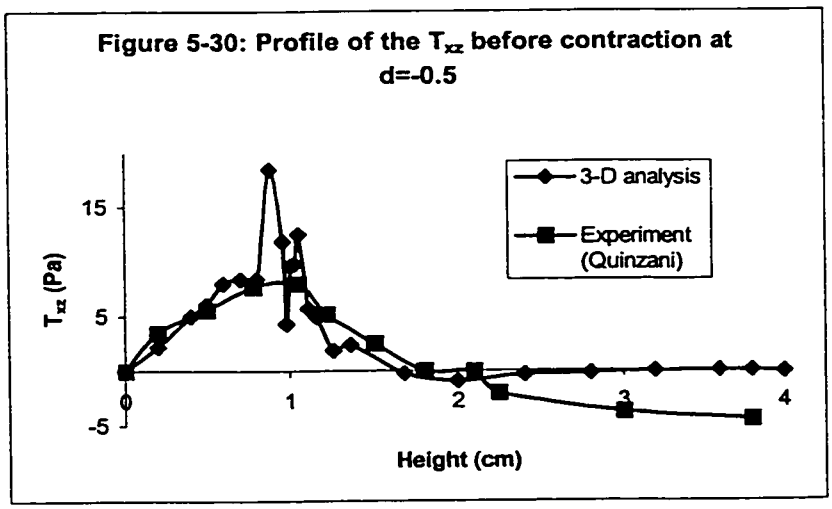

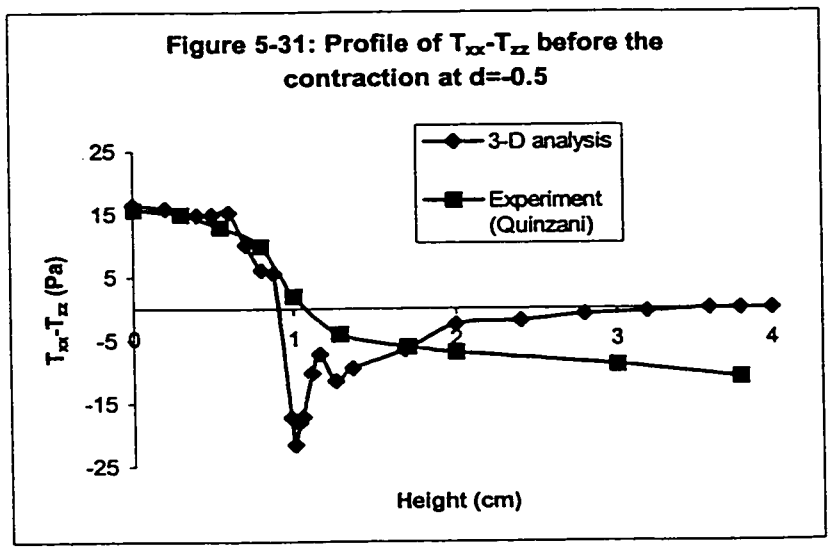

Figures 5-30, 5-31 shows fluctuations in the calculated stress near the re-entrant corner. There is good agreement between results, in the first section of the curves (0<h<1), while there is a qualitative difference in the rest of the curve (1<h<4).

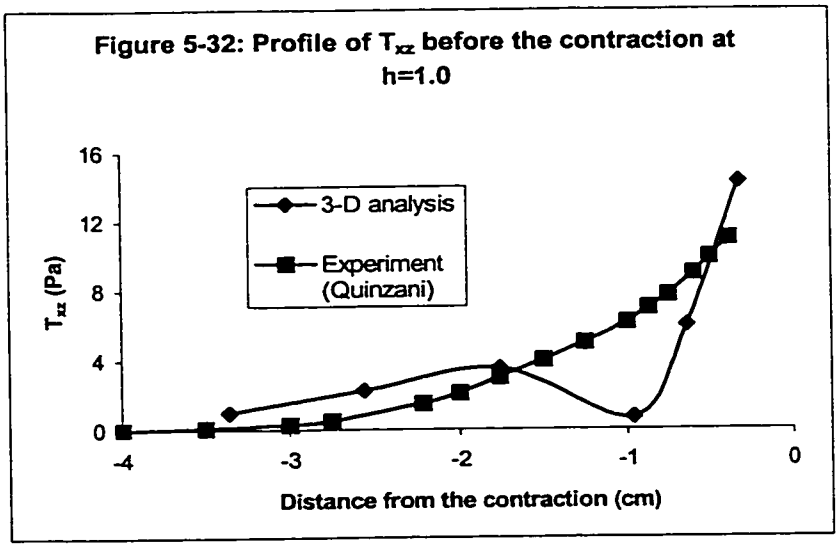

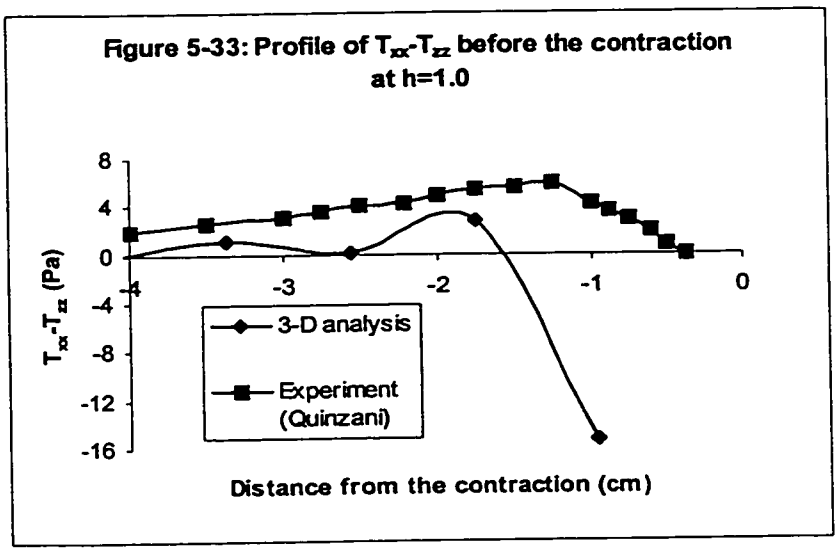

Figures 5-32, and 5-33 show qualitative agreement between computational and experimental results, while computational results show fluctuations near the contraction plane.

Comparing the computed results with the experimental results shows that there is close agreement between results the predictions of velocity profiles and the experimental values. In the prediction of the stresses there appears to be considerable oscillation near the re-entrant corner (as expected in the absence of stabilizing techniques); however, there is generally a good qualitative agreement in the region far from vicinity of the re-entrant corner.

Results from 3-D analysis for the mid-plane (y=0.5) were consistent with the results from 2-D analysis, except that there was more oscillation in the results of stress in case of 3-D analysis.

It can be concluded, that the 3-D algorithm has been shown to be capable of modeling flow in complex geometries; however, for the cases involving singular points, special techniques (as described earlier in the section) are required for any further studies. To explore flow in complex geometries, faster and more efficient solvers are required for larger and denser meshes. And of course, using fast computers and optimized software must be considered in any effort that seeks to study the flow in complex geometries for different meshes and different parameters of the model.

5.3- Concluding remarks

In this chapter, the fully segregated 3-D algorithm was examined for cases of the flow in complex geometries. For this evaluation, two cases of flow in complex geometries were selected from the literature where the experimental results were available. The model parameters were extracted from literature where 2-D analysis on those experiments had been performed. Furthermore, 2-D creeping flow formulation of the segregated algorithm was also developed and employed to model planar flow in complex geometry as a basis for comparison. The agreement between the computational (both 2-D and 3-D) and experimental results was generally good.

The efforts that were made here were to show that the 3-D segregated algorithm is an appropriate method to employ toward the final goal of quantitative prediction of the flow variables in complex geometries. 3-D segregated algorithm has features, that make it a good candidate for further improvements. These features include memory and time saving, which could be further improved by using iterative solvers. The EVSS method that was employed can be extended for multi-mode constitutive equations, which are necessary in modeling the flow in complex geometries.

Chapter 6

Conclusions and Recommendations

The goal of this study was to develop a 3-D numerical algorithm for analyzing viscoelastic fluid flow in straight ducts and in more complex geometries. Since the size of the problem and number of variables increase considerably in 3-D analysis, the primary task was to explore methods that result in saving computer time and memory.

At the beginning, the marching method was examined as it was potentially very attractive for saving time and memory. The marching method was abandoned because its formulation involves elimination of the terms that are important in analysis of the flow in complex geometries. Consequently a 3-D algorithm based on creeping flow formulation and EVSS method was introduced to model the flow of MPTT fluid in simple and complex geometries. The pressure correction segregated method that was used in

modeling the creeping flow was studied for its performance, convergence and speed. It was also compared with fully coupled method in solving generalized Newtonian flow.

In Chapter Three a fully segregated 2.5-D algorithm for the analysis of fully developed viscoelastic flows in straight ducts was introduced to study secondary flows. After verifying the algorithm and confirming the results by comparing them with results from literature, the results were used as a basis for evaluation of the results from 3-D analysis of the viscoelastic flow in a straight duct.

Different boundary conditions were studied for 3-D analysis of the viscoelastic flow in a straight duct in Chapter Four. It was observed that near the outlet a solution appears that is physically different from the rest of the domain and inconsistent with the vortex pattern. The outlet flow anomaly was attributed to the inconsistency between the boundary conditions and the presence of the source terms in momentum equations. A solution for avoiding such problem was to decouple the pressure at the end section. In Chapter Five, the performance of the 3-D algorithm in analyzing the flow in complex geometries was evaluated by comparing the results with experimental measurements.

6.1- Contributions

Achievements of this study can be summarized to be in two main areas; progress on 3-D analysis of visoelastic flow and the analysis of the secondary flows in straight non-circular ducts.

On 3-D analysis of viscoelastic flows, and what is unique in this study, is the special attention that is given to two issues of:

1- Savings in computer time and memory
2- Problems with boundary conditions for velocities

The marching method (Appendix A) was an ideal formulation considering these two issues. No boundary conditions were required at the outlet, and the 3-D problem was broken into a series of 2-D plane problems, which required less memory and time to solve. The problem with the marching method was in the area of flow in complex geometries. Therefore, an alternative formulation (based on the creeping flow formulation) was selected and pursued. Segregated methods were employed to save computer time and memory.

The creeping flow formulation was applied to the viscoelastic flow (for a MPTT fluid) in a straight duct using a decoupled scheme. The problem of the boundary

condition, which had been ignored previously, was reported. The problem was carefully analyzed. Appropriate methods were then suggested to circumvent the problem. Moreover, it was shown that this formulation is indeed capable of being used for analysis of flow in complex geometries.

Another problem that has been extensively discussed in this study was the fully developed flow of a viscoelastic fluid in straight non-circular ducts. It was shown that the solution that is obtained based on the assumptions of fully developed flow is consistent with the solution from 3-D analysis. The algorithmic steps for a 2.5-D segregated method were described in detail and tested.

The algorithm was applied for the cases of high Wi (up to 20). At high Wi (Wi>1), the intensity of the secondary flows was shown to reach a plateau independent of Wi, which is very different from sharp increase that is seen at low Wi. The momentum equations in 2.5-D algorithm was further modified to study the effects of Re, and it was shown that an increase in the value of Re could result in a higher number of vortices. The new patterns of secondary flows for square and rectangular ducts were reported for the first time.

It was emphasized that obtaining the correct u-velocity profile is essential for the correct prediction of secondary flows and a method was suggested to directly relate N_2 (or related parameters in the model) to the intensity of the secondary flows. One can

hope that this method will result in a test that provides accurate prediction of more viscoelastic properties for polymeric liquids.

6.2- Recommendations

In the study of secondary flows, there are several issues that are of further interest.

- Inclusion of the effect of temperature to evaluate the effect of secondary flows on heat transfer would also be interesting. The effect of temperature and the equation of energy can be added as a separate module to the existing code and no major modifications would be required to the structure of the code.

- The marching code can be extended for viscoelastic flow as explained by Torres (1995), with the modification introduced in Appendix A. The results at the outlet can be compared with the results from this study of the secondary flow considering Re.

For 3-D analysis, the first necessity would be to develop an iterative solver that is faster and more efficient in solving for larger meshes than the one presently available. For complex geometries, where the cross velocity components are significant, upwinding methods seem to be necessary as well. By employing methods that have been developed in 2-D studies of viscoelastic fluids (e.g. upwinding); a 3-D method can be improved to

have a larger range of performance and convergence. After using stabilizing methods, extending the 3-D algorithm to include Re effects would also be of interest.

In moving towards quantitative prediction of flow variables of a viscoelastic fluid in complex geometries, it is very important to employ constitutive equations that are valid in a wide range of shear rates (e.g. multi-mode constitutive equations).

References

Anderson, D. A., Tannehill, J. C., Pletcher, R. H., Computational Fluid Mechanics and Heat Transfer, Hemisphere, 1984.

Azaiez, J., Guenette, R., Ait-Kadi, A. "Numerical Simulation of Viscoelastic Flows Through a Planar Contraction" J. Non-Newt. Fluid Mech., 62, 253, 1996.

Batchelor, G. K., An Introduction to Fluid Dynamics, Cambrige University Press, 1967.

Beavers G. S., Sparrow E. M., Magnuson R. A. "Experiments on Hydrodynamically Developing Flow in Rectangular Ducts of Arbitrary Aspect ratio" Int. J. Heat Mass Transfer 13, 689, (1970).

Benim, A. C., Zinser, W. "A Segregated Formulation of Navier-Stokes Equations with Finite Elements" Comp. Meth. Appl. Mech. Eng., 57, 223, 1986.

Bird, R.B., Armstrong, R.C., Hassager, O. Dynamics of Polymeric Liquids, vol. 1, Wiley (1987).

Boger, D. V. "Viscoelastic Flows Through Contractions" Ann. Rev. Fluid Mech., 19, 157, 1987.

Briley, W. R. "Numerical Method for Predicting Three Dimensional Steady Viscous Flow in Ducts", J. Comp. Phys., 14, 8, 1974.

Bravo, V. "Finite Element Simulation of Flow in Twin Screw Extruder Mixing Elements" Ph. D. Thesis, McMaster University, Hamilton, Canada, 1998.

Brown, R.A., Armstrong, R. C., Beris, A. N. and Yeh, P.-W "Galerkin Finite Element Analysis of Complex Viscoelastic Flows" Comp. Meth. Appl. Mech. Engng., 58, p201, 1986.

Burnett, D. Finite Element Analysis Addisson Wesley, 1987.

Chorin, A. J., "Numerical Solution of The Navier-Stokes Equations", Math. Comput., 22, 745, 1968.

Cohen, Y., Metzner, A. B. "Apparent Slip Flow of Polymer Solutions" J Rheo., 29(1), 67, 1985.

Comini, G., Del Giudice, S., Strada, M. "Finite Element Analysis of Laminar Flow in the Entrance Region of Ducts" Int. J. Num. Meth. Eng., 15, 507, (1980).

Comini, G., Del Giudice, S. "Parabolic Systems: Finite Element Method", in Numerical Heat Transfer Handbook, chapter 4, ed. Minkowycz, W. J., Wiley (1988).

Debbaut B., Avalosse T., Dooley J., Hughes K., "On The Development of Secondary Motions in Straight Channels Induced by The Second Normal Stress Difference: Experiments and Simulations" J. Non-Newt. Fluid Mech., 69, 255 (1997)

Denn M. M., "Surface-Induced Effects in Polymer Melt Flow" Proc XIth, Int. Congress on Rheology, Brussels, 45, 1992.

Dooley J., Dietsche, L. "Numerical Simulation of Viscolelastic Polymer Flow - Effect of Secondary Flows on Multilayer Coextrusion" Plastics Engineering, April 1996.

Dodson, A.G., Townsend, P., Walters, K. "Non-Newtonian Flow in Pipes of Non-Circular Cross Section" Comp. & Fluids, 2, 317, 1974.

Dooley, J., Hughes, K. "Coextrusion Layer Thickness Variation - Effect of Polymer Viscoelasticity on Layer Uniformity" SPE ANTEC, Boston, 1995.

Dussan, E.B., Davis, S. H. "On the Motion of a Fluid-Fluid Interface Along a Solid Surface" J. Fluid Mech., 65, 71, 1974.

Gervang, B., Larson, P. S. "Secondary Flows in Straight Ducts of Rectangular Cross Section" J. Non-Newt. Fluid Mech., 39, 217, 1991.

Ghia, K. N., and Sokhey, J. S., "Laminar Incompressible Viscous Flow in Curved Ducts of Regular Cross Sections", J. Fluids Eng., 99, p 640, 1977.

Giesekus, H.,"A Simple Constitutive Equation for Polymer Fluids Based on the Concept of Deformation-Dependent Tensorial Mobility", J. Non-Newt. Fluid Mech. 11, p69, 1982.

Goldstein R. J., Kreid D. K. "Measurement of Laminar Flow Development in a Square Duct Using a Laser-Doppler flowmeter" J. Appl. Mech. 34, p813, 1967.

Han L. S. "Hydrodynamic Entrance Lengths for Incompressible Laminar Flow in Rectangular Ducts" J. Appl. Mech. 27, p403, 1960.

Haroutunian, V., Engelman, M.S., Hasbani, I. "Segregated Finite Element Algorithms for the Numerical solution of Large-Scale Incompressible Flow Problems" Int. J. Num. Meth. Fluids, 17, 323, 1993.

Hatzikiriakos, S.G., Dealy, J. M. "Wall Slip of Molten High Density Polyethylenes I. Sliding Plate Rheometer Studies" J. Rheol., 35, 497, 1991.

Hatzikiriakos, S.G., Dealy, J. M. "Wall Slip of Molten High Density Polyethylenes II. Capillary Rheometer Studies" J. Rheol., 36, 703, 1992a.

Hatzikiriakos, S.G., Dealy, J. M. "Start-Up Pressure Transients in a Capillary Rheometer" SPE ANTEC, 1992b.

Hatzikiriakos, S.G., Dealy, J. M. "Role of Slip and Fracture in the Oscillating Flow of HDPE in a Capillary" J. Rheol., 36, 845, 1992c.

Hatzikiriakos, S.G. "A Slip Model for Linear Polymers Based on Adhesive Failure" Int. Polym. Proc. VII, 135, 1993.

Hill, D. A., Hasegawa, T., Denn, M. M. "On The Apparent Relation Between Adhesive Failure and Melt Fracture" J. Rheol., 34, 891, 1990.

Hu H. H., Joseph D. D., "Numerical Simulation of Viscoelastic Flow Past a Cylinder" J. Non-Newt. Fluid Mech., 37, 347, 1990.

Hughes, T. J. R., Brooks, A. "A Theoretical Framework for Petrov-Galerkin Methods with Discontinous Weighting Functions Applied to Streamline-Upwind Procedure" Finite Elements in Fluids, 4, 47, 1982.

Joseph, D. D., Renardy, M., and Saut, J. C. "Hyperbolicity and Change of Type in the Flow of Viscoelastic Fluids" Arch. rational Mech. Anal., 87, 213 (1985).

Kajiwara, T., Ninomoiya, S., Kuwano, Y., Funatsu, K.,"Numerical Simulation of Converging Flow of Polymer Melts Through a Tapered Slit Die" J. Non-Newt. Fluid Mech., 48, 111, 1993.

Kihara, S., Hashimoto, Y., Godha, T., Matsunaga, K. and Funatsu, K. "Numerical Simulation of Three-dimensional Viscoelastic Flows Using a Thermodynamic Interpolation Models" PPS-14, Yokohama, Japan, 1998.

Keunings, R. "Simulation of Viscoelastic Fluid Flow" in Computational Modeling for Polymer Processing, Charles Tucker III, ed., Hanser, 1989.

Langlois, W. E., Rivlin, R. S. "Steady Flow of Slightly Viscoelastic Fluids" Brown Univ. Tech. Rept. No.3 to the Office of Ordnance Research, U.S. Army, under Contract DA-19-020-ORD-4725, 1959.

Langlois, W. E., Rivlin, R. S. "Slow Steady-State Flow of Viscoelastic Fluids Through Non-Circular Tubes" Rend. Mat. Roma, 22, 169, 1963.

Langlois, W.E. "The Steady Flow of a Slightly Viscoelastic Fluid Between Rotating Spheres" Quart. Appl. Math., 21, 61, 1963.

Langlois, W. E. "A Recursive Approach to the Theory of Slow Steady-State Viscoelastic Flow" Trans. Soc. Rheol. 7, 75, 1963.

Langlois, W. E. "A Recursive Approach to the Theory of Slow Steady-State Viscoelastic Flow" Trans. Soc. Rheol. 8, 33, 1964.

Larson R.G."A Constitutive Equation for Polymer Melts Based on Partially Extending Strand Convection" J. Rheol. 28(5), p545, 1984.

Luo X.-L., Tanner R. I. "A Streamline Element Scheme for Solving Viscoelastic Flow Problems. Part I. Differntial Constitutive Equations" J. Non-Newt. Fluid Mech., 21, 179, 1986.

Luo X.-L., Tanner R. I. "A Decoupled Finite Element Streamline-Upwind Scheme for Viscoelastic Flow Problems" J. Non-Newt. Fluid Mech., 31, 143, (1989).

Macosko, C. W. Rheology Principles, Measurements and Applications VCH Publishers, 1994.

Magda, J.J., Baek, S.G., DeVries, K.L., Larson, R.G. "shear Flows of Liquid Crystal Polymers: Measurements of the Second Normal Stress Difference and the Doi Molecular Theory" Macromolecules, 24, 4460, (1991).

Magda, J.J., Lee, C-S, Muller, S., Larson, R.G. "Rheology, Flow Instabilities, and shear-Induced Diffusion in Polystyrene Solutions" Macromolecules 26, 1696, (1993).

Matsunaga K., Sakaki K., Kajiwara T., Funatsu K., "Approximate Simulation Method on The Three-dimensional Polymer Melts Flow in a Die" Intern. Polymer Processing X, Hanser Publishers, Munich (1995).

Meissner, J., Garbella, R.W., Hostettler, J. "Measuring Normal Stress Differences in Polymer Melt Shear Flow" J. Rheol., 33, 843, 1989.

Millsaps, K., Pohlhausen K., "Thermal Distributions in Jeffery-Hamel Flows Between Nonparallel Plane Walls", J. Aero. Sci., p 187, March 1953.

Mompean, G., Deville, M. "Unsteady Finite Volume Simulation of Oldroyd-B Fluid Through a Three-Dimensional Planar Contraction" J. Non-Newtonian Fluid Mech. 72, 253, 1997.

Patankar, S.V., Spalding, D.B. "Calculation Procedure for Heat, Mass and Momentum Transfer in Three-Dimensional parabolic Flows" Int. J. Heat Mass Transfer, 15, 1787, 1972.

Patankar, S.V. Numerical Heat Transfer and Fluid Flow, Hemisphere, 1980.

Phan-Thien, N., Tanner, R.I. "A New Constitutive Equation Derived From Network Theory" J. Non-Newt. Fluid Mech., 2, 353, 1977.

Quinzani L.M., Armstrong R.C., Brown R.A. "Birefringence and Laser Doppler Velocimetry (LDV) Studies of Viscoelastic Flow Through a Planar Contraction" J. Non-Newt. Fluid Mech., 52, 1, (1994).

Raithby, G. D., Schneider, G. E., "Numerical Solution of Problems in Incompressible Fluid Flow: Treatment of the Velocity-Pressure Coupling", Numer. Heat Transfer, 2, 417, 1979.

Rajagopalan, D., Armstrong, R.C., Brown, R.A. "Finite Element Methods for Calculation of Steady, Viscoelastic Flow Using Constitutive equations with a Newtonian Viscosity" J. Non-Newt. Fluid Mech., 36, 159, 1990.

Reddy, J. N. Introduction to The Finite Element Method McGraw-Hill, 1984.

Rice, J. G., Schnipke, R. J. "An Equal-Order Velocity-Pressure Formulation That Does Not Exhibit Spurious Pressure Modes" Comp. Meth. Appli Mech. Eng. 58, 135, 1986.

Rivlin, R. S. "Second and Higher-Order Theories for The Flow of a Viscoelastic Fluid in a Non-Circular Pipe"

Roache, P. J. Computational Fluid Dynamics Hermosa Publishers, Albuquerque, 1976.

Schlichting, H., Boundary-Layer Theory, McGraw-Hill, 1979.

Shah, R.K., London, A.L., Laminar Flow Forced Convection in Ducts, Advances in Heat Transfer, Supplement 1, academic Press, 1978.

Shaw, C. T. "Using a Segregated Finite Element Scheme to Solve The Incompressible Navier-Stokes Equations" Int. J. Num. Meth. Fluids, 12, 81, 1991.

Shiojima, T., Shimazaki, Y. "Three Dimensional Finite Element Method for Extrudate Swells of a Maxwell Fluid" J. Non-Newt. Fluid Mech., 34, 269, 1990.

Sizaire, R., Legat V. "Numerical Prediction of the Encapsulation Effect for Polymer Melts" Progress and Trends in Rheology V, Proceedings of the Fifth European Rheology Conference, Emri, I., ed., Portoroz, Slovenia September 1998.

Takase, M., Gohda, T., Kihara, S. and Funatsu K. "Numerical Analysis of Encapsulation Phenomena in Coextrusion" PPS-14, Yokohama, Japan, 1998.

Thangam, S., Speziale, C. G., "Non-Newtonian Secondary Flows in Ducts of Rectangular Cross-Section" Acta Mechanica 68, 121, 1987.

Torres, A., Finite Element Analysis of Layer Non-Uniformity in Polymer Coextrusion Flows Ph.D. Thesis, McMaster University, Hamilton, Canada, 1995.

Townsend, P., Walters K., Waterhouse, W.M. "Secondary Flows in Pipes of Square Cross-Section and the measurement of the second Normal Stress Difference" J. Non-Newt. Fluid Mech., 1, 107, 1976.

Tran-Cong, T., Phan-Thien, N. "Three Dimensional Study of Extrusion Process by Boundary Element Method. II. Extrusion of a Viscoelastic Liquid" Rheol. Acta, 27, 639, 1988.

Wesson, R. D., Papanastasiou, T.C. "Flow Singularity and Slip Velocity in Plane Extrudate Swell Computations" J. Non-Newt. Fluid Mech., 26, 277, 1988.

Wheeler, J. A., Wisseler, E. H. "Steady Flow of Non-Newtonian Fluids in a Square Duct" Trans. Soc Rheol, 10:1, 353, 1966.

White, J. L., Ide Y.,"Investigation of Failure During Elongational Flow of Polymer Melts" J. Non-Newt. Fluid Mech., 2, p281, 1977.

White, S. A., Gotsis, A. D., Baird, D., G. "Review of the Entry Flow Problem: Experimental and Numerical" J. Non-Newt. Fluid Mech., 24, 121, 1987.

Xue, S.-C., Phan-Thien, N., Tanner, R.I, "Numerical Study of Secondary Flows of Viscoelastic Fluid in Straight Pipes by an Implicit Finite Volume Method" J. Non-Newt. Fluid Mech., 59, 191, 1995.

Xue, S.-C., Phan-Thien, N., Tanner, R.I, "Three Dimensional Numerical Simulations of Viscoelastic Flows Through Planar Contractions" J. Non-Newt. Fluid Mech., 74, 195, 1998.

Appendix A

Parabolic Formulation and Marching Method

In this Appendix a marching algorithm based on parabolic formulation of momentum equations as proposed by Torres (1995) has been studied. The interest in this method arises from the fact that this formulation eliminates the need for imposing boundary conditions at the outlet by reducing the order of the differential equation in terms of x (flow direction) derivative. It also converts the solution of the 3-D problem to the solution of a sequence of 2-D plane problems, for which large savings in memory and CPU time are expected.

Newtonian flow in a straight duct, using parabolized Navier-Stokes equations (PNSE) formulation was studied here to examine the method and address some of the convergence problems that were reported by Torres (1995) in modeling viscoelastic flows.

A.1- PNSE Formulation

The complete set of Navier-Stokes equations which govern the flow field, constitute a system of second-order non-linear partial differential equations (PDE). Unfortunately, the Navier-Stokes equations are very difficult to solve in their complete form due to their nonlinearity and require a very large amount of computer time and storage to obtain a solution. Therefore, different approximations of Navier-Stokes equations based on the physical nature of the flows are used, such as boundary layer equations to model some viscous flows and Euler's equations to solve inviscid flow.

For the cases of the flow which satisfy certain conditions, a set of reduced Navier-Stokes equations has been developed which satisfactorily model those flows. Considering x as the direction of the main flow these conditions may be stated as follows.

1- The x direction is the dominant flow direction and there is no flow recirculation in the x direction.
2- The diffusion of momentum in that direction is negligible, compared with advection.
3- The downstream pressure field has no effect on the upstream flow conditions.

These reduced equations are often referred to as the thin-layer or parabolized Navier-Stokes equations. Although the formulations vary slightly, the equations all

contain a non-zero normal pressure gradient and do not contain the second derivative terms with respect to the streamwise direction of the flow. The reduced Navier-Stokes equations, for steady flow, can therefore be presented in Cartesian coordinates as (where first derivative of stress terms in x direction have been dropped)

$$\rho u\frac{\partial u}{\partial x}+\rho v\frac{\partial u}{\partial y}+\rho w\frac{\partial u}{\partial z}=-\frac{dP}{dx}+\frac{\partial T_{xy}}{\partial y}+\frac{\partial T_{xz}}{\partial z} \qquad (A.1)$$

$$\rho u\frac{\partial v}{\partial x}+\rho v\frac{\partial v}{\partial y}+\rho w\frac{\partial v}{\partial z}=-\frac{\partial p}{\partial y}+\frac{\partial T_{yy}}{\partial y}+\frac{\partial T_{yz}}{\partial z} \qquad (A.2)$$

$$\rho u\frac{\partial w}{\partial x}+\rho v\frac{\partial w}{\partial y}+\rho w\frac{\partial w}{\partial z}=-\frac{\partial p}{\partial z}+\frac{\partial T_{zy}}{\partial y}+\frac{\partial T_{zz}}{\partial z} \qquad (A.3)$$

where P is an average pressure in each cross section and is assumed to vary only in the x direction. p is the "in-plane" pressure, representing the variation of pressure in a cross-section. Therefore pressure $p^{*}(x,y,z)$ at each point can be described as;

$$p^{*}(x,y,z)=\Delta P.x+p(y,z) \qquad (A.4)$$

u, v, and w are velocity components in x, y, and z directions and ρ is the density of the fluid. T is the stress tensor.

Reducing the Navier-Stokes equations to the parabolized Navier-Stokes equations accommodates a marching procedure that solves the 3-D problem as a series of 2-D problems which requires less memory. The computational strategy that is most commonly used solves the conservation equation for each individual variable sequentially

(sometimes called "segregated" approach). Once the pressure field is specified, the solution can march in the main flow direction using the x-momentum equation to obtain u profile in the next cross section. Then the y-momentum equation is solved to obtain v and z-momentum equation to obtain w. If the pressure distribution in cross plane is correctly specified, the velocity components will satisfy the continuity equation.

Different approaches to the solution of reduced set of Navier-Stokes equations have been proposed and studied by Chorin (1968), Patankar (1972), Briley (1974), Ghia and Sokhey (1977), and Comini (1988). The marching algorithm that has been studied here is the one that is suggested by Torres (1995) based on Comini et. al (1988). Torres (1995) employed a marching algorithm by decoupling elastic stresses to model the flow of viscoelastic fluid in a straight duct. However, the algorithm failed to converge where the step sizes were smaller than 0.01 or larger than 1. Therefore to address these problems Newtonian flow was studied to discover the source of the possible problems that caused the failure of the marching code as the step sizes decreased.

A.2- Description of The Marching Algorithm

The average velocity (u_{av}) is the velocity scale and the width of the duct (D) is the length scale in equations 2.1 to 2.3 which were made dimensionless. Re is defined as

$$Re = \frac{\rho u_{av} D}{\eta_0} \qquad (A.5)$$

Pressure was made dimensionless by dividing by $\rho(u_{av})^2$. The marching algorithm for Newtonian flow can be described as follows.

The solution is presumed known at station x^n (plane of constant x) and the algorithm to find flow variables at station x^{n+1} is:

1-Solve x-momentum equation to obtain u, using previously calculated values for Δp, u, v and w (from the previous station).

$$u^n\left(\frac{\partial u}{\partial x}\right)^* = \frac{1}{Re}\left[\frac{\partial^2 u^*}{\partial y^2} + \frac{\partial^2 u^*}{\partial z^2}\right] - \left[v^n \frac{\partial u^*}{\partial y} + w^n \frac{\partial u^*}{\partial z}\right] - \frac{\partial P}{\partial x} \qquad (A.6)$$

2- Calculate the flow rate Q* (for rectangular ducts of width W and height H)

$$\int_{-H/2}^{+H/2}\int_{-W/2}^{+W/2} u^* dydz = Q^* \qquad (A.7)$$

3- Use (Q-Q*) to calculate new ΔP, using bi-section method, where Q is the initial flow rate.

4- If $|Q-Q^*| <$ tolerance, then $u^{n+1}=u^*$ and go to 5, else go to 1.

5- Solve the y-momentum equation to obtain v*.

$$u^n\left(\frac{\partial v}{\partial x}\right)^* = \frac{1}{Re}\left[\frac{\partial^2 v^*}{\partial y^2} + \frac{\partial^2 v^*}{\partial z^2}\right] - \left[v^n \frac{\partial v^*}{\partial y} + w^n \frac{\partial v^*}{\partial z}\right] - \left(\frac{\partial p}{\partial y}\right)^n \qquad (A.8)$$

6- Solve the z-momentum equation to obtain w*.

$$u^n\left(\frac{\partial w}{\partial x}\right)^* = \frac{1}{Re}\left[\frac{\partial^2 w^*}{\partial y^2} + \frac{\partial^2 w^*}{\partial z^2}\right] - \left[v^n \frac{\partial w^*}{\partial y} + w^n \frac{\partial w^*}{\partial z}\right] - \left(\frac{\partial p}{\partial z}\right)^n \qquad (A.9)$$

7- Use continuity differential equation to obtain pressure correction p(y,z).

$$\frac{\partial}{\partial y}\left(\frac{1}{u^n}\frac{\partial p}{\partial y}\right) + \frac{\partial}{\partial z}\left(\frac{1}{u^n}\frac{\partial p}{\partial z}\right) = \frac{1}{\Delta x}\left(\frac{u^{n+1} - u^n}{\Delta x} + \frac{\partial v^*}{\partial y} + \frac{\partial w^*}{\partial z}\right) \qquad (A.10)$$

8- Use pressure correction to calculate corrective values v′, and w′.

$$v' = -\Delta x \frac{\partial p'}{\partial y} \qquad (A.11)$$

$$w' = -\Delta x \frac{\partial p'}{\partial z} \qquad (A.12)$$

9- Add corrective values to the estimated value v*, and w* to obtain corrected values.

$$v^{n+1} = v^* + v' \qquad (A.13)$$

$$w^{n+1} = w^* + w' \qquad (A.14)$$

To improve estimates of velocities and pressure under-relaxation of the following form has been used.

$$\phi^n = (1-\alpha)\phi^{n-1} + \alpha\phi^c \qquad (A.15)$$

ϕ^c stands for corrected value of any of the variables and α is the relaxation factor.

10- If changes in v, w, and p are larger than tolerance, go to step 5, otherwise convergence is achieved and proceed to the next cross section.

The finite element formulation of the problem is given in Torres (1995).

A.3- Evaluating Marching Method for The Duct Flow

This section contains the results of the marching method (as developed by Torres, 1995) and its evaluation for the duct flow of a Newtonian fluid, using different initial conditions.

In the first stage of this study, parameters related to the analysis such as; mesh density, step size, and relaxation factors were analyzed. Use of symmetry conditions allowed only one quarter of the cross section of the channel to be modeled using 3x3, 5x5, and 10x10 biquadratic, nine node elements. These meshes were analyzed for flow at low Reynolds number ($Re=10^{-3}$), with a step size in the axial direction of 0.1 L/D.

In a study of the effect of relaxation factors, four cases were studied by choosing α_p and α_v as 0.1 and 1 (α_p and α_v are relaxation factors for pressure and velocity

components). It was found that the convergence of the program was sensitive to changing α_v but not α_p. While changing α_p did not change rate of convergence, the program did not converge to a solution for α_v=1. Tolerance for largest change in the magnitude of v, w and p values was 10^{-5}.

The program was run on IBM (RS 6000-370) workstation. The memory required was about 10 MB for the average size of mesh (5x5). The time required for the solution to march down one step was about 8 minutes for a 5x5 mesh.

A.3.1- Flow Cases

The study on the algorithm performance in duct flow started by using fully developed flow as the initial condition, as the most trivial case. After removing some minor difficulties and ensuring that the outlet flow profile is consistent with the solution from creeping flow (that was obtained using commercial software, FIDAP™ from Fluent Inc.).

It was found that large tolerances (higher than 10^{-3}) in the calculation of the flow rate (step 4 of the algorithm) results in fluctuation of the pressure drop along the duct, therefore the tolerance had to be selected 10^{-4} or smaller.

A major problem that was reported by Torres (1995), was the divergence of the method as the size of the steps (Δx) was reduced. To understand the source of the problem, the size of the steps were reduced until divergence. For this case (i.e. Newtonian flow) divergence occurred for step sizes smaller than 10^{-7}. Divergence appeared in the form of producing very high values of p(y,z), v, w, and further affecting u values.

Probing the problem showed that error is generated in step 7 where values for pressure are calculated and then the error propagated through the corrective values of v and w in step 8. The source of the error was the finite difference derivative of u relative to x. . As the step size (i.e. Δx) reduces, the error in $\Delta u/\Delta x$ increases resulting in divergence. For the case of fully developed flow, $\partial u / \partial x$ can be forced to zero. By doing so, the problem of divergence for small steps was averted and it showed that this term is indeed the source of the problem. $\partial u / \partial x$ cannot be neglected in general, however it was important to realize the source of the problem and the limits that it imposes on the size of the step sizes that can be selected.

One possible explanation for an increased error in the calculation of $\Delta u/\Delta x$, due to decrease in Δx, is that the error in the calculation of u, and therefore in Δu, remains the same and of order of magnitude of 10^{-6} (depending on the tolerance in calculation of flow

rate and pressure drop). The error in Δu becomes comparable to Δu as Δx becomes smaller and that results in further errors in the calculations.

The second case of the flow that was studied was the case of developing flow of a Newtonian fluid in straight ducts, applying a flat velocity profile as the initial condition. As a primary check the results for the u profile at the outlet were compared against the FIDAP™ solution of the same problem and no differences were observed. Other aspects of the flow, including pressure drop and velocity at the centre showed some inconsistencies. In comparison with experimental results (Beavers et.al 1970), a clear difference in pressure drop values was observed. Predictions for the pressure drop near the inlet were 50% lower than the experimental values reducing to about 5% at $\Delta x/Re=0.03$. While there was a gradual decrease in pressure drop from inlet to outlet, the pressure drop at the first step was predicted unexpectedly lower than the second step. This error was approximately equal to the difference between experimental and calculated results along the duct. Figure A-1 shows the result from the algorithm before and after modifications (the discussion of the modifications in the algorithm and initial conditions (I.C.) follows later in this section).

Figure A-1: Prediction of pressure drop before and after modifications

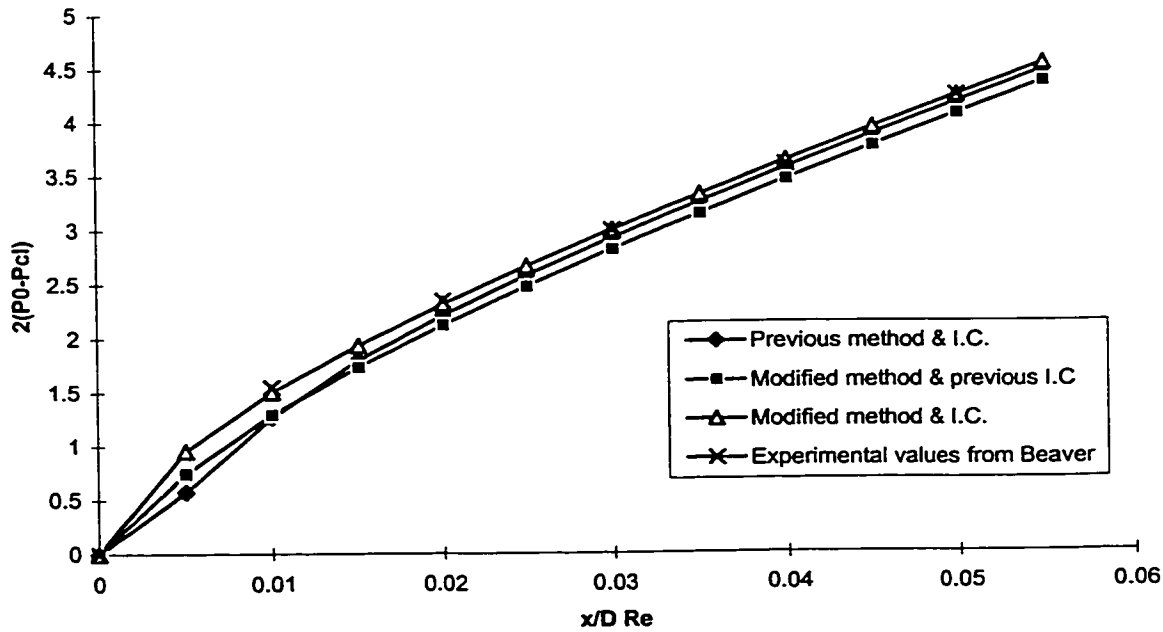

The other problem with results was that the results near the edge of the duct were dependent on the mesh (for the cross section) and the step size. This is an especially important problem, as mesh independence is one of the requirements to verify the results in the later stages of the application of this algorithm (e.g. for viscoelastic flow). These problems were investigated and the results could be summarized as follows.

Firstly, it was found that continuity is not preserved. The flow-rate was being underestimated (between 5-10%, depending on the mesh and step size) in the first step

(from x^o to x^1) and slightly (about 1% and gradually diminishing) overestimated in the next steps.

Comparing the marching algorithm to the SIMPLE algorithm (Patankar, 1980) shows that in the SIMPLE algorithm, corrections from continuity are applied to u, v, and w while in the marching algorithm it was only applied to v and w only. Comparing the marching algorithm to Comini's method (Comini et. al, 1988), the difference is in the calculation of pressure drop. The pressure drop (Δp) is checked against a flow-rate in the marching method while in Comini's method the mechanical energy is being used in the calculation of Δp which is far more sensitive to errors in u values (energy depends on the velocity to the power of 3 while flow-rate depends on velocity itself).

Considering marching method solution for plane x^1 based on information from plane x^o, it was noted that v and w are zero at x^o. This results in an error in equation A.6 where u distribution is obtained. Δp that is obtained after calculation of u-velocity profile will therefore is underestimated. In the following steps, the problem of considering v, and w from previous stages still exists but to a lesser extent.

To remedy the problem another step was introduced to check the flow-rate at each section, once the calculation of pressure and velocity components was completed (after step 10, and before proceeding to the next cross-section) therefore taking into account v

and w effect. This new loop continues until continuity is satisfied at each cross section. It generally took three or four iterations in the first step to satisfy overall continuity and fewer iterations in the following steps. Effects of the continuity check on the prediction of velocity at the centreline (u_c) are shown in Figure (A-2).

Figure A-2: Prediction of center line velocity before and after modifications

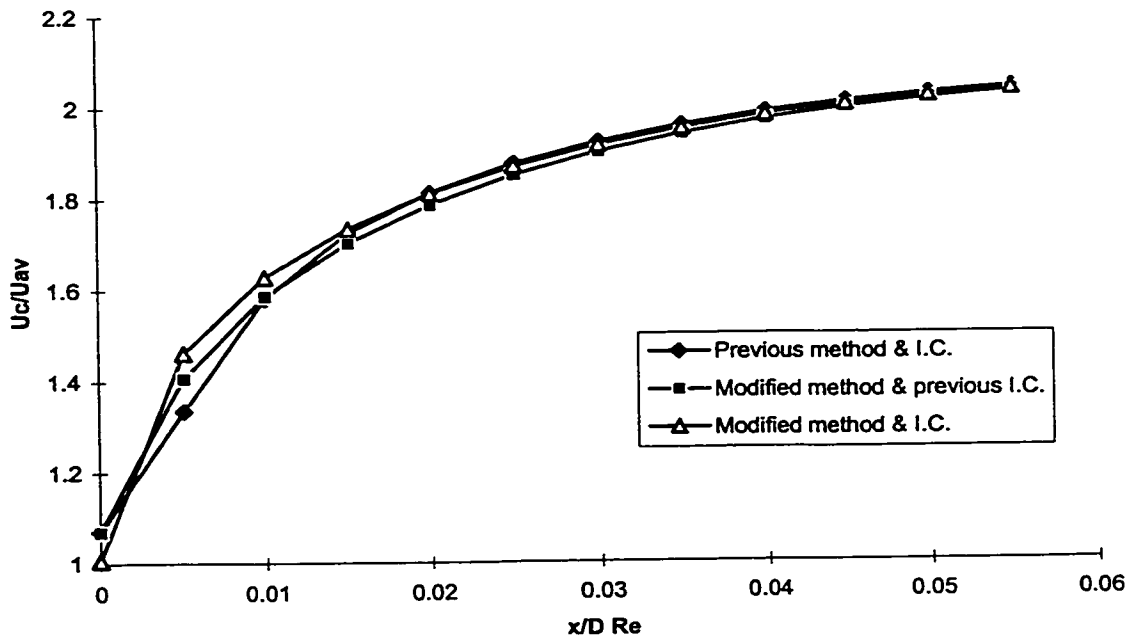

Satisfying continuity, removed the problem of pressure drop in the first step being smaller than the pressure drop in second step, however the difference between the calculated and experimental values still remained (Figure A-1).

Another problem that was contributing to the mesh dependence was the imposition of flat velocity profile as an initial condition. Since the velocity is zero at the wall, to maintain an average dimensionless velocity of 1 requires slightly different profiles depending on how close the mesh is to the wall.

By having nodes closer to the wall, and by satisfying continuity at every plane very good agreement with experimental values were found, as shown in Figure A-3. Figure A-3 also shows how the mesh density near the wall influences the results. These results (Figure A-3) were obtained from the meshes, with first element distance from the wall as 0.005, 0.01, and 0.015D. Even for these meshes proper Δx had to be chosen, otherwise too small steps would have resulted in erroneous results. The proper value of Δx was the minimum value that produces a harmonic function of u against x (i.e. du/dx does not change sign).

The fundamental reason for having so much difficulty near the inlet is the fact that the diffusion term in the direction of the flow ($\partial^2 u / \partial x^2$) is not negligible near the inlet for the case of developing flow. The same problem also exists for the case of flow in complex geometries. In converging or diverging ducts or ducts with a sudden contraction or expansion, second order (diffusion) terms in the direction of the flow are definitely not zero.

Figure A-3: Effects of Initial condition & density of the mesh near the wall

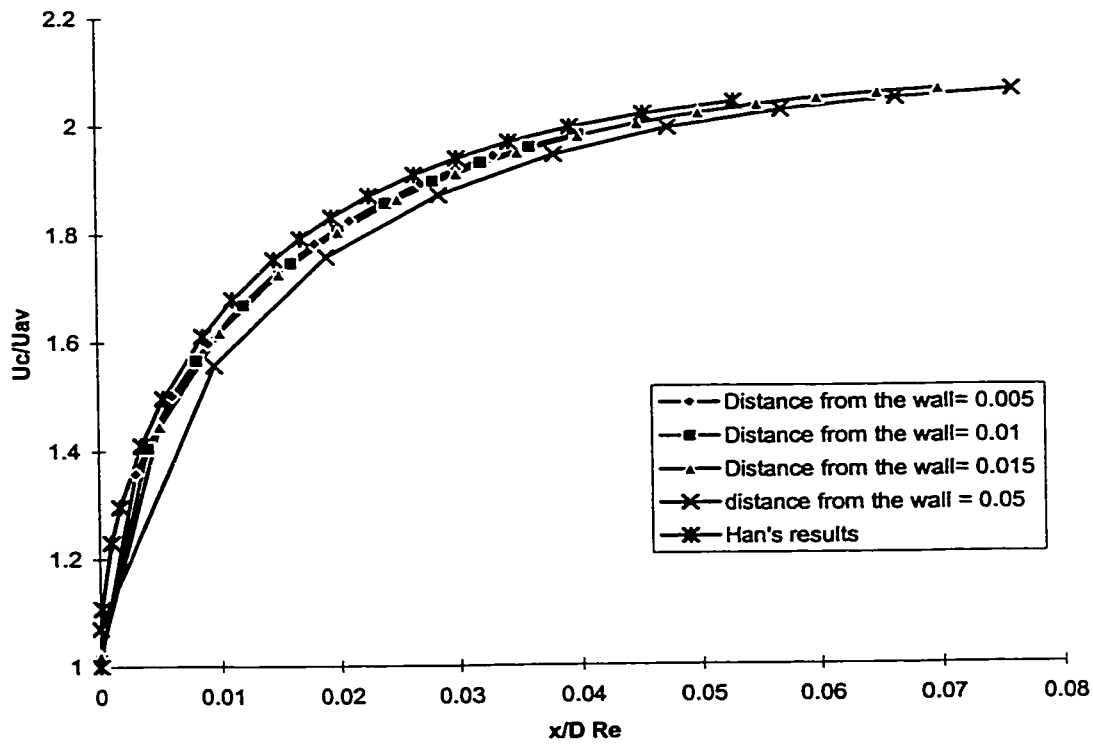

In decoupling the pressure it was assumed that the pressure variation within each plane is very small compared to the pressure drop in flow direction. This is certainly not true for the flow in the neighborhood of sudden contraction or expansion. . There is also the possibility of having re-circulation in such flows as well, resulting in a violation of the assumptions that the marching algorithm is built on.

As for the prediction of the longitudinal vortices, there are a couple of problems associated with the marching code. The first one is in calculation of p(y,z) where we have (step 7 in the algorithm):

$$\frac{\partial}{\partial y}\left(\frac{1}{u^n}\frac{\partial p}{\partial y}\right)+\frac{\partial}{\partial z}\left(\frac{1}{u^n}\frac{\partial p}{\partial z}\right)=\frac{1}{\Delta x}\left(\frac{u^{n+1}-u^n}{\Delta x}+\frac{\partial v^*}{\partial y}+\frac{\partial w^*}{\partial z}\right) \qquad \text{(A.10)}$$

The variation of u from positive values to negative values implies having zero at some points for u^n in equation (A.10). Secondly, since the pressure in downstream affects the upstream domain, there is a need for an algorithm that is able to correctly carry downstream effects upstream (Anderson, 1984).

For a converging or diverging flow as the angle of convergence increases, the pressure in each cross section and also the transverse velocity components increase. Therefore assuming a small variation or a dominant flow in the direction of main flow is no longer valid.

Flows in a diverging duct are amenable to a separation that is detrimental to the basic assumptions of parabolic flow. Point of separation, can be described as the point at which one streamline intersects the wall at a definite angle, and can be mathematically defined as the point where

$$\left.\frac{\partial u}{\partial y}\right|_{wall}=0 \qquad \text{(A.16)}$$

In a divergent channel, pressure increases in the direction of the flow. An adverse pressure gradient together with friction near the wall causes a particle that is moving near the wall to consume its kinetic energy and to stop eventually. After the point of separation, the adverse pressure gradient makes the particle move in the opposite direction (Schlichting, 1979). The region where the purely divergent flow is possible is given by Batchelor (1967) in terms of Re and angle of divergence. At a very low Re or very small angle of divergence (approximately 7°) purely divergent flow can be expected.

Appendix B

Coefficients for equations of viscoelastic stress

$$A_{xx} = (\zeta - 1)(2\frac{\partial u}{\partial x})$$

$$A_{xy} = (\zeta - 1)(\frac{\partial u}{\partial x} + \frac{\partial v}{\partial y})$$

$$A_{xz} = (\zeta - 1)(\frac{\partial u}{\partial x} + \frac{\partial w}{\partial z})$$

$$A_{yy} = (\zeta - 1)(2\frac{\partial v}{\partial y})$$

$$A_{yz} = (\zeta - 1)(\frac{\partial v}{\partial y} + \frac{\partial w}{\partial z})$$

$$A_{zz} = (\zeta - 1)(2\frac{\partial w}{\partial z})$$

$$B_{xx} = \zeta(T_{xy}\frac{\partial v}{\partial x} + T_{xz}\frac{\partial w}{\partial x}) + (\zeta - 2)(T_{xy}\frac{\partial u}{\partial y} + T_{xz}\frac{\partial u}{\partial z})$$

$$B_{xy} = \frac{\zeta}{2}(T_{yy}\frac{\partial v}{\partial x} + T_{yz}\frac{\partial w}{\partial x} + T_{xx}\frac{\partial u}{\partial y} + T_{xz}\frac{\partial w}{\partial y}) + (\frac{\zeta}{2} - 1)(T_{yy}\frac{\partial u}{\partial y} + T_{yz}\frac{\partial u}{\partial z} + T_{xx}\frac{\partial v}{\partial x} + T_{xz}\frac{\partial v}{\partial z})$$

$$B_{xz} = \frac{\zeta}{2}(T_{zz}\frac{\partial w}{\partial x} + T_{yz}\frac{\partial v}{\partial x} + T_{xx}\frac{\partial u}{\partial z} + T_{xy}\frac{\partial v}{\partial z}) + (\frac{\zeta}{2} - 1)(T_{zz}\frac{\partial u}{\partial z} + T_{yz}\frac{\partial u}{\partial y} + T_{xx}\frac{\partial w}{\partial z} + T_{xy}\frac{\partial w}{\partial y})$$

$$B_{yy} = \zeta(T_{xy}\frac{\partial u}{\partial y} + T_{yz}\frac{\partial w}{\partial y}) + (\zeta - 2)(T_{xy}\frac{\partial v}{\partial x} + T_{yz}\frac{\partial v}{\partial z})$$

$$B_{yz} = \frac{\zeta}{2}(T_{zz}\frac{\partial w}{\partial y} + T_{xz}\frac{\partial u}{\partial y} + T_{yy}\frac{\partial v}{\partial z} + T_{xy}\frac{\partial u}{\partial z}) + (\frac{\zeta}{2} - 1)(T_{zz}\frac{\partial v}{\partial z} + T_{xz}\frac{\partial v}{\partial x} + T_{yy}\frac{\partial w}{\partial y} + T_{xy}\frac{\partial w}{\partial x})$$

$$B_{zz} = \zeta(T_{xz}\frac{\partial u}{\partial z} + T_{yz}\frac{\partial v}{\partial z}) + (\zeta - 2)(T_{xz}\frac{\partial w}{\partial x} + T_{yz}\frac{\partial w}{\partial y})$$

$$E_{xx} = B_{xx} + \zeta(\gamma_{xy}\frac{\partial v}{\partial x} + \gamma_{xz}\frac{\partial w}{\partial x}) + (\zeta - 2)(\gamma_{xy}\frac{\partial u}{\partial y} + \gamma_{xz}\frac{\partial u}{\partial z})$$

$$E_{xy} = B_{xy} + \frac{\zeta}{2}(\gamma_{yy}\frac{\partial v}{\partial x} + \gamma_{yz}\frac{\partial w}{\partial x} + \gamma_{xx}\frac{\partial u}{\partial y} + \gamma_{xz}\frac{\partial w}{\partial y}) + (\frac{\zeta}{2} - 1)(\gamma_{yy}\frac{\partial u}{\partial y} + \gamma_{yz}\frac{\partial u}{\partial z} + \gamma_{xx}\frac{\partial v}{\partial x} + \gamma_{xz}\frac{\partial v}{\partial z})$$

$$E_{xz} = B_{xz} + \frac{\zeta}{2}(\gamma_{zz}\frac{\partial w}{\partial x} + \gamma_{yz}\frac{\partial v}{\partial x} + \gamma_{xx}\frac{\partial u}{\partial z} + \gamma_{xy}\frac{\partial v}{\partial z}) + (\frac{\zeta}{2} - 1)(\gamma_{zz}\frac{\partial u}{\partial z} + \gamma_{yz}\frac{\partial u}{\partial y} + \gamma_{xx}\frac{\partial w}{\partial z} + \gamma_{xy}\frac{\partial w}{\partial y})$$

$$E_{yy} = B_{yy} + \zeta(\gamma_{xy}\frac{\partial u}{\partial y} + \gamma_{yz}\frac{\partial w}{\partial y}) + (\zeta - 2)(\gamma_{xy}\frac{\partial v}{\partial x} + \gamma_{yz}\frac{\partial v}{\partial z})$$

$$E_{yz} = B_{yz} + \frac{\zeta}{2}(\gamma_{zz}\frac{\partial w}{\partial y} + \gamma_{xz}\frac{\partial u}{\partial y} + \gamma_{yy}\frac{\partial v}{\partial z} + \gamma_{xy}\frac{\partial u}{\partial z}) + (\frac{\zeta}{2} - 1)(\gamma_{zz}\frac{\partial v}{\partial z} + \gamma_{xz}\frac{\partial v}{\partial x} + \gamma_{yy}\frac{\partial w}{\partial y} + \gamma_{xy}\frac{\partial w}{\partial x})$$

$$E_{zz} = B_{zz} + \zeta(\gamma_{xz}\frac{\partial u}{\partial z} + \gamma_{yz}\frac{\partial v}{\partial z}) + (\zeta - 2)(\gamma_{xz}\frac{\partial w}{\partial x} + \gamma_{yz}\frac{\partial w}{\partial y})$$

$$H_{xx} = u\frac{\partial \gamma_{xx}}{\partial x} + v\frac{\partial \gamma_{xx}}{\partial y} + w\frac{\partial \gamma_{xx}}{\partial z}$$

$$H_{xy} = u\frac{\partial \gamma_{xy}}{\partial x} + v\frac{\partial \gamma_{xy}}{\partial y} + w\frac{\partial \gamma_{xy}}{\partial z}$$

$$H_{xz} = u\frac{\partial \gamma_{xz}}{\partial x} + v\frac{\partial \gamma_{xz}}{\partial y} + w\frac{\partial \gamma_{xz}}{\partial z}$$

$$H_{yy} = u\frac{\partial \gamma_{yy}}{\partial x} + v\frac{\partial \gamma_{yy}}{\partial y} + w\frac{\partial \gamma_{yy}}{\partial z}$$

$$H_{yz} = u\frac{\partial \gamma_{yz}}{\partial x} + v\frac{\partial \gamma_{yz}}{\partial y} + w\frac{\partial \gamma_{yz}}{\partial z}$$

$$H_{zz} = u\frac{\partial \gamma_{zz}}{\partial x} + v\frac{\partial \gamma_{zz}}{\partial y} + w\frac{\partial \gamma_{zz}}{\partial z}$$